SKBF
KBS
TEKNISK
RAPPORT
80-19

Hydrothermal conditions around a radioactive waste repository

Part 1 A mathematical model for the flow of ground-water and heat in fractured rock
Part 2 Numerical solutions

Roger Thunvik
Royal Institute of Technology, Stockholm, Sweden

Carol Braester
Israel Institute of Technology, Haifa, Israel, December 1980

SVENSK KÄRNBRÄNSLEFÖRSÖRJNING AB / PROJEKT KÄRNBRÄNSLESÄKERHET

POSTADRESS: Kärnbränslesäkerhet, Box 5864, 102 48 Stockholm, Telefon 08-67 95 40

HYDROTHERMAL CONDITIONS AROUND A RADIOACTIVE WASTE REPOSITORY

Part 1 A mathematical model for the flow of groundwater and heat in fractured rock
Part 2 Numerical solutions

Roger Thunvik
Royal Institute of Technology, Stockholm, Sweden

Carol Braester
Israel Institute of Technology, Haifa, Israel

December 1980

A list of other reports published in this series is attached at the end of this report. Information on KBS technical reports from 1977-1978 (TR 121) and 1979 (TR 79-28) is available through SKBF/KBS.

HYDROTHERMAL CONDITIONS AROUND A RADIOACTIVE WASTE REPOSITORY

Part 1 - A Mathematical Model for the Flow of Groundwater and Heat in Fractured Rock

Roger Thunvik
Royal Institute of Technology
Stockholm, Sweden

Carol Braester
Israel Institute of Technology
Haifa, Israel

ABSTRACT

A mathematical model describing the hydrothermal conditions around a hard rock repository for disposal of nuclear fuel waste is presented. The model was developed to study the effect of heat released from a radioactive waste repository on the flow times from the repository to the ground surface. The model consists of a set of coupled non-linear partial differential equations for heat and ground water flow. In addition there are two equations of state relating fluid density and viscosity to pressure and temperature. The system of equations is solved numerically using the finite element method in either two or three dimensions. The model is based on the continuum approach. The fractured rock is treated either as two overlapping continua in which the one represents the network of fractures and the other the solid blocks or as a single equivalent medium. The first approach assumes quasi-steady state heat transfer from the rock to the fluid, allowing a linear heat transfer function to be used. The second approach assumes instantaneous equilibrium between the fluid and the rock. This report presents the theoretical background of the model. Numerical solutions for the problems are contained in a separate report entitled "HYDROTHERMAL CONDITIONS AROUND A RADIOACTIVE WASTE REPOSITORY, Part 2 - Numerical Solutions".

CONTENTS

NOMENCLATURE

Symbol	Description	Dimension	SI unit
a	equivalent block radius	L	m
c	compressibility	$M^{-1}LT^{2}$	1/Pa
C	specific heat capacity	$L^{2}T^{-2}K^{-1}$	J/(kgK)
D	thermal diffusivity	$L^{2}T^{-1}$	m^{2}/s
e^{n}	heat flux normal to the flow boundary	MT^{-3}	W/m^{2}
g	acceleration of gravity	LT^{-2}	m/s^{2}
h	heat transfer coefficient	$ML^{-1}T^{-3}K^{-1}$	$W/(m^{3}K)$
H	characteristic length of flow domain	L	m
J	heat flux	MT^{-3}	W/m^{2}
k	permeability	L^{2}	m^{2}
l	thickness of slab	L	m
p	pressure	$ML^{-1}T^{-2}$	Pa
q	specific discharge	LT^{-1}	m/s
q^{n}	specific discharge normal to the flow boundary	LT^{-1}	m/s
Q^{T}	total heat flux	$ML^{2}T^{-3}$	W
R	flow region	-	-
Ra	Rayleigh number	-	-
t	time	T	s
T	temperature	K	K
T_{u}	ultimate temperature at the surface of a sphere or a slab	K	K
x_{i}	Cartesian coordinate	L	m
v	fluid velocity	LT^{-1}	m/s
w	heat transfer function	$ML^{-1}T^{-3}$	W/m^{3}

β	coefficient of thermal volume expansion of the fluid	K^{-1}	1/K
γ	coefficient to determine exponential decrease in permeability with depth	-	-
Γ	boundary of flow domain	-	-
δ	coefficient for the approximation of the heat transfer at the surface of a sphere or a slab	-	-
Δt	time step	T	s
ΔT	characteristic temperature difference	K	K
θ	coefficient for increase in temperature per unit time	KT^{-1}	K/s
λ	thermal conductivity	$MLT^{-3}K^{-1}$	W/(mK)
μ	dynamic viscosity	$ML^{-1}T^{-1}$	Pas
ν	kinematic viscosity	L^2T^{-1}	m^2/s
ρ	density	ML^{-3}	kg/m^3
ϕ	porosity	-	-
Ψ	shape function	-	-

<a> space average defined as

$$\langle a \rangle \equiv \frac{1}{V} \int_V a \, dV$$

<a,b> inner product of two functions a and b defined as

$$\langle a,b \rangle \equiv \int_R a \cdot b \, dR$$

{ } column vector

( ) matrix

superscripts

f fluid

r rock

d	dimensionless parameter
o	reference value
*	equivalent medium
n	time level

subscripts

i,j	indices used for Cartesian tensor notation, repeated indices indicate summation over these indices (i,j = 1,2,3)
	$p_{,t}$ partial time derivative
	$p_{,j}$ gradient of p
I,J,K,L	node indices, repeated indices indicate summation over these indices (I,J,K,L = 1,2,...N, where N is the number of nodal points)

above symbol

~	perturbation term

SUMMARY

This report describes a mathematical model for the flow of groundwater and heat through a fractured rock mass. The model was developed to study the effect of heat released from a radioactive waste repository on the groundwater flow pattern.

Heat released from the waste will increase the temperature of the rock, changing the groundwater density gradients and creating convective currents. Physical parameters such as porosity and hydraulic conductivity are also dependent on temperature. The mathematical model presented describes the flow of groundwater and heat through a fractured rock mass using a system of coupled nonlinear partial differential equations. The model takes into account the dependence of fluid density and viscosity on pressure and temperature.

The motivation for this project came as a result of plans in Sweden for permanent disposal of radioactive waste from nuclear power plants in hard rock repositories deep below the ground surface. The feasibility of a prospective site for waste disposal depends in part on the groundwater conditions. This is due to the capability of a fractured rock mass to transport contaminated groundwater from the repository to the ground surface, should any of the waste canisters be breached. It is therefore of great interest in the safety analysis to assess potential transport times for the groundwater under various conditions.

The main purpose of the present model is to obtain flow patterns in the area around the repository for subsequent calculation of

flow transit times. Major interest has been directed towards the influence of various parameters on the travel times of water particles from the repository to the ground surface.

The fractured rock mass is modelled either as a single equivalent medium or as two separate media. The first case is analagous to an ordinary porous medium in which it is assumed that thermal equilibrium between the rock and the fluid phase is reached instantaneously. In the second case, the two separate media are represented by an interconnected network of fractures through which the fluid flow takes place and solid blocks which are considered impervious to the fluid flow. Convective heat transport takes place in the fractures while conductive heat transport takes place in both media. The second case also takes into account the exchange of heat between the two phases. In the present version of the model this is described by a linear function of the temperature difference between the rock and the fluid. This assumes that quasi-steady state heat transfer from the one phase to the other is reached instantaneously.

The model consists of a set of coupled non-linear partial differential equations for the flow of heat and groundwater through a fractured rock mass. The model is represented by two equations when instantaneous thermal equilibrium is assumed, one for the fluid flow and one for heat flow through both fluid and rock. The model is represented by three equations when quasi-steady heat exchange between the fluid and the solid phase is assumed: one for the fluid flow, one for the heat flow through the fluid, and one for the heat flow through the rock. In addition there are two equations of state relating density and viscosity of the fluid to

pressure and temperature.

The governing equations are solved numerically by the finite element Galerkin method in either two or three dimensions. The flow domain is discretized into a number of elements and the governing equations are transformed into a set of algebraic equations which are solved by Gauss' elimination using the frontal method.

The governing equations in the present model describe the large scale transport of mass and thermal energy through a fractured rock mass. This assumes that it is possible to find a scale at which meaningful space average parameters may be defined. Moreover, the characteristic sizes of the features in the fracture pattern must be significantly smaller than the total dimensions of the rock formation under consideration. Thus, the present model is applicable to fractured rocks with well developed fracture patterns. Further research on the subject of flow conditions around a radioactive waste repository should examine the more complex problems encountered in less developed fracture systems.

1. INTRODUCTION

This report describes a mathematical model developed to study the flow of groundwater and heat through a fractured rock mass. The purpose of the presented model is to describe the physical behaviour of the groundwater around a prospective hard rock repository for disposal of radioactive waste. The present report contains the theoretical development of the flow model presented. Numerical solutions to some problems of interest are presented in a separate report entitled "HYDROTHERMAL CONDITIONS AROUND A RADIOACTIVE WASTE REPOSITORY, Part 2 - Numerical Solutions".

The present investigation was initiated by the Swedish KBS (Nuclear Fuel Safety) project having plans for deep burial of high level nuclear fuel waste. The radioactive waste from the nuclear power plants is planned to be permanently stored in hard rock repositories at a depth of about 500 metres. Definite repository sites have not yet been selected but the general principles for the construction of a repository regarding the layout, the method of encapsulation, etc. have been devised (KBS, 1978).

The feasibility of a prospective site for disposal of radioactive waste depends highly on the geohydrological conditions at the site. This means that in order to determine the suitability of a prospective site for the disposal of radioactive waste, the physical behaviour of the groundwater around the repository must be predicted.

The groundwater flow plays an important role owing to its capability of transporting hazardous waste material through the fractures

of the rock to the biosphere, should a canister be breached. It is therefore of significant interest in the safety analysis of a radioactive waste repository to determine the travel times for water particles from the repository to the ground surface.

The present study is an extension of a previous investigation, in which only the flow patterns induced by piezometric gradients were investigated (Stokes and Thunvik, 1978). In that investigation the groundwater flow around a hypothetical radioactive waste repository was studied under isothermal steady state conditions.

The overall objective of the present groundwater flow study is to develop a more comprehensive model for the flow of groundwater through fractured granite eventually including the main phenomena related to radioactive waste repositories. These phenomena are among others:

- Heat induced phenomena such as convection currents due to the disturbance of initial water density gradients, modifications in the fracture pattern due to dilation of the rock, and changes in the initial rock stress distribution.

- Transport phenomena such as the transport of contaminated groundwater, should any of the canisters be breached.

This investigation is restricted to studying the influence on the groundwater flow patterns and flow transit times due to hydrothermal convection around a hypothetical radioactive waste repository. The initial step in this development is the choice of a conceptual model capable of representing the actual physical phenomenon. The problem is then formulated mathematically and the partial differ-

ential equations are solved for some important problems, e.g. the influence of the topography on the induced patterns of water flow both with and without the repository heat source, using a finite element Galerkin method.

Heat is emitted by the decaying radioactive nuclides for some time after the emplacement of the waste. The effect of the heat is to cause the groundwater to rise in the vicinity of the repository because of the buoyancy effects. The thermally induced uplift of the groundwater above the repository will in general change the flow pattern and under certain conditions decrease the flow transit times for the water particles to travel from the repository to the ground surface. Thus, transport times for various hazardous radioactive nuclides may also decrease in the event of a breached canister.

The flow transit times depend upon the thermal and hydraulic properties of the rock and the appropriate boundary and initial conditions for the flow problem. Moreover, the physical properties of the fluid medium, such as viscosity and density, are pressure and temperature dependent. For example hydraulic conductivity is a function of pressure and temperature because the fluid density and viscosity are functions of pressure and temperature. Thus, the hydraulic conductivity increases when the temperature increases.

The mathematical model presented is used to produce flow patterns to determine the travel times of the water particles from the repository to the surface through a fractured rock mass. The fluid flow in granitic rocks takes place only in the fractures.

Thus, the flow patterns depend on the geometry as well as the physical properties of the fractures.

Fractured granite is highly inhomogeneous and anisotropic due to complex networks of fractures of varying density, distance between adjacent fractures, opening and orientation. The model presented in this report contains simplified representations of fractured granite. Because mathematical solutions require simplifications, care must be taken in drawing conclusions based on this simplified model.

A significant difficulty in the modelling of the flow through a fractured rock mass is due to the great complexity of the fracture pattern. There may be several fracture systems within the same rock mass. The physical characteristics of a fracture system may be distributed within such a wide range that the flow problem becomes impossible to solve properly unless only a very small number of fractures need to be taken into account.

The idea is then to consider only the large scale flow through the rock and to use space average values of the physical properties of the rock in the calculations. This is the common approach to porous media where the solid grains and void interstices are small in relation to the considered scale.

Solutions for groundwater flow through fractured granite are in this report based on the equations for flow through continua, i.e. the actual discontinuum is replaced by a fictitious continuum with average parameters such as permeability defined at every mathematical point. Solving a flow problem using the continuum approach

requires that the investigated flow domain be large in comparison to the "representative sample" of the formation for which the average parameters are defined. Therefore, the question of scale is critical when using the continuum approach. The continuum approach is a reasonable approximation for a fractured rock with a well developed network of fractures. The best locations for repositories are in good quality rock intersected by only a few fractures. In such cases the formation should be treated as discontinuous.

The discrete approach implies that one describes the flow through individual fractures and solid blocks. This requires a description of the physical properties as well as the geometrical characteristics of the fractures and blocks throughout the whole flow domain. Not only is a detailed geometrical description of the fracture pattern practically impossible to obtain in the field, but the mathematical problem increases in complexity since a large number of internal boundary conditions must be imposed upon the flow problem.

Nevertheless, discrete analysis may have to be considered if the continuum approach is not satisfactory for certain hard rock formations. For instance the distributions of the fracture width, the spacing between the fractures and the connectivity between the fractures may be such that the aforementioned requirements of a continumm cannot be fulfilled.

Extensive literature covers various problems of flow through ordinary porous media. Little is known, however, about flow through fractured rocks with very low permeabilities and in particular

about flow through crystalline rocks. Existing mathematical models assume that fractured rocks may be treated as ordinary porous media. The limitations of the application of the porous medium approach to granitic rocks have yet to be determined (Stokes, 1980).

The use of a mathematical model to predict the flow patterns at a site requires that adequate data on the physical parameters, as well as the boundary and initial conditions, are available. It is also required that these data be measured and interpreted using methods which are based on the same theory as the mathematical model itself.

2. MATHEMATICAL FORMULATION OF THE FLOW PROBLEM

The objective of this chapter is to describe the set of partial differential equations characterizing the physical behaviour of groundwater heated by a radioactive waste repository in a hard rock formation. The first section is devoted to the basic concepts of the flow model. The remaining sections are devoted to the derivation of the governing flow equations, the dimensionless form of the flow equations, boundary conditions, and general considerations regarding the exchange of heat between the solid and fluid phases.

2.1 General concepts

A fractured medium may be modelled mathematically either as a continuous or a discrete system. As already pointed out, the continuum approach is the standard approach to flow through granular porous media, but the limits of application to fractured rocks and in particular to crystalline rocks are not quite clear at present. The presented flow model assumes however that the continuum approach is valid for the considered rock formations. The correctness of this assumption should be verified by field tests.

When treating mathematically a fractured medium as a continuum, one must consider various properties such as permeability, pressure, fluid and rock temperature as averages over some volume elements. These elements must be large in comparison with individual fractures and solid blocks, but small in comparison with the characteristic dimensions of the total flow domain. Significant features such as major faults may be included as inhomogeneities,

i.e. as zones with physical properties, which are different from those of the surrounding rock.

Two basic approaches are considered for the heat transport. The first one treats the fluid and solid phases as a single equivalent phase by assuming instantaneous thermal equilibrium between the two phases. The second one treats the heat flow in each one of the two phases separately. In the first approach the model will be represented by one equation for the fluid flow and another equation for the heat flow and the model parameters have to be averaged over both phases. In the second approach the heat flow will be represented by two equations, one for the heat flow in the fluid phase and another equation for the heat flow in the solid phase. The latter approach also requires that the heat transfer from the one phase to the other be calculated.

For the mathematical analysis of the present flow problem the fractured rock mass is conceptualized as a configuration of interconnected fractures and solid blocks. It is assumed that flow of mass takes place only in the fractures, implying that the solid blocks are impervious to the fluid flow. The heat will, however, be conducted through both the solid blocks and the fluid in the fractures. Thus, the heat flow occurs in two different phases, a fluid and a solid phase with continuous exchange of heat at the interface between the two phases.

Pressure and thermal gradients have been proved to be uncoupled in the momentum equation (Bin Guine B. Huang and Dybbs, 1975). This means that the fluid flow is only induced by pressure gradients and not by thermal gradients. Thus, thermally induced flow is

only due to changes in the fluid density.

To apply a discrete approach to the fractured rock mass requires that the interface between the two phases be geometrically described and that the heat transfer along the interface be determined. The geometrical structure of the fracture pattern in a rock mass may be very complex, which implies that this is also true of the geometrical structure of the interface between the fluid and rock phase. Moreover, the heat transfer is dependent on the geometrical shapes of the blocks as well as the physical properties of the flow domain. This makes the problem extremely complicated to deal with at a microscopic scale. The justification for applying the continuum approach to the fractured rock mass is that the various physical parameters may be treated as space averages at a certain macroscopic scale and that the governing equations may be derived accordingly.

In order to derive a set of governing equations for a macroscopic scale the fundamental laws of the conservation of mass, momentum and thermal energy must also be expressed for a macroscopic scale. This requires that it is possible to define a scale, which is large enough to give stable average values of the physical parameters, but small with regard to the dimensions of the exterior boundaries of the considered rock mass.

2.2 Basic equations of the flow model

The macroscopic equations expressing the conservation of mass and momentum of the fluid are considered to be known and will be introduced without a derivation. It is assumed that the terms

related to the inertia forces in the momentum equation can be neglected. Hence this equation is reduced to a form, which is identical to Darcy's law. This means that the fluid flow through the fractures in the rock mass will be treated analogously to the fluid flow through an ordinary porous medium.

A great amount of work has been devoted to derive equations for the conservation of thermal energy for composite porous media at a macroscopic scale by averaging the equations of the individual phases for a microscopic scale. For the sake of completeness a derivation of these equations will be presented. The derivation follows a method described by Gray and O'Neill (1976). Basic definitions and average theorems which are used in the derivation are given in Appendix 1.

2.2.1 Derivation of the macroscopic equations of thermal energy in the solid and fluid phase

The microscopic equation of thermal energy in the solid phase is (De Groot and Mazor, 1963)

$$(\rho^r C^r T^r)_{,t} + J^r_{i,i} = 0 \qquad (2.1)$$

which averaged over an element of the composite medium, taking

into consideration the stated average theorems, becomes

$$\langle \rho^r C^r T^r \rangle_{,t} - \frac{1}{V} \int_S \rho^r C^r T^r v_i n_i \, dS + \langle J_i \rangle_{,i} +$$

$$+ \frac{1}{V} \int_S J_i^r n_i \, dS = 0 \tag{2.2}$$

The velocity at the solid-fluid interface is zero and therefore the second term of (2.2) vanishes. The last term in (2.2) represents the transfer of energy from the solid to the fluid phase, denoted w in the sequel.

The thermal flux is expressed by

$$J_i^r = - \lambda_{ij}^r T_{,j}^r \tag{2.3}$$

We consider averages of the expressions involved in (2.2)

$$- \langle J_i^r \rangle = \langle \lambda_{ij}^r T_{,j}^r \rangle = \langle \lambda_{ij}^r \rangle \langle T_{,j}^r \rangle + \langle \tilde{\lambda}^r \tilde{T}_{,j}^r \rangle \tag{2.4}$$

or (Gray and O'Neill, 1976)

$$- \langle J_{,i}^r \rangle = \langle \lambda_{ij}^r \rangle \langle T_{,j}^r \rangle + \langle \tilde{\lambda}_{ij}^r \tilde{T}_{,j}^r \rangle \tag{2.5}$$

and

$$\langle \rho^r C^r T^r \rangle = \langle \rho^r \rangle \langle C^r \rangle \langle T^r \rangle + \langle \tilde{\rho}^r \tilde{C}^r \tilde{T}^r \rangle \tag{2.6}$$

Neglecting the perturbation terms in (2.5) and (2.6), which are assumed to be small within the element, and substituting these expressions into (2.2) we finally obtain:

$$(\rho^r C^r T^r)_{,t} - (\lambda^r_{ij} T^r_{,j})_{,i} + w^r = 0 \tag{2.7}$$

The average over the element volume is according to (A1.5)

$$((1-\phi)\rho^r C^r T^r)_{,t} - ((1-\phi)\, \lambda^r_{ij} T^r_{,j})_{,i} + w^r = 0 \tag{2.8}$$

or

$$((1-\phi)\rho^r C^r T^r)_{,t} - (\lambda^{r*}_{ij} T^r_{,j})_{,i} + w^r = 0 \tag{2.9}$$

where $\lambda^{r*}_{ij} = (1-\phi)\lambda^r_{ij}$ is the thermal conductivity of the solid rock averaged over the element of the composite medium, and ϕ is porosity.

A similar equation as for the solid phase holds for the fluid

phase, i.e.

$$(\rho^f C^f T^f)_{,t} + J^f_{i,i} = 0 \tag{2.10}$$

which averaged over the phase volume becomes

$$\langle \rho^r C^f T^f \rangle_{,t} - \frac{1}{V} \int_S \rho^f C^f T^f v_i n_i dS + \langle J^f_i \rangle_{,i} + \\ + \frac{1}{V} \int_S J^f_i n_i dS = 0 \tag{2.11}$$

For the same reason as for the solid phase the second term of (2.11) vanishes. The last term represents the transfer of heat from the fluid to the solid, which for continuity reasons is equal to the transfer of heat from the solid to the fluid.

By replacing the flux through the fluid phase by

$$J^f_i = - \lambda^f_{ij} T^f_{,j} + \rho^f C^f v_i T^f \tag{2.12}$$

we obtain after similar average calculations as for the solid phase

$$(\phi \rho^f C^f T^f)_{,t} - (\lambda^{f*}_{ij} T^f_{,j})_{,i} + (\rho^f C^f q_i T^f)_{,i} + w^f = 0 \tag{2.13}$$

where $\lambda^{f*}_{ij} = \phi \lambda^f_{ij}$ is the thermal conductivity of the fluid phase averaged over the composite element volume and q is the specific

fluid flux.

Equations (2.9) and (2.13) are the macroscopic equations for the conservation of thermal energy for the solid and fluid phases respectively. These equations contain a heat transfer function w between the two media, which is difficult to evaluate. This transfer function does not appear when considering the equation for the conservation of thermal energy for the composite medium as a whole, i.e. by adding equations (2.9) and (2.13). Such an approach assumes instantaneous exchange of heat between the two phases and the thermal conductivity is treated as one equivalent parameter in the composite medium.

2.2.2 Macroscopic equations of the flow model

This section is devoted to the development of the macroscopic equations expressing the laws of the conservation of mass, momentum and thermal energy. The fractured rock mass is mathematically treated as two overlapping continua, where the one represents the network of fractures saturated with fluid and the other the solid rock matrix. The two systems are coupled through a heat transfer function calculating the exchange of thermal energy between the two media. The thermal energy transport in the fractures is governed by convection and conduction. The thermal energy transport in the solid blocks is governed only by conduction. The macroscopic conservation laws are expressed by the following set of partial differential equations:

(i) The equation for the conservation of mass of the fluid

$$(\phi\rho^f)_{,t} + (\rho^f q_i)_{,i} = 0 \tag{2.14}$$

(ii) The equation for the conservation of momentum of the fluid

$$q_i = -\frac{k}{\mu}_{ij}(p_{,j} - \rho^f g_j) \tag{2.15}$$

which is equivalent to Darcy's law.

(iii) The equation for the conservation of thermal energy of the fluid

$$(\phi\rho^f C^f T^f)_{,t} - (\lambda^{f*} T^f_{,i})_{,i} + (\rho^f C^f q_i T^f)_{,i} + w^f(x_i,t) = 0 \quad (2.16)$$

(iv) The equation for the conservation of thermal energy of the rock

$$((1-\phi)\rho^r C^r T^r)_{,t} - (\lambda^{r*} T^r_{,i})_{,i} + w^r(x_i,t) = 0 \quad (2.17)$$

where λ^{f*} and λ^{r*} represent the equivalent thermal conductivities of the fluid and the rock media. For simplicity in the ensuing derivations the thermal conductivity tensors are assumed isotropic. However, they may readily be redefined and treated as anisotropic tensors whenever desirable.

The fluid density ρ^f and the dynamic viscosity μ are functions of pressure and temperature. Therefore the previous set of equations must be supplemented by the equations of state of the fluid density and viscosity respectively

$$\rho^f = \rho^f(p,T^f) \quad (2.18)$$

$$\mu = \mu(p,T^f) \quad (2.19)$$

For the present we let the heat transfer terms w^f and w^r denote only the exchange of heat between the fluid medium and the rock medium, omitting other types of heat sources in the ensuing equa-

tions. Since w^f and w^r will have the same absolute values but opposite signs, the superscripts of w will hereafter be dropped.

Regarding the heat exchange between the fluid and the rock, three basic types of assumptions can be made:

(i) Transient exchange of heat between the fluid and the rock

(ii) Instantaneous quasi-steady state exchange of heat between the fluid and the rock

(iii) Instantaneous thermal equilibrium between the fluid and the rock

The temperature response of the solid blocks to fluid temperature changes is always transient. For large block sizes the transients are slow.

For small block sizes the transients become rapid and a quasi-steady state heat transfer function may be applied. Then the heat transfer function describing the exchange of heat between the fluid and the rock may be simplified to a linear function of the difference between the fluid and the rock temperatures.

Equations (2.18) and (2.19) may be written as

$$(\phi\rho^f C^f T^f)_{,t} - (\lambda^{f*} T^f_{,i})_{,i} + (\rho^f C^f q_i T^f)_{,i} + h(T^f - T^r) = 0 \quad (2.20)$$

$$((1-\phi)\rho^r C^r T^r)_{,t} - (\lambda^{r*} T^r_{,i})_{,i} - h(T^f - T^r) = 0 \quad (2.21)$$

where h is the heat transfer coefficient, being a function of the

physical properties of the two media.

For an ordinary porous medium the usual approach is to assume that the fluid medium and the rock medium will instantaneously attain thermal equilibrium. That is to say, no distinction is made between the temperatures of the two media. Then the two previous equations for the conservation of thermal energy may be replaced by a single equation such as the following

$$((\rho C)^{*}T)_{,t} - (\lambda^{*}T_{,i})_{,i} + (\rho^{f}C^{f}q_{i}T)_{,i} = 0 \qquad (2.22)$$

where $(\rho C)^{*}$ is the equivalent volumetric heat capacity and λ^{*} is the equivalent thermal conductivity of the two media.

Further discussion about the concepts of the heat transfer function and the thermal properties of the fluid and rock media will be carried out in section 2.3.

The remaining part of the present section will be devoted to further development of the governing equations by the introduction of fluid compressibility, rock compressibility, thermal volume expansion, etc.

Compressibility of the fluid, compressibility of the solid matrix, and the coefficient of thermal volume expansion of the fluid are

defined as

$$c^f = \frac{1}{\rho^f} \frac{\partial \rho^f}{\partial p} \tag{2.23}$$

$$c^r = \frac{1}{\phi} \frac{d\phi}{dp} \tag{2.24}$$

$$\beta = - \frac{1}{\rho^f} \frac{\partial \rho^f}{\partial T^f} \tag{2.25}$$

With these definitions the time derivative term in the equation for the conservation of mass of the fluid may be expanded and rewritten in the following way

$$(\phi\rho^f)_{,t} = \phi\rho^f_{,t} + \rho^f\phi_{,t} = \phi(\frac{\partial \rho}{\partial p} p_{,t} + \frac{\partial \rho^f}{\partial T^f} T^f_{,t}) + \rho^f \frac{d\phi}{dp} p_{,t} \tag{2.26}$$

Making use of the previous definitions of compressibility and thermal volume expansion we obtain

$$(\phi\rho^f)_{,t} = \phi\rho^f(c^f + c^r) p_{,t} - \phi\rho^f\beta T^f_{,t} \tag{2.27}$$

The equation for the conservation of mass of the fluid can now be

written as

$$\phi\rho^f(c^f+c^r)\, p_{,t} - \phi\rho^f\beta T^f_{,t} + (\rho^f q_i)_{,i} = 0 \qquad (2.28)$$

Substituting equation (2.15) into this equation, we obtain

$$\phi\rho^f(c^f + c^r)\, p_{,t} - \phi\rho^f\beta T^f_{,t} - (\rho^f \frac{k}{\mu}_{ij}(p_{,j} - \rho^f g_j))_{,i} = 0 \qquad (2.29)$$

Expanding the time derivative term and the convective divergence term in equation (2.16), we obtain

$$\phi\rho^f C^f T^f_{,t} + C^f T^f(\phi\rho^f)_{,t} - (\lambda^{f*} T^f_{,i})_{,i} + \rho^f C^f q_i T^f_{,i}$$

$$+ C^f T^f(\rho^f q_i)_{,i} + w = 0 \qquad (2.30)$$

Applying the equation for the conservation of mass of the fluid to the previous equation, we obtain

$$\phi\rho^f C^f T^f_{,t} - (\lambda^{f*} T^f_{,i})_{,i} + \rho^f C^f q_i T^f_{,i} + w = 0 \qquad (2.31)$$

Expanding the time derivative in equation (2.16), we obtain

$$((1-\phi)\rho^r C^r T^r)_{,t} = (1-\phi)\rho^r C^r T^r_{,t} - \rho^r C^r T^r \phi_{,t} \qquad (2.32)$$

or

$$((1-\phi)\rho^r C^r T^r)_{,t} = (1-\phi)\rho^r C^r T^r_{,t} - \rho^r C^r T^r \phi c^r p_{,t} \tag{2.33}$$

The equation for the conservation of thermal energy of the rock can now be written as

$$-- (1-\phi)\rho^r C^r T^r_{,t} - \rho^r C^r T^r \phi c^r p_{,t} - (\lambda^{r*} T^r_{,i})_{,i} - w = 0 \tag{2.34}$$

We now have the following set of equations to solve

$$\phi\rho^f(c^f + c^r) p_{,t} - \phi\rho^f \beta T^f_{,t} - (\rho^f \frac{k}{\mu}_{ij} (p_{,j} - \rho^f g_j))_{,i} = 0 \tag{2.35}$$

$$\phi\rho^f C^f T^f_{,t} - (\lambda^{f*} T^f_{,i})_{,i} + \rho^f C^f q_i T^f_{,i} + w = 0 \tag{2.36}$$

$$(1-\phi)\rho^r C^r T^r_{,t} - \rho^r C^r T^r \phi c^r p_{,t} - (\lambda^{r*} T^r_{,i})_{,i} - w = 0 \tag{2.37}$$

$$\rho^f = \rho^f(p, T^f) \tag{2.38}$$

$$\mu = \mu(T^f) \tag{2.39}$$

where w may represent either a transient or a quasi-steady state heat transfer function. The dynamic viscosity of the fluid has been restated as a function of temperature only, since in the model the pressure dependence has been neglected in this equation.

In brief, the model is represented by a system of non-linear partial differential equations. One of the equations governs the fluid flow, one the flow of heat by the fluid in the fractures, and one the flow of heat through the rock matrix. The fluid flow equation is coupled with the thermal energy balance equations through the convective term in the fluid energy equation and through the fluid density and viscosity. There is another coupling between the fluid flow equation and the fluid energy equation through the term with the time derivative of the fluid temperature, due to the thermal volume expansion of the fluid. Since one of the terms in the thermal energy equation of the rock contains a time derivative of pressure, there is also a coupling between this equation and the fluid flow equation. The two energy balance equations are strongly coupled through the heat transfer function, governing the exchange of heat between the fluid in the fractures and the rock matrix.

The heat transport will be conductive or convective dominant depending on the relative significance of the conduction and convection terms in the equation of thermal energy (2.36). One can see from this equation that the flow of heat will be dominated by

conduction for low fluid velocities and low temperature gradients, while it will be dominated by convection for high fluid velocities and high temperature gradients.

2.3 Heat transfer considerations

This section presents some mathematical concepts which describe the exchange of heat between the rock and the fluid. The principles of the heat exchange between the two different phases are of interest when dealing with fractured media that cannot be treated like ordinary porous media. That is to say, the flow model parameters cannot be lumped into single equivalent parameters which represent both phases of the fractured rock medium.

An idea when treating mathematically a fractured medium is to conceive the medium as a configuration of blocks and fractures, where the blocks represent the solid phase and the fractures the fluid phase. A fundamental problem is then to calculate the heat transfer from the one phase to the other.

2.3.1 Simplifying assumptions

For the calculation of the heat transfer from the one phase to the other, geometrical descriptions of the blocks are needed. This makes the problem very complicated from a computational as well as from a practical point of view. In order to simplify these calculations the blocks are approximated to spheres or slabs. Hereby the geometrical properties of the blocks may be represented by a single parameter characterizing the overall sizes of the blocks.

Investigations carried out by Kuo et al. (1976) show that irregular shaped solids under imposed flux at the surface behave like spheres of equivalent radii. The equivalent radii for some regular shapes, e.g. cylinders, parallelepipeds and several irregular

shapes, were analyzed theoretically and experimentally. A rough estimate for the radius of an equivalent sphere is a=3V/A where a is the radius of the sphere, V is the volume and A is the area of the block. More accurate values are given in the report by Kuo.

The most important reason for approximating the solid blocks in the fracture pattern to equivalent spheres or slabs is that it enables the use of some analytical solutions of the heat conduction equation for solids. Analytical solutions may, however, only be used to calculate the heat flux through the surface of a sphere or a slab under ideal conditions, but analytical solutions may yet be very useful to estimate the relation between response times and block sizes, to estimate the heat transfer coefficient for quasi-steady state heat transfer conditions, etc.

The solutions used herein were taken from Carlslaw and Jaeger. From these solutions one may readily derive expressions for the temperature gradient at the surface of the block and apply Fourier's law to obtain the heat flux. Two types of boundary conditions will be considered a) linear increase in temperature at the surface of the block and zero initial temperature within the block and b) constant temperature at the surface of the block and constant initial temperature within the block. In each case expressions of the heat flux for exact as well as averaged solutions to the temperature distributions will be derived.

Preference is given to adopt the sphere when investigating the heat transfer properties of a fractured rock mass with a well developed fracture pattern forming a system of blocks. The slab may be more appropriate to adopt when investigating the heat

transfer properties of a fractured rock mass with a less developed fracture pattern formed by a limited number of fractures.

2.3.2 Calculation of the heat flux through the surface of a sphere

The sphere is assumed to be heated by surrounding water. Assuming that the heat flow within the sphere is only governed by conduction we may use the well-known diffusion equation

$$(\rho C)^r T_{,t} - \lambda^r T^r_{,ii} = 0 \tag{2.40}$$

Derivatives of solutions to (2.40) may be substituted into Fourier's law to calculate the total heat flux at the surface of the sphere

$$Q^T = 4\pi a^2 \lambda^r \left(\frac{\partial T^r}{\partial r}\right)_{r=a} \tag{2.41}$$

which expressed as thermal energy flux per unit volume can be written as

$$w = Q^T / \frac{4}{3}\pi a^2 = \frac{3\lambda^r}{a}\left[\frac{\partial T^r}{\partial r}\right]_{r=a} \tag{2.42}$$

Two particular cases will be investigated: a) linear increase in temperature at the surface of the sphere and zero initial temperature within the sphere, b) constant temperature on the surface of the sphere and constant initial temperature within the sphere.

a) Linear increase in temperature at the surface of the sphere and zero intial temperature within the sphere heated by surrounding water

The solution of equation (2.40) for this case is 1)

$$T(r,t) = \theta\left(t - \frac{a^2 - r^2}{6D}\right) - \frac{2\theta a^3}{D\pi r} \sum_{n=1}^{\infty} \frac{(-1)^n}{n^3} e^{-\frac{Dn^2\pi^2}{a^2}t} \sin\frac{n\pi r}{a} \qquad (2.43)$$

Using (2.43), the temperature derivative within the sphere becomes equal to

$$\frac{\partial T}{\partial r} = \theta\frac{2r}{6D} - \frac{2\theta a^3}{D\pi^3 r} \sum_{n=1}^{\infty} \frac{(-1)^n}{n^3} e^{-\frac{Dn^2\pi^2}{a}t} \frac{n\pi}{a} \cos\frac{n\pi r}{a}$$

$$+ \frac{2\theta a^3}{D\pi r^2} \sum_{n=1}^{\infty} \frac{(-1)^n}{n^3} e^{-\frac{Dn^2\pi^2}{a^2}t} \sin\frac{n\pi r}{a} \qquad (2.44)$$

at r=a this expression becomes

$$\left.\frac{\partial T}{\partial r}\right|_{r=a} = \frac{\theta a}{3D} - \frac{2\theta a}{D\pi^2} \sum_{n=1}^{\infty} \frac{1}{n^2} e^{-\frac{Dn^2\pi^2}{a^2}t} \qquad (2.45)$$

and

$$\left.\frac{\partial T}{\partial r}\right|_{r=a} = \frac{\theta a}{3D} \qquad (2.46)$$

for $t \to \infty$

---

1) Carlslaw and Jaeger, p. 235.

The average temperature of the sphere is

$$T = \theta(t - \frac{a^2}{15D}) + \frac{6\theta a^2}{\pi^4 D} \sum_{n=1}^{\infty} \frac{1}{n^4} e^{-\frac{Dn^2\pi^2}{a^2} t} \tag{2.47}$$

The difference between the surface temperature and the average temperature of the sphere is

$$T^f - T = \frac{\theta a^2}{D} (\frac{1}{15} - \frac{6}{\pi^4} \sum_{n=1}^{\infty} \frac{1}{n^4} e^{-\frac{Dn^2\pi^2}{a^2} t}) \tag{2.48}$$

The derivative is approximated as

$$\frac{T^f - T}{\delta a} = \frac{\theta a}{D\delta} (\frac{1}{15} - \frac{6}{\pi^4} \sum_{n=1}^{\infty} \frac{1}{n^4} e^{-\frac{Dn^2\pi^2}{a^2} t}) \tag{2.49}$$

Approximating (2.49) to (2.46), we obtain $\delta = 0.2$.

Using (2.42), (2.45) and (2.49) to express the exact solution for the heat flux as energy per unit volume, we obtain

$$w = \frac{\lambda^r \theta}{D} - \frac{6\lambda^r \theta}{D\pi^2} \sum_{n=1} \frac{1}{n^2} e^{-\frac{Dn^2\pi^2}{a^2} t} \tag{2.50}$$

and for the averaged solution we obtain

$$w = \frac{3\lambda^r \theta}{D\delta} (\frac{1}{15} - \frac{6}{n^4} \sum_{n=1}^{\infty} \frac{1}{n^4} e^{-\frac{Dn^2\pi^2}{a^2} t}) \tag{2.51}$$

(2.50) and (2.51) are displayed in Figure 2.1.

b) Constant temperature at the surface of the sphere and constant initial temperature

The solution of equation (2.40) for this case is 1)

$$T(r,t) = T_u + \frac{2aT_u}{\pi r} \sum_{n=1}^{\infty} \frac{(-1)^n}{n} \sin \frac{n\pi r}{a} e^{-\frac{Dn^2\pi^2}{a^2} t} \tag{2.52}$$

The temperature derivative for the sphere becomes equal to

$$\frac{\partial T}{\partial r} = \frac{2a}{\pi r} \sum_{n=1}^{\infty} \frac{(-1)^n}{n} \frac{n\pi}{a} \cos \frac{n\pi r}{a} e^{-\frac{Dn^2\pi}{a^2} t} -$$

$$- \frac{2aT}{\pi r^2 u} \sum_{n=1}^{\infty} \frac{(-1)^n}{n} \sin \frac{n\pi r}{a} e^{-\frac{Dn^2\pi^2}{a^2} t} \tag{2.53}$$

at r=a this expression becomes

$$\left.\frac{\partial T}{\partial r}\right|_{r=a} = \frac{2T_u}{a} \sum_{n=1}^{\infty} e^{-\frac{Dn^2\pi^2}{a^2} t} \tag{2.54}$$

and

$$\left.\frac{\partial T}{\partial r}\right|_{r=a} = 0 \qquad t \to \infty \tag{2.55}$$

The average temperature of the sphere is

$$T = T_u - \frac{6T_u}{\pi^2} \sum_{n=1}^{\infty} \frac{1}{n^2} e^{-\frac{Dn^2\pi^2}{a^2} t} \tag{2.56}$$

---

1) Carlslaw and Jaeger, p. 233.

The difference between the surface temperature and the average temperature of the sphere is

$$T^f - T = \frac{6T_u}{\pi^2} \sum_{n=1}^{\infty} \frac{1}{n^2} e^{-\frac{Dn^2\pi^2}{a^2}t} \tag{2.57}$$

The derivative is approximated as

$$\frac{\partial T}{\partial r}\Big|_{r=a} \cong \frac{T^f - T}{\delta a} = \frac{6T_u}{\delta a \pi^2} \sum_{n=1}^{\infty} \frac{1}{n^2} e^{-\frac{Dn^2\pi^2}{a^2}t} \tag{2.58}$$

In the present case the derivative vanishes as time goes to infinity. Therefore, the value of δ could not be obtained in the same way as for the previous case. Instead (2.58) was experimentally approximated to (2.54) and the best fit was obtained for $\delta \cong 0.30$.

"sing (2.42),(2.54) and (2.58) to express the exact solution for the heat flux as energy per unit volume, we obtain

$$w = \frac{6\lambda^r T_u}{a^2} \sum_{n=1}^{\infty} e^{-\frac{Dn^2\pi^2}{a^2}t} \tag{2.59}$$

and for the approximate solution we obtain

$$w = \frac{18\lambda^r T_u}{\delta a^2 \pi^2} \sum_{n=1}^{\infty} \frac{1}{n^2} e^{-\frac{Dn^2\pi^2}{a^2}t} \tag{2.60}$$

(2.59) and (2.60) are displayed in Figure 2.2. In figures (2.1) and (2.2) the following transformation into dimensionless time was

used

$$t^d = \frac{D}{a^2} t \tag{2.61}$$

where D is the thermal diffusivity, a is the equivalent block radius and t is time.

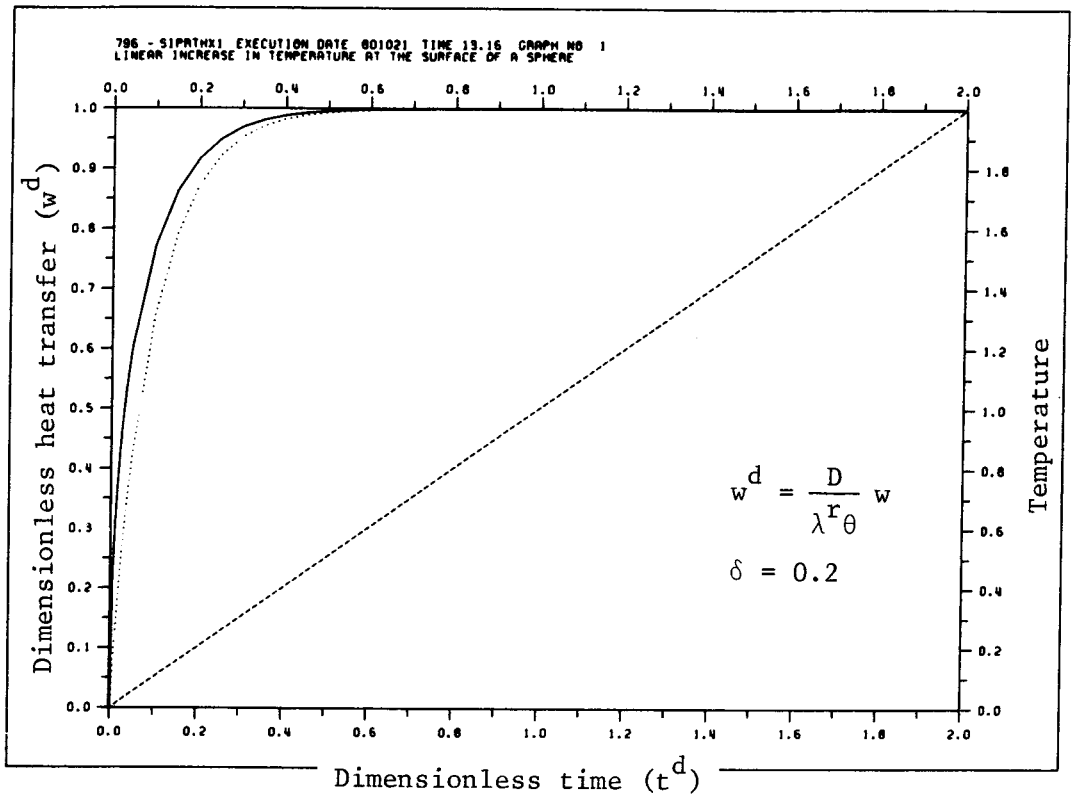

Figure 2.1 Exact (solid line) and approximate (dotted line) solutions for the heat flux on the surface of a sphere. Linear increase in surface temperature and constant initial temperature within the sphere.

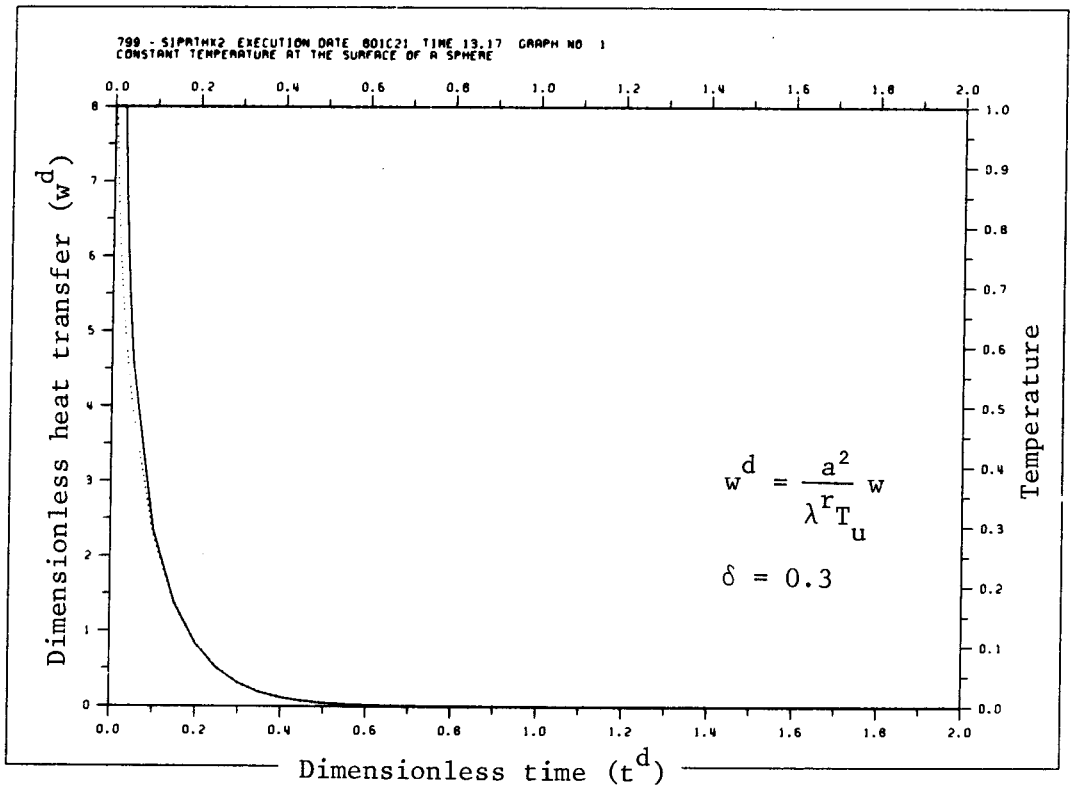

Figure 2.2 Exact (solid line) and approximate (dotted line) solutions for the heat flux at the surface of a sphere. Constant surface temperature and constant initial temperature within the sphere.

2.3.3 Calculation of the heat flux through the surface of the slab

The analysis carried out for the slab is quite similar to that of the sphere. One dimensional solutions to (2.40) with boundary and initial conditions comparable to the sphere were taken from Carlslaw and Jaeger. That is to say the temperature at the surface of the slab at x=+l is either assumed to increase linearly with time or kept constant. The initial temperature is assumed to be zero in both cases.

The thermal energy flux per unit volume is

$$w = \frac{1}{l}\,\lambda^r\left(\frac{\partial T}{\partial x}\right)_{x=l} \tag{2.62}$$

As for the sphere, the derivative of the temperature at the surface of the slab, using exact as well as averaged temperature distributions, will be presented.

a) Linear increase in temperature at the surface of the slab and zero initial temperature.

The solution of (2.40) for this case is 1)

$$T(x,t) = \theta\left(t + \frac{x^2-l^2}{2D}\right) - \frac{16\theta l^2}{D\pi^3}\sum_{n=0}^{\infty}\frac{(-1)^n}{(2n+1)^3}\, e^{-\frac{D(2n+1)^2\pi^2}{4l^2}t}$$

$$\cos\frac{(2n+1)\pi x}{2l} \tag{2.63}$$

1) Carlslaw and Jaeger, p. 104.

The derivative of the temperature at the surface of the slab is

$$\frac{\partial T}{\partial x}\Big|_{x=l} = \frac{\theta l}{D} - \frac{8\theta l}{D\pi^2} \sum_{n=0}^{\infty} \frac{1}{(2n+1)^2} e^{-\frac{D(2n+1)^2\pi^2}{4l^2} t} \qquad (2.64)$$

The average temperature is

$$T = \theta(t - \frac{l^2}{3D}) + \frac{32\theta l^2}{D\pi^4} \sum_{n=0}^{\infty} \frac{1}{(2n+1)^4} e^{-\frac{D(2n+1)^2\pi^2}{4l^2} t} \qquad (2.65)$$

and the difference between the surface and the average temperature is

$$T^f - T = \frac{\theta l^2}{3D} - \frac{32\theta l^2}{D\pi^4} \sum_{n=0}^{\infty} \frac{1}{(2n+1)^4} e^{-\frac{D(2n+1)^2\pi^2}{4l^2} t} \qquad (2.66)$$

The derivative of the temperature is approximated by

$$\frac{\partial T}{\partial x}\Big|_{x=l} \quad \frac{T^f - T}{\delta l} = \frac{1}{\delta} \frac{\theta l}{D} \left(\frac{1}{3} - \frac{32}{\pi^4} \sum_{n=0}^{\infty} \frac{1}{(2n+1)^4} e^{-\frac{D(2n+1)^2\pi^2}{4l^2} t}\right) \qquad (2.67)$$

Approximating (2.67) to (2.64) for $t \to \infty$, we obtain $\delta = \frac{1}{3}$.

Using (2.62), (2.64) and (2.67) to express the exact solution for the heat flux as energy per unit volume, we obtain

$$w = \frac{\lambda^r \theta}{D} \left(1 - \frac{8}{\pi^2} \sum_{n=0}^{\infty} \frac{1}{(2n+1)^2} e^{-\frac{D(2n+1)^2\pi^2}{4l^2} t} \right) \qquad (2.68)$$

and for the approximate solution we obtain

$$w = \frac{\lambda^r \theta}{\delta D} \left(\frac{1}{3} - \frac{32}{\pi^4} \sum_{n=0}^{\infty} \frac{1}{(2n+1)^4} e^{- \frac{D(2n+1)^2\pi^2}{4l^2} t} \right) \qquad (2.69)$$

(2.68) and (2.69) are displayed in figure 2.3.

b) Constant temperature at the surface of the slab

The solution for this case is 1)

$$T(x,t) = T_u - \frac{4T_u}{\pi} \sum_{n=0}^{\infty} \frac{(-1)^n}{2n+1} e^{- \frac{D(2n+1)^2\pi^2}{4l^2} t} \cos \frac{(2n+1)\pi x}{2l} \qquad (2.70)$$

and the derivative at x=l is

$$\left.\frac{\partial T}{\partial x}\right|_{x=l} = \frac{2T_u}{l} \sum_{n=0}^{\infty} e^{- \frac{D(2n+1)^2\pi^2}{4l^2} t} \qquad (2.71)$$

The average temperature is

$$T = T_u - \frac{8T_u}{\pi^2} \sum_{n=0}^{\infty} \frac{1}{(2n+1)^2} e^{- \frac{D(2n+1)^2\pi^2}{4l^2} t} \qquad (2.72)$$

and the derivative is approximated by

$$\left.\frac{\partial T}{\partial x}\right|_{x=l} \cong \frac{T_u - T}{\delta l} = \frac{8T_u}{\pi^2 \delta l} \sum_{n=0}^{\infty} \frac{1}{(2n+1)^2} e^{- \frac{D(2n+1)^2\pi^2}{4l^2} t} \qquad (2.73)$$

---

1) Carlslaw and Jaeger, p. 100.

In this case (2.73) was experimentally approximated to (2.71) and the best fit was obtained for $\delta \cong 0.40$.

Using (2.62),(2.71) and (2.73) to express the exact solution for the heat flux as energy per unit volume, we obtain

$$w = \frac{\lambda^r 2T_u}{l^2} \sum_{n=0}^{\infty} e^{-\frac{D(2n+1)^2\pi^2}{4l^2} t} \tag{2.74}$$

and for the approximate solution we obtain

$$w = \frac{\lambda^r 8T_u}{\pi\delta l^2} \sum_{n=0}^{\infty} \frac{1}{(2n+1)^2} e^{-\frac{D(2n+1)^2\pi^2}{4l^2} t} \tag{2.75}$$

The results of the calculations carried out for the slab are presented in figures (2.3) and (2.4), in which the same dimensionless time as for the sphere applies (see eq. 2.61).

A general conlusion that may be drawn from the previous analysis of the heat flux through the surface of a sphere or slab under various conditions, is that the heat exchange between the fluid and rock media, in most cases, may be approximated by a quasi-steady state heat transfer function.

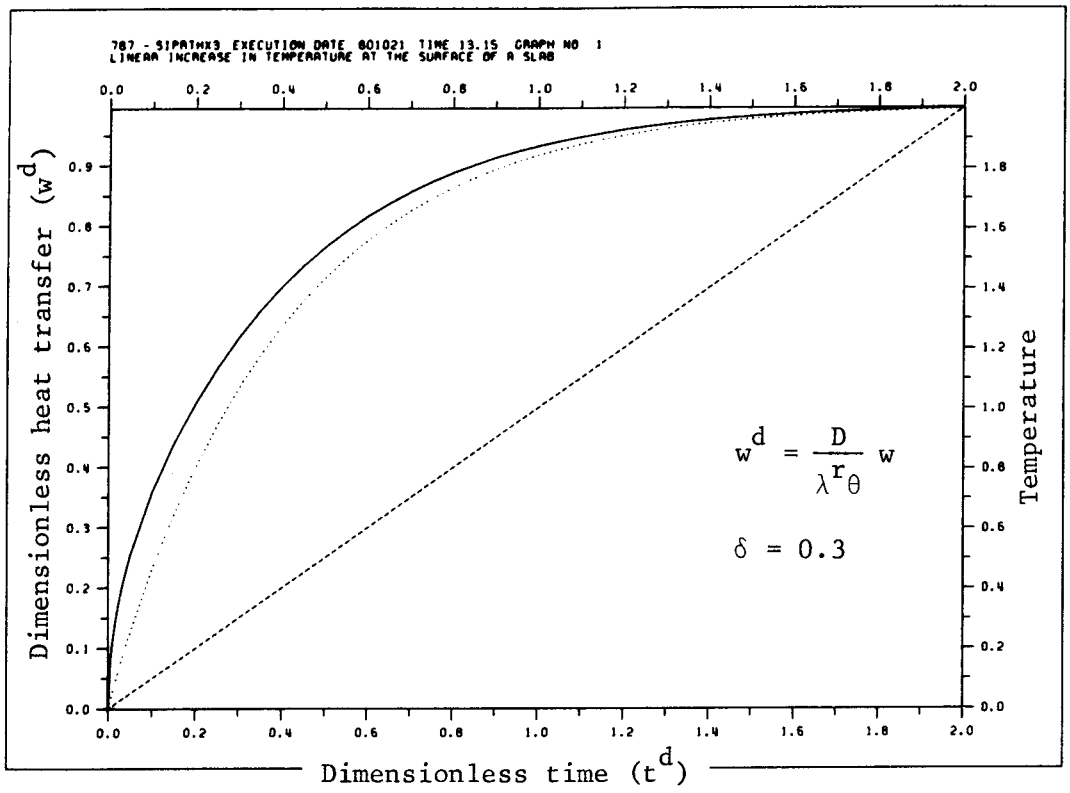

Figure 2.3 Exact (solid line) and approximate (dotted line) solutions for the heat flux at the surface of a slab. Linear increase in surface temperature and constant initial temperature of the slab.

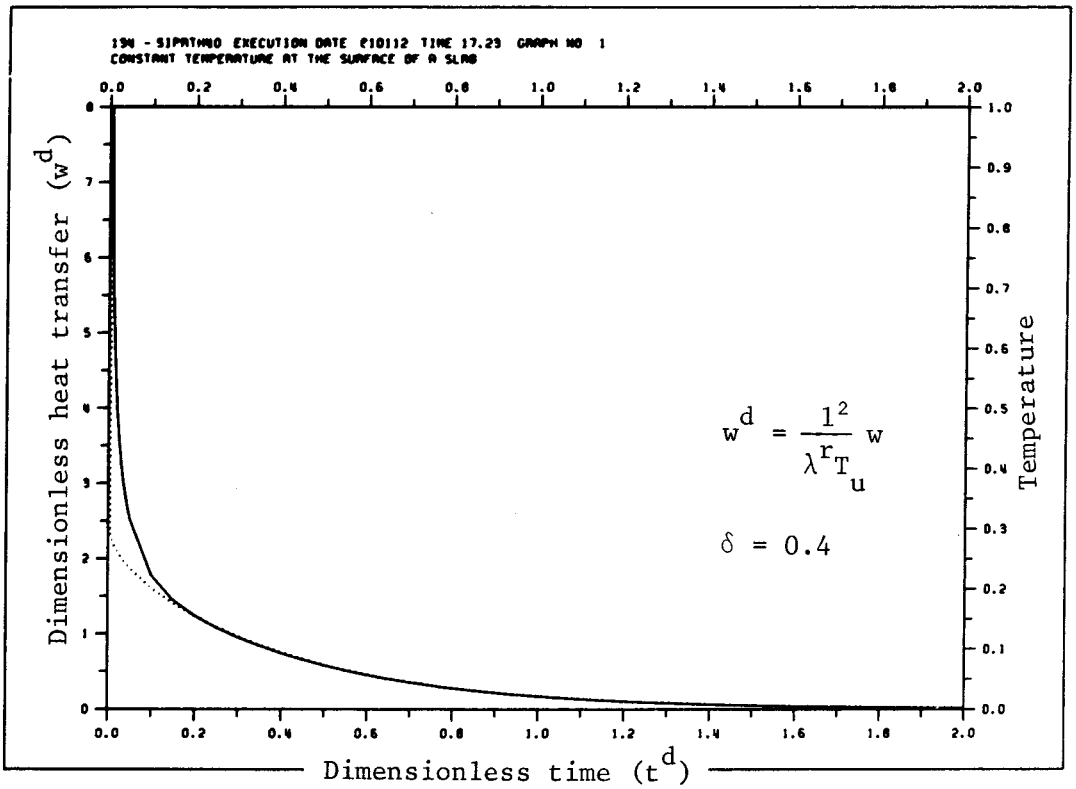

Figure 2.4 Exact (solid line) and approximate (dotted line) solutions for the heat flux at the surface of a slab. Constant surface temperature and constant initial temperature of the slab.

2.3.4 Quasi-steady state heat transfer function

We assume a quasi-steady state heat transfer function of the following form

$$w = h(T^f - T^r) \tag{2.76}$$

where h is the heat transfer coefficient.

The thermal energy flux per unit volume through the surface of a sphere is approximated by

$$w = \frac{3\lambda^r}{a} \frac{\partial T}{\partial r}\Big|_{r=a} = \frac{3\lambda^r}{a} \frac{(T^f - T^r)}{\delta a} \tag{2.77}$$

Making use of (2.76) and (2.77), h may be solved as

$$h = \frac{3\lambda^r}{\delta a^2} \tag{2.78}$$

The thermal energy flux through the surface of a slab is

$$w = \frac{1}{l} \lambda^r \frac{\partial T}{\partial x}\Big|_{x=l} = \frac{\lambda^r}{l} \frac{(T^f - T^r)}{\delta l} \tag{2.79}$$

Making use of (2.76) and (2.79) h becomes

$$h = \frac{\lambda^r}{\delta l^2} \tag{2.80}$$

The value of the coefficient δ was determined experimentally (see sections 2.3.2 and 2.3.3).

2.4 Dimensionless form of equations

We consider equations (2.14) to (2.17) to obtain the dimensionless form of the flow equations.

To obtain the dimensionless form of Darcy's law, that is to say equation (2.15), the following dimensionless parameters are defined

$$k_{ij}^{d} = \frac{k_{ij}}{k^{o}} , \quad \mu^{d} = \frac{\mu}{\mu^{o}} , \quad \rho^{d} = \frac{\rho}{\rho^{o}\beta\Delta T} ,$$

$$p^{d} = \frac{p - p^{o}}{\rho^{o} g H} , \quad x_{i}^{d} = \frac{x_{i}}{H} \tag{2.81}$$

where ΔT is a characteristic temperature difference taken over some characteristic length H of the flow domain. The superscripts d and o are used to indicate dimensionless parameters and reference values, respectively. Using the definitions given in (2.81) and substituting into (2.15) we obtain

$$q_{i}^{d} = - \frac{k_{ij}^{d}}{\mu^{d}} \left(p_{,j}^{d} - \rho^{fd} \beta \Delta T \frac{g_{j}}{g} \right) \tag{2.82}$$

To obtain the dimensionless form of the equation for the conservation of mass of the fluid (2.14), the following dimensionless time

is defined

$$t^{d1} = \frac{k^o \rho^o g}{\mu^o H} t \tag{2.83}$$

Substitution of (2.83) together with the definitions of fluid density and specific flux, as given in (2.81) above, into (2.14) yields the following dimensionless form of the equation for the conservation of mass of the fluid

$$(\phi \rho^{fd})_{,t^{d1}} + (\rho^{fd} q_i^d)_{,i} = 0 \tag{2.84}$$

For the equations for the conservation of thermal energy (2.16) and (2.17), we define in addition to (2.81) the following dimensionless parameters

$$\lambda^d = \frac{\lambda}{\lambda^o} \quad , \quad C^d = \frac{C}{C^o} \quad , \quad T^d = \frac{T}{\Delta T} \quad ,$$

$$w^d = \frac{H^2}{\lambda^o \Delta T} w \tag{2.85}$$

The dimensionless time for the equations of thermal energy is defined as

$$t^{d2} = \frac{\lambda^o}{\rho^o C^o H^2 \beta \Delta T} t \tag{2.86}$$

Making use of the previous definitions and substituting into

(2.16), we obtain

$$(\phi \rho^{fd} C^{fd} T^{fd})_{,t} d2 - (\lambda^{f*d} T^{fd}_{,i})_{,i} + \\ + Ra (\rho^{fd} C^{fd} q^{d}_{i} T^{fd})_{,i} + w^{rd} = 0 \qquad (2.87)$$

where Ra denotes the Rayleigh number, expressing the ratio of heat transported by free convection to that by conduction, here defined as

$$Ra = \frac{\rho^{o} C^{o} k^{o} H \beta \Delta T g}{\lambda^{o} \nu^{o}} \qquad (2.88)$$

For the equation of conservation of energy of the rock we apply the same reference values as for the conservation of energy of the fluid and obtain

$$((1-\phi) \rho^{rd} C^{rd} T^{rd})_{,t} d2 - (\lambda^{r*d} T^{rd}_{,i})_{,i} + w^{rd} = 0 \qquad (2.89)$$

Thus, there are different dimensionless time parameters in the equations for the conservation of mass and energy respectively. The time parameter in (2.83) is proportional to the permeability, fluid density and gravity respectively, and inversely proportional to the viscosity and the characteristic length. The time parameter in (2.86) is proportional to the thermal conductivity and inversely proportional to the volumetric heat capacity, the square of the characteristic length, the thermal volume expansion of the fluid and the characteristic temperature difference respectively.

The dimensionless form of the equations facilitates the qualitative evaluation of the significance of various parameters to the results. Therefore, a presentation of the results in dimensionless form gives a more general aspect to the study, in particular with regard to the uncertainties in some model data. Furthermore, it makes it possible to consider a wide range of parameter values.

2.5 Boundary and initial conditions

The governing equations must be supplemented by the boundary and initial conditions that are appropriate for the problem.

For the fluid flow equation these are of the following types

a) Prescribed pressure at a boundary

b) Prescribed normal flux through a boundary

The first type of boundary condition is relevant to the top boundary of the flow domain when the aquifer is to be considered unconfined. The top boundary may either be a fixed or a moving boundary. If it is a moving boundary then its position is usually unknown and therefore a part of the solution. If the top of the aquifer is confined by an impervious layer then the second type of boundary condition should be considered with zero normal flux prescribed at the boundary.

The lateral extent of the flow domain should in general be considered infinite. This is also true of the bottom of the flow domain. However, the calculations must be limited to a finite part of the flow domain. In certain cases a finite part may be localized using symmetry reasoning by considering an infinite series of identical repositories. In general, imaginary boundaries must be imposed upon the flow domain and they must be chosen in such a way that their effects on the solution values become negligible.

For the temperature equations the following types are of interest

c) Prescribed temperature at a boundary

d) Prescribed thermal flux through a boundary

The first type is considered for the top and the bottom boundaries of the flow domain. The prescribed temperature at the top boundary corresponds to the temperature at the ground surface or at the water table if this is below the ground surface. As for the fluid flow equation, a boundary condition corresponding to an imaginary bottom of the flow domain must be imposed. The temperature at the bottom boundary will, together with the prescribed temperature at the top boundary, specify the natural geothermal gradient. In a similar way as for the fluid flow equation the considered flow domain is confined laterally by the introduction of imaginary vertical boundaries.

3. NUMERICAL METHOD OF SOLUTION

The governing equations are transformed into a set of algebraic equations using Galerkin's method. The obtained matrix system is non-linear and is therefore solved in an iterative way.

3.1 Finite element formulation of the flow equations

To solve the governing equations of flow, using the Galerkin finite element method, we first introduce the following trial functions

$$p \cong \Psi_J p_J \tag{3.1}$$

$$T^f \cong \Psi_J T^f_J \tag{3.2}$$

$$T^r \cong \Psi_J T^r_J \tag{3.3}$$

where $\Psi_J = \Psi_J(x_i)$ represents the basis functions chosen to satisfy the essential boundary conditions. The same basis functions are also used to represent the variations in the material properties etc. over the elements, e.g.

$$\rho^f \cong \Psi_K \rho^f_K \tag{3.4}$$

which represents the variation in the fluid density over the elements.

Making use of the orthogonality conditions in Galerkin's method we obtain

(i) The fluid flow equation

$$< \phi\rho^f (c^f + c^r) p_{,t} , \Psi_I > - < \phi\rho^f \beta T^f_{,t} , \Psi_I > -$$

$$- <(\rho^f \frac{k}{\mu}_{ij} (p_{,j} - \rho^f g_j))_{,i} , \Psi_I > = 0 \qquad (3.5)$$

(ii) The fluid temperature equation

$$< \phi\rho^f C^f T^f_{,t} , \Psi_I > - < (\lambda^{f*} T^f_{,i})_{,i} , \Psi_I > + < \rho^f C^f q_i T^f_{,i} , \Psi_I > +$$

$$+ < w , \Psi_I > = 0 \qquad (3.6)$$

(iii) The rock temperature equation

$$< (1-\phi) \rho^r C^r T^r_{,t} , \Psi_I > - < \rho^r C^r T^r \phi c^r p_{,t} , \Psi_I > -$$

$$- < (\lambda^r T^r_{,i})_{,i} , \Psi_I > - < w , \Psi_I > = 0 \qquad (3.7)$$

Applying Green's theorem to all second order terms we obtain

(i) The fluid flow equation

$$< \phi\rho^f (c^f + c^r)\, p_{,t} \,,\, \Psi_I > - < \phi\rho^f \beta\, T^f_{,t} \,,\, \Psi_I > +$$

$$+ < \rho^f \frac{k}{\mu}_{ij} (p_{,j} - \rho^f g_j) \,,\, \Psi_{I,i} > -$$

$$- \int \rho^f \frac{k}{\mu}_{ij} (p_{,j} - \rho^f g_j)\, \Psi_I \, d\Gamma_i = 0 \qquad (3.8)$$

(ii) The fluid temperature equation

$$< \phi\rho^f C^f T^f_{,t} \,,\, \Psi_I > + < \lambda^{f*} T^f_{,i} \,,\, \Psi_{I,i} > +$$

$$+ < \rho^f C^f q_i T^f_{,i} \,,\, \Psi_I > + < w \,,\, \Psi_I > -$$

$$- \int_\Gamma \lambda^{f*} T^f_{,i}\, \Psi_I \, d\Gamma_i = 0 \qquad (3.9)$$

(iii) The rock temperature equation

$$< (1-\phi)\rho^r C^r T^r_{,t} \,,\, \Psi_I > - < \rho^r C^r T^r c^r p_{,t} \,,\, \Psi_I > +$$

$$+ < \lambda^{r*} T^r_{,i} \,,\, \Psi_I > - < w \,,\, \Psi_I > -$$

$$- \int_\Gamma \lambda^{r*} T^r_{,i}\, \Psi_I \, d\Gamma_i = 0 \qquad (3.10)$$

Substitution of (3.1-3.4) into (3.8-3.10) yields

(i) The fluid equation

$$\phi (c^f + c^r) \rho^f_K p_{J,t} \int_R \Psi_I \Psi_J \Psi_K \, dR - \phi\beta\rho^f_K T^f_{J,t} \int_R \Psi_I \Psi_J \Psi_K \, dR +$$

$$+ p_J \rho^f_K \left(\frac{k}{\mu}ij\right)_L \int_R \Psi_{I,i} \Psi_{J,j} \Psi_K \Psi_L \, dR -$$

$$- g_j \rho^f_K \left(\frac{k}{\mu}ij\right)_L \rho^f_M \int \Psi_{I,i} \Psi_K \Psi_L \Psi_M \, dR -$$

$$- \rho^f_K \int_\Gamma q^n \Psi_I \Psi_K \, d\Gamma = 0 \qquad (3.11)$$

(ii) The fluid temperature equation

$$\phi C^f T^f_{J,t} \rho^f_K \int_R \Psi_I \Psi_J \Psi_K \, dR + T^f_J \int_R \lambda^{f*} \Psi_{I,i} \Psi_{J,i} \, dR +$$

$$+ C^f T^f_J \rho^f_K \int_R \Psi_I q_i \Psi_{J,i} \Psi_K \, dR + w_K \int_R \Psi_I \Psi_K \, dR -$$

$$- \int_\Gamma e^n \Psi_I \, d\Gamma = 0 \qquad (3.12)$$

where

$$q_i \cong - \left(\frac{k}{\mu}ij\right)_L \Psi_L (p_M \Psi_{M,j} - \rho^f_G \Psi_G g_j) \qquad (3.13)$$

(iii) The rock temperature equation

$$(1-\phi)\,\rho^r C^r T^r_{J,t} \int_R \Psi_I\,\Psi_J\,dR - \rho^r C^r T^r_K \phi\; c^r p_{L,t} \int_R \Psi_I\,\Psi_K\,\Psi_L\,dR +$$

$$+ T^r_J \int_R \lambda^{r*}\,\Psi_{I,i}\,\Psi_{J,i}\,dR - w_K \int_R \Psi_I\,\Psi_K\,dR -$$

$$- \int_\Gamma e^n\,\Psi_I\,d\Gamma = 0 \qquad (3.14)$$

As can be seen the heat transfer function has been introduced explicitly into the two temperature equations (3.6) and (3.7), requiring that it be evaluated at the nodal points prior to the solution of these equations. This is inevitable when applying a non-linear heat transfer function. As a consequence, the two temperature equations must be decoupled and each of the equations must be solved separately in an iterative way. The previous system of equations may then be written in matrix form as

$$(a_{11})\,\{p_{,t}\} + (a_{12})\,\{T^f_{,t}\} + (a_{13})\,\{p\} + \{c_1\} = 0 \qquad (3.15)$$

$$(a_{21})\,\{T^f_{,t}\} + (a_{22})\,\{T^f\} + \{c_2\} = 0 \qquad (3.16)$$

$$(a_{31})\,\{T^r_{,t}\} + (a_{33})\,\{T^r\} + (a_{34})\,\{p_{,t}\} + \{c_3\} = 0 \qquad (3.17)$$

A quasi-steady state heat transfer function such as

$$w = h\ (T^f - T^r) \tag{3.18}$$

is linear and may be introduced implicitly into the two temperature equations reducing the number of iterations, since in this case these equations may be solved simultaneously. Applying Galerkin's method to this term we obtain

$$< h\ (T^f - T^r),\ \Psi_I > \tag{3.19}$$

or

$$h\ (T^f_J \int_R \Psi_I \Psi_J\ dR - T^r_J \int_R \Psi_I \Psi_J\ dR) \tag{3.20}$$

The matrix system may now instead be written as

$$(a_{11})\ \{p_{,t}\} + (a_{12})\ \{T^f_{,t}\} + (a_{13})\ \{\ p\ \} + \{c_1\} = 0 \tag{3.21}$$

$$(a_{21})\ \{T^f_{,t}\} + (a_{22})\ \{T^f\} + (a_{23})\ \{T^r\} + \{c_2\} = 0 \tag{3.22}$$

$$(a_{31})\ \{T^r_{,t}\} + (a_{32})\ \{T^f\} + (a_{33})\ \{T^r\} + (a_{34})\ \{p_{,t}\} + \{c_3\} = 0 \tag{3.23}$$

where the two temperature variables may be solved for implicitly.

Using the finite difference approach to approximate the time derivatives in equations (3.21), (3.22) and (3.23) we obtain

$$\frac{1}{\Delta t}(a_{11})\left(\{p\}^{n+1} - \{p\}^{n}\right) + \frac{1}{\Delta t}(a_{12})\left(\{T^f\}^{n+1} - \{T^f\}^{n}\right) + \\ + (a_{13})\{p\}^{n+1} + \{c_1\} = 0 \tag{3.24}$$

$$\frac{1}{\Delta t}(a_{21})\left(\{T^f\}^{n+1} - \{T^f\}^{n}\right) + (a_{22})\{T^f\}^{n+1} + (a_{23})\{T^r\}^{n+1} + \\ + \{c_2\} = 0 \tag{3.25}$$

$$\frac{1}{\Delta t}(a_{31})\left(\{T^r\}^{n+1} - \{T^r\}^{n}\right) + (a_{32})\{T^f\}^{n+1} + (a_{33})\{T^r\}^{n+1} + \\ + \frac{1}{\Delta t}(a_{34})\left(\{p\}^{n+1} - \{p\}^{n}\right) + \{c_3\} = 0 \tag{3.26}$$

where n denotes the time level. Rearranging we obtain

$$\left(\frac{1}{\Delta t}(a_{11}) + (a_{13})\right)\{p\}^{n+1} = \frac{1}{\Delta t}(a_{11})\{p\}^{n} - \\ - \frac{1}{\Delta t}(a_{12})\left(\{T^f\}^{n+1} - \{T^f\}^{n}\right) - \{c_1\} \tag{3.27}$$

$$\left(\frac{1}{\Delta t}(a_{21}) + (a_{22})\right)\{T^f\}^{n+1} + (a_{23})\{T^r\}^{n+1} = \\ = \frac{1}{\Delta t}(a_{21})\{T^f\}^{n} - \{c_2\} \tag{3.28}$$

$$\left(\frac{1}{\Delta t}\left(a_{31}\right) + \left(a_{32}\right)\right)\{T^f\}^{n+1} + \left(a_{33}\right)\{T^r\}^{n+1} =$$

$$= \frac{1}{\Delta t}\left(a_{31}\right)\{T^r\}^n - \frac{1}{\Delta t}\left(a_{34}\right)\left(\{p\}^{n+1} - \{p\}^n\right) - \{c_3\} \qquad (3.29)$$

or

$$\left(A_{11}\right)\{p\} = \{C_1\} \qquad (3.30)$$

$$\left(A_{22}\right)\{T^f\} + \left(B_{23}\right)\{T^r\} = \{C_2\} \qquad (3.31)$$

$$\left(A_{32}\right)\{T^f\} + \left(B_{33}\right)\{T^r\} = \{C_3\} \qquad (3.32)$$

3.2 Numerical procedure

In the numerical model the system of non-linear equations is solved using the frontal method. In this method the forward elimination according to Gauss' elimination method is performed during the element assembly. A significant advantage of this technique is that less incore storage is usually required, allowing larger problems to be solved in comparison with conventional band-matrix solution techniques.

The non-linearities in the system of equations are treated iteratively in a simple way. After each iteration the non-linear coefficients are updated as weighted averages of the most recent iterations. The procedure is repeated until the stipulated convergence criteria have been achieved.

A numerical model based on integration over finite element volumes may for practical reasons only be applied to a finite region. Thus, when dealing with an infinite region it becomes necessary to localize a finite region, where the imposed boundaries are located in such a way that the solution is not significantly affected in the region as well as within the period of interest.

4. REFERENCES

1 Bin Guine B. Huang and Dybbs, A., 1975, Mass and Energy Transport Phenomena in Porous Media, Dept. of Fluid, Thermal and Aerospace Sciences, Case Institute of Technology, June 1975, Cleveland, Ohio, USA.

2 Carlslaw, H.S., Jaeger, J.C., 1960, Conduction of Heat in Solids, Oxford at the Clarendon Press.

3 Combarnous, M.A., 1975, Hydrothermal Convection in Saturated Porous Media, Advances i Hydroscience, Volume 10-1975, p. 231-307, Academic Press.

4 KBS, 1978, Handling and Final Storage of Unreprocessed Spent Nulear Fuel, Volume II.

5 Gray, W.G., O'Neill, K., 1976, On the General Equations of Flow in Porous Media and Their Reduction to Darcy's Law, Water Resources Research, Vol. 12, No 2, p. 148-154.

6 De Groot, S.R., Mazur, P., 1962, Non-Equilibrium Thermodynamic, North Holland Publishing Company-Amsterdam.

7 Kuo, M.C.T., Kruger, P., Brigham, W.E., 1976, Shape Factor Correlations for Transient Heat Conduction from Irregular-Shaped Rock Fragments to Surrounding Fluid, Stanford Geothermal Program, SGP-TR-16, Stanford University, California.

8 Stokes, J., Thunvik, R., 1978, Investigations of Groundwater Flow in Rock around Repositories for Nuclear Waste, KBS-TR-47.

9 Stokes, J., 1980, On the Description of the Properties of Fractured Rock using the Concept of a Porous Medium, SKBF-KBS-TR-80-05.

Appendix 1 Space averaging definitions and theorems

In the derivation of the macroscopic equations the following definitions and averaging theorems are used:

(i) The phase average of a parameter P^i of the phase i over the volume V of the composite element is defined as

$$\langle P^i \rangle = \frac{1}{V} \int_{V^i} P^i dV \tag{A1.1}$$

(ii) The phase average of a parameter P^i of the phase i over the phase volume V^i within the volume V (also the intrinsic phase average) is defined as

$$\langle P^i \rangle_{V^i} = \frac{1}{V^i} \int_{V^i} P^i dV \tag{A1.2}$$

(iii) The average of the average equals the average

$$\langle\langle P^i \rangle\rangle = \langle P^i \rangle \tag{A1.3}$$

(iv) The fractional volume of the phase i within the volume of the element is defined as

$$\phi^i = \frac{V^i}{V} = \frac{1}{V} \int_{V^i} dV \tag{A1.4}$$

(v) The average and the phase average are related to the frac-

tional volume as follows

$$\langle P^i \rangle = \frac{1}{V} \int_{V^i} P^i dV = \frac{1}{V} \langle P^i \rangle_{V^i} V\phi^i = \phi^i \langle P^i \rangle \tag{A1.5}$$

(vi) A parameter value may be represented as the sum of the average and its deviation from the average as

$$P = \langle P \rangle + \tilde{P} \tag{A1.6}$$

Then with the previous definitions, the average of a product is given by

$$\langle P^1 P^2 \rangle = \langle P^1 \rangle \langle P^2 \rangle + \langle \tilde{P}^1 \tilde{P}^2 \rangle \tag{A1.7}$$

(vii) The average of the time derivative of a parameter P^i (also the transport theorem, Whitaker, 1973)

$$\langle P^i_{,t} \rangle = \langle P^i \rangle_{,t} - \frac{1}{V} \int_S P^i v_j n^i_j \, dS \tag{A1.8}$$

where v is the velocity at the boundary of phase i and n the outer unit normal vector.

(viii) Averaging theorem (Whitaker, 1967)

$$\langle P^i_{,j} \rangle = \langle P^i \rangle_{,j} + \frac{1}{V} \int_S P^i n^i_j \, dS \tag{A1.9}$$

References

1 Whitaker, S., 1973, The transport equations for multi-phase systems, Chemical Engineering Science, 1973, Vol. 28, pp. 139-147, Pergamon Press.

2 Whitaker, S., 1967, Diffusion and Dispersion in Porous Media, AIChE Journal, 1967, Vol. 13, No 3, pp. 420-427.

Appendix 2 Model validation

A fully satisfactory validation of the numerical realization of the mathematical model is very difficult to achieve. This is mainly due to the non-linearities in the system of partial differential equations. The non-linearities in the flow problem makes it impossible to obtain analytical solutions compatible with the numerical solutions. In order to enable a comparison with analytical solutions simplified assumptions have to be made regarding the flow conditions. Partial verifications of the computer code may only be performed by making the necessary assumptions to decouple the governing equations.

The fluid flow equation was checked against two dimensional analytical solutions to an isothermal groundwater flow equation with the appropriate boundary and initial conditions. This was done by assuming the fluid density and viscosity to be independent of pressure and temperature. Thereby, the fluid flow equation is decoupled from the heat flow equations for the fluid and rock media.

The heat flow equations were checked against solutions to the one dimensional convective heat flow equation. First, the two heat flow equations must be decoupled from the fluid flow equation. This is be done by assuming steady state fluid flow conditions. Second, analytical solutions to the heat flow equations cannot be obtained, if they are coupled to each other. Assuming instantaneous thermal equilibrium between the rock and the fluid, the two energy equations may be replaced by a single heat flow equation, representing both the fluid and rock media. In one dimension this

equation may be written as

$$(\rho C)^* \frac{\partial T}{\partial t} - \lambda^* \frac{\partial^2 T}{\partial x^2} + \rho^f C^f q \frac{\partial T}{\partial x} = 0 \qquad \text{(A2.1)}$$

where

$$(\rho C)^* = \phi \rho^f C^f + (1-\phi)\, \rho^r C^r \qquad \text{(A2.2)}$$

and

$$\lambda^* = \phi \lambda^f + (1-\phi)\, \lambda^r \qquad \text{(A2.3)}$$

A solution to equation (A2.1) is 1)

$$\frac{T - T_i}{T_o - T_i} = \frac{1}{2} \left\{ \operatorname{erfc}\left(\frac{x}{2\sqrt{at}} - \sigma \sqrt{at}\right) + e^{2x\sigma} \operatorname{erfc}\left(\frac{x}{2\sqrt{at}} - \sigma \sqrt{at}\right) \right\} \qquad \text{(A2.4)}$$

where

$$a = \frac{\lambda^*}{(\rho C)^*} \qquad \text{(A2.5)}$$

and

$$\sigma = \frac{\rho^f C^f q}{2\lambda^*} \qquad \text{(A2.6)}$$

In figure 1, two examples are presented to allow a simple comparison between numerical solutions from the model and analytical solutions to the one dimensional convective heat flow equation using (A2.4). In these examples the fluid and rock media are treated as a single equivalent medium with properties such as

fluid density and viscosity independent of pressure and temperature. In figure 2, three examples are presented treating the fluid and rock media as two separate media, which are coupled to each other by a quasi-steady state heat transfer function. In figure 3, two examples are presented with fluid and rock treated as separate media, as for the previous set of examples, but fluid density and viscosity are functions of pressure and temperature.

The following material properties are assumed in the examples:

Thermal conductivity of the rock	3.5	W/(mK)
Specific heat capacity of the rock	800	J/(kgK)
Rock density	2700	kg/m^3
Thermal conductivity of the fluid	0.6	W/(mK)
Specific heat capacity of the fluid	4180	J/(kgK)
Porosity	0.003	-
Fluid density	998	kg/m^3
Dynamic viscosity	0.0018	Pas

A mesh of 20 elements is used in the examples. A pressure gradient equivalent to a slope of 1 in 1000 is applied. The initial time step is 5 years. In the first five time steps, the time step is increased by a factor of 1.2 and thereafter by 1.5.

The presented examples show good agreement between the numerical and the analytical solutions. However, they provide only a limited verification of the presented flow model owing to the oversimplified assumptions made for the solutions. A significant difficulty in applying the presented flow model to more complicated problems is that solutions from the model are in general higly

sensitive to the discretization of the considered flow domain as well as the time step procedure. To provide an inherent check upon the calculations the computer model performs mass and energy balances at each time step.

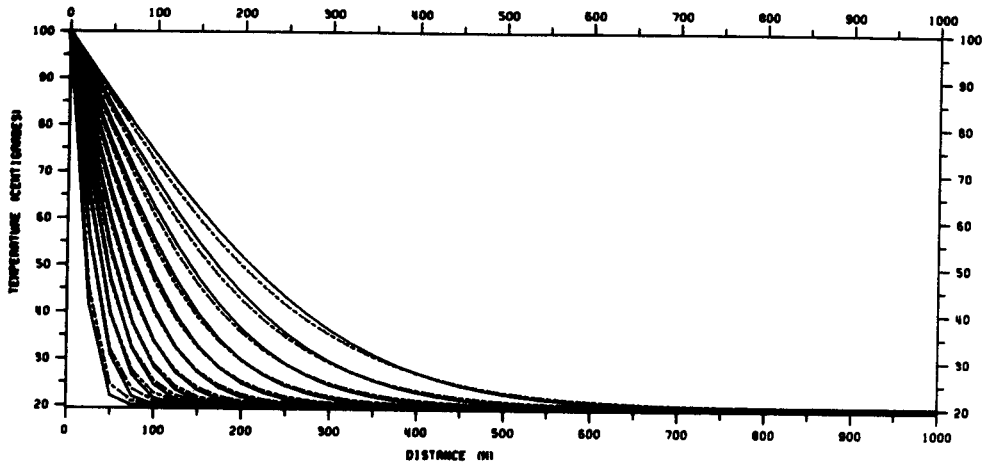

(a)

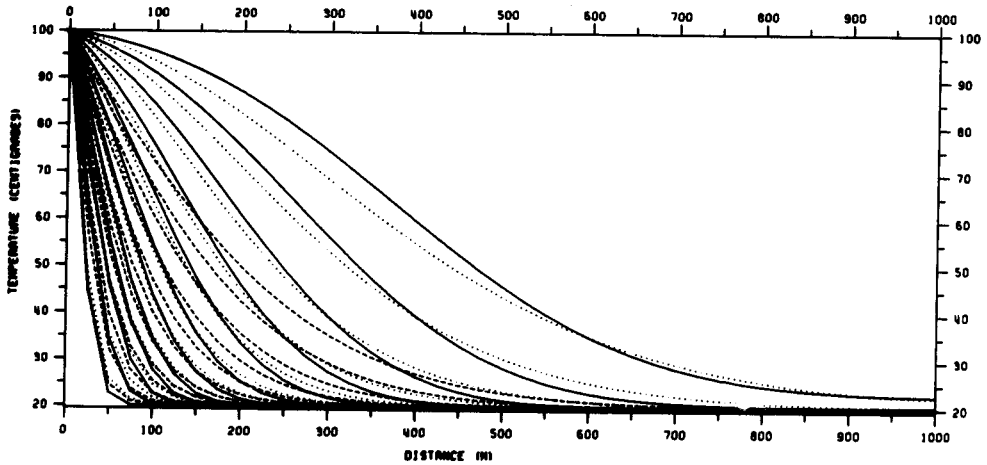

(b)

Figure 1. Numerical (dotted line) and analytical (solid line) solutions to the one dimensional convective heat flow equation representing both the fluid and rock media, Solutions to the conductive heat flow equation for the rock are also presented (dashed line). (a) Permeability is 10^{-14}, (b) Permeability is 10^{-12}.

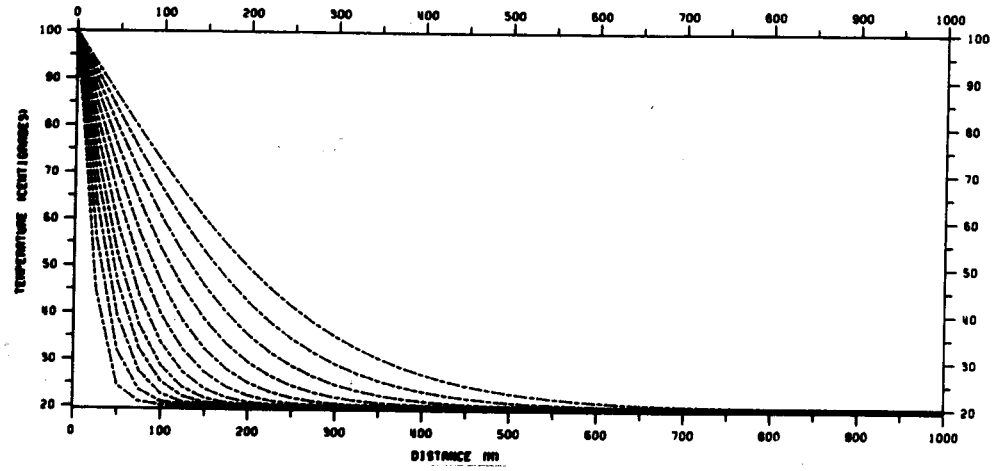

(a)

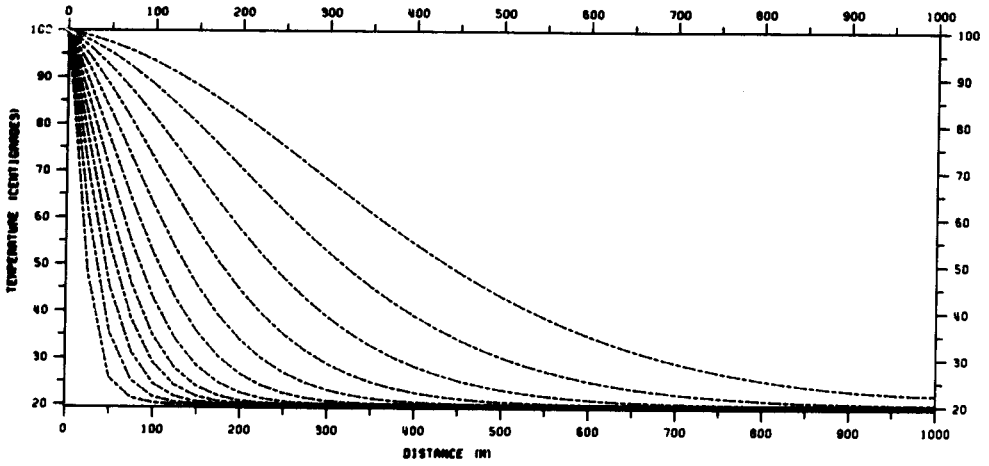

(b)

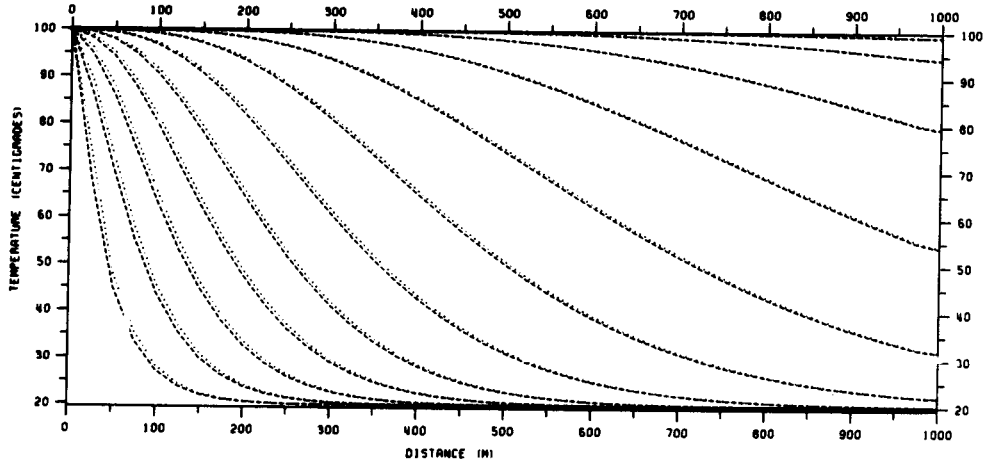

(c)

Figure 2. Numerical solutions to the one dimensional convective heat flow equation for the fluid (dotted line) and the conductive heat flow equation for the rock (dashed line). The two equations are coupled to each other by a quasi-steady heat transfer function, (a) Permeability is 10^{-14}, (b) Permeability is 10^{-12}, (c) Permeability is 10^{-11}.

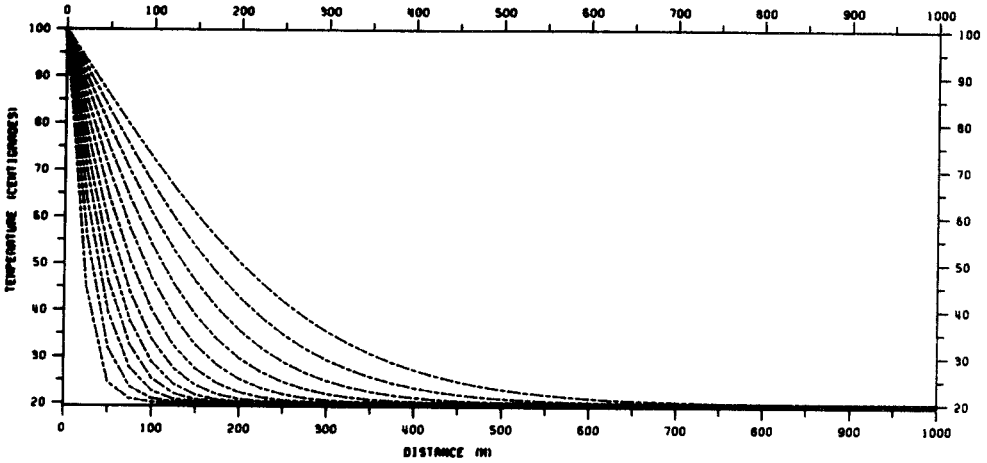

(a)

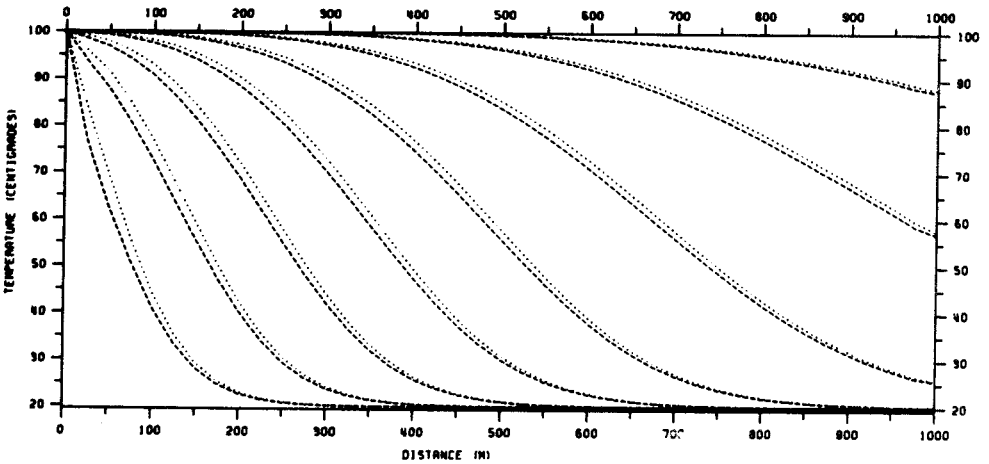

(b)

Figure 3. Numerical solutions to the one dimensional convective heat flow equation for the fluid (dotted line) and the conductive heat flow equation for the rock (dashed line). The two equations are coupled to each other by a quasi-steady heat transfer function. Fluid density and viscosity are functions of pressure and temperature. (a) Permeability is 10^{-14}, (b) Permeability is 10^{-11}.

References

1 Lagarde, A., 1965, Considerations sur le Transfert de Chaleur en Milieu Poreux, Revue de l'Institute Francais de Petrole, Fevrier 1965, p.396.

HYDROTHERMAL CONDITIONS AROUND A RADIOACTIVE WASTE REPOSITORY

Part 2 - Numerical Solutions

Roger Thunvik
Royal Institute of Technology
Stockholm, Sweden

Carol Braester
Israel Institute of Technology
Haifa, Israel

ABSTRACT

Numerical solutions for the hydrothermal conditions around a hard rock repository for nuclear fuel waste are presented. The presented solutions illustrate the effect of heat released from a hypothetical radioactive waste repository under various conditions with regard to topography, the location of the repository, permeability, porosity and adjacent fracture zones. Major interest in the analysis is directed towards flow patterns and travel times for water particles from the repository to the ground surface or alternatively to a major fracture zone in the vicinity of the repository. The solutions were obtained using a mathematical model for the flow of groundwater and heat through a fractured rock mass. The model consists of a set of coupled non-linear partial differential equations for heat and groundwater flow. The set of equations is solved numerically using the finite element method in two or three dimensions. The presented results show that the heat emitted by the decaying radioactive waste may have a significant influence on the initial flow patterns and subsequently also on the travel times from the repository under certain conditions.

CONTENTS

NOMENCLATURE

Symbol	Description	Dimension	SI unit
a	equivalent block radius	L	m
b	fracture width	L	m
c	compressibility	$M^{-1}LT^2$	1/Pa
C	specific heat capacity	$L^2T^{-2}K^{-1}$	J/(kgK)
D	thermal diffusivity	L^2T^{-1}	m^2/s
g	acceleration of gravity	LT^{-2}	m/s^2
h	heat transfer coefficient	$ML^{-1}T^{-3}K^{-1}$	$W/(m^3K)$
H	charateristic length of flow domain	L	m
k	permeability	L^2	m^2
K	hydraulic conductivity	LT^{-1}	m/s
L	characteristic block size	L	m
p	pressure	$ML^{-1}T^{-2}$	Pa
q	specific discharge	LT^{-1}	m/s
Q	heat flow rate	ML^2T^{-3}	W
Ra	Rayleigh number	-	-
t	time	T	s
T	temperature	K	K
x_i	Cartesian coordinate	L	m
v	fluid velocity	LT^{-1}	m/s
w	heat transfer function	$ML^{-1}T^{-3}$	W/m^3
β	coefficient of thermal volume expansion of the fluid	K^{-1}	1/K
ΔT	characteristic temperature difference	K	K
λ	thermal conductivity	$MLT^{-3}K^{-1}$	W/(mK)
μ	dynamic viscosity	$ML^{-1}T^{-1}$	Pas

ν	kinematic viscosity	L^2T^{-1}	m^2/s
ρ	density	ML^{-3}	kg/m^3
ϕ	porosity	-	-

superscripts

f	fluid
r	rock
d	dimensionless parameter
o	reference value
*	equivalent medium

subscripts

i,j	indices used for Cartesian tensor notation, repeated indices indicate summation over these indices (i,j = 1,2,3)
	$p_{,t}$ partial time derivative of p
	$p_{,j}$ gradient of p

SUMMARY

This report presents a number of numerical solutions for the flow of groundwater and heat around a radioactive waste repository. The solutions were obtained using a mathematical model for the flow of groundwater and heat through fractured rock.

The objective of the present investigation is to study the effect of heat released from a radioactive waste repository on the initial groundwater flow pattern. In order to facilitate the interpretation of the results of the calculations simplified assumptions are made regarding the properties of the flow domain as well as the repository. Thus, topography is assumed horizontal or linearly sloping. The flow domain is bounded downwards by an impervious bottom, laterally by noflow boundaries and upwards by the water table. The water table is assumed to coincide with the topography. Permeability is assumed constant or exponentially decreasing with depth over the flow domain. The effect of major vertical fracture zones located close to a repository is also studied.

The initial flow pattern is assumed to be governed by the topography. and in the event of adjacent fracture zones of high permeability, the flow conditions in these fracture zones. The initial distribution of the fluid and rock temperatures is assumed to follow the natural geothermal gradient. The effect of the heat emitted by the decaying radionuclides is investigated for four idealized cases with regard to the boundary and initial conditions as well as the properties of the flow domain.

The presented cases illustrate the hydrothermal conditions around a radioactive waste repository situated below a horizontal ground surface, the crest of a hill, and a hillside. As a special case, the effect of two major vertical fracture zones situated on either side of the repository is investigated. In each of the cases the effect of decreasing versus constant permeability and porosity with depth is analyzed.

The results are presented in the form of tables of flow times for water particles to travel from the repository to the ground surface, or alternatively to the major fracture zones, and in the form of pathlines. The hydrothermal flow conditions are illustrade by vector plots showing the direction and magnitude of the groundwater fluxes, and isotherms showing the temperature distribution at different moments.

A single level repository is considered and it is assumed to be located at a depth of about 500 metres below the ground surface. It consists of a system of parallel tunnels, spaced 25 metres apart. The radioactive waste is stored in canisters in drillholes along the bottoms of the tunnels. The lateral extent of the repository is about 1 km. For simplicity in the calculations the waste is assumed to be instantaneously emplaced. Flow patterns are studied for a repository situated below a horizontal ground surface, the crest of a hill, or a hillside.

1. INTRODUCTION

The objective of the present investigation is to exemplify in principle the effect of heat released from a radioactive waste repository on the initial groundwater flow pattern under various conditions. This report contains a number of preliminary examples worked out in order to illustrate the influence of a hypothetical radioactive waste repository on the groundwater flow around the repository. Thus, no specific site is referred to in the analysis and the assumptions regarding the characteristics of the flow domain as well as the repository are made simple to facilitate the interpretation of the results.

Heat released from the radioactive waste will increase the temperature of the rock, changing the groundwater density gradients and creating convective currents. This means that the initial groundwater flow pattern is changed and subsequently also the flow times for contaminated groundwater from the repository to the biosphere, should any of the canisters be breached.

The solutions presented herein were obtained using a mathematical model developed for studying the flow of groundwater and heat through fractured rock. The model is thoroughly described in a previous report entitled "HYDROTHERMAL CONDITIONS AROUND A RADIOACTIVE WASTE REPOSITORY, Part 1 - A Mathematical Model for the Flow of Groundwater and Heat in Fractured Rock". The used flow model is therefore only briefly described in the present report.

The model is based on the continuum approach, implying that vari-

ous properties such as permeability, pressure, fluid and rock temperature are defined as averages over some volume elements. These elements must be large in comparison with individual fractures, but small with regard to the dimensions of the exterior boundaries of the rock formation under consideration. The model is represented by a set of partial differential equations, which is solved numerically using the finite element method.

2. THE FLOW MODEL

The mathematical flow model used herein consists of a set of partial differential equations describing the flow of mass and heat through a fractured rock. The model treats the fractured rock either as a single equivalent continumm representing both fluid and rock, or as two overlapping continua, where one represents the fluid in the fractures and the other the solid rock. The first approach assumes that local thermal equilibrium between the fluid and the rock is reached instantaneously. The second approach assumes that quasi-steady state exchange of heat between the fluid and the rock media is reached instantaneously.

2.1 Governing equations of the flow model

The model consists of the following set of partial differential equations

$$\phi\rho^f(c^f+c^r)\,p_{,t} - \phi\rho^f\beta\,T^f_{,t} - \left(\rho^f \frac{k}{\mu}_{ij}(p_{,j} - \rho^f g_j)\right)_{,i} = 0 \qquad (2.1)$$

$$\phi\rho^f C^f\,T^f_{,t} - (\lambda^{f*}\,T^f_{,i})_{,i} + \rho^f C^f\,q_i T^f_{,i} + w = 0 \qquad (2.2)$$

$$(1-\phi)\rho^r C^r\,T^r_{,t} - \rho^r C^r T^r\,\phi\,c^r p_{,t} - (\lambda^{r*} T^r_{,i})_{,i} - w = 0 \qquad (2.3)$$

When instantaneous thermal equilibrium between the fluid and the rock is assumed, the last two equations of the previous set of

equations reduces to

$$(\rho C)^* T_{,t} - (\lambda^* T_{,i})_{,i} + \rho^f C^f q_i T_{,i} = 0 \qquad (2.4)$$

where λ^* denotes the thermal conductivity and $(\rho C)^*$ the volumetric heat capacity of the single equivalent medium representing both the fluid and rock media.

In addition to the previous equations, there are two equations of state relating the density and viscosity of the fluid to pressure and temperature

$$-- \quad \rho^f = \rho^f(p, T^f) \qquad (2.5)$$

$$\mu^f = \mu(T^f) \qquad (2.6)$$

In brief, the model is represented by a system of non-linear partial differential equations. One of the equations governs the fluid flow, one the flow of heat by the fluid in the fractures, and one the flow of heat through the rock matrix. The fluid flow equation is coupled with the thermal energy balance equations by the convective term in the fluid energy equation and by the fluid density and viscosity. There is another coupling between the fluid flow equation and the fluid energy equation by the term with the time derivative of the fluid temperature, due to the thermal volume expansion of the fluid. Since one of the terms in the thermal energy equation of the rock contains a time derivative of pressure, there is also a coupling between this equation and the fluid flow equation. The two energy balance equations are strongly coupled through the heat transfer function, governing the

exchange of heat between the fluid in the fractures and the rock matrix.

The heat transport will be conductive or convective dominant depending on the relative significance of the conduction and convection terms in the equation for the thermal energy of the fluid. One can see from this equation that the heat flow is dominated by conduction for low fluid velocities and low temperature gradients, while it is dominated by convection for high fluid velocities and high temperature gradients. The heat transport in the present problem was concluded to be dominated by conduction. As a consequence, equation (2.4) may be employed in the calculations, reducing the computational effort.

2.2 Dimensionless parameters

The following dimensionless parameters are defined (see section 2.4 in part 1)

$$k_{ij}^d = \frac{k_{ij}}{k^o}\,,\quad \mu^d = \frac{\mu}{\mu^o}\,,\quad \rho^d = \frac{\rho}{\rho^o \beta \Delta T}\,,\quad p^d = \frac{p - p^o}{\rho^o g H}\,,\quad x_i^d = \frac{x_i}{H}$$

$$\lambda^d = \frac{\lambda}{\lambda^o}\,,\quad C^d = \frac{C}{C^o}\,,\quad T^d = \frac{T}{\Delta T}\,,\quad w^d = \frac{H^2}{\lambda^o \Delta T}\, w \tag{2.7}$$

$$Ra = \frac{\rho^o C^o k^o H \beta \Delta T g}{\lambda^o \nu^o}$$

Major interest in the present investigation is directed towards the travel times of water particles from the repository to the ground surface. The influence of various physical properties of the fractured rock mass is analyzed using the following transformation into dimensionless time for the fluid flow equation

$$t^{d1} = \frac{k^o \rho^o g}{\mu^o H}\, t \equiv \frac{K^o}{H}\, t \tag{2.8}$$

and

$$t^{d2} = \frac{\lambda^o}{\rho^o C^o H^2 \beta \Delta T}\, t \equiv \frac{D^o}{H^2 \beta \Delta T}\, t \tag{2.9}$$

for the heat flow equation.

With the exception of permeability and porosity, the parameters in equations (2.8) and (2.9) are not expected to vary significantly from place to place. As follows from equation (2.8), the travel time is directly proportional to the hydraulic conductivity K and inversely proportional to the characteristic length H of the flow domain.

The dimensionless time t^{d1} should be used for problems dominated by the fluid flow, while t^{d2} should be used for problems dominated by the heat flow. In certain problems both t^{d1} and t^{d2} must be used. It is then possible to relate t^{d1} and t^{d2} to each other, for example by the following relationship

$$t^{d2} = \frac{D^o}{K^o H\beta\Delta T} t^{d1} \equiv \frac{1}{Ra} t^{d1} \qquad (2.10)$$

where Ra is the Rayleigh number. Thus, a change in the hydraulic conductivity will change the value of t^{d1} according to (2.8) and change the value of t^{d2} according to (2.10). Porosity, however, does not appear in (2.10) and a change in porosity will have the same effect on both t^{d1} and t^{d2}.

2.3 Boundary and initial conditions

Most of the previous work on the flow of mass and heat through aquifers has been devoted to problems of hydrothermal convection in confined aquifers. In the present problem the aquifer should be considered unconfined, implying that the flow domain is bounded upwards by a water table. This complicates the problem since the position of the groundwater table is usually unknown and therefore a part of the solution. In the present numerical solutions the upper boundary is assumed to coincide with the ground surface, simplifying the mathematical treatment of this boundary. The downward as well as the lateral extent of the flow domain should in principle be considered infinite, unless there should exist some predominant geological features bounding the flow domain under consideration. The present analysis is carried out in two dimensions for a vertical cross-section through the repository and the following boundary conditions are considered:

2.3.1 A horizontal bottom which is impervious to fluid flow and at constant temperature.

In general, below a certain depth the location of an impervious bottom has little influence on the groundwater flow around and above the location depth of a radioactive waste repository. This is particularly true if the permeability decreases with depth. The temperature at this boundary is set in accordance with the geothermal gradient.

2.3.2 Vertical sides which are impervious to fluid flow and adiabatic to heat.

This boundary condition is either due to a physical barrier that

prevents exchange of water as well as heat with the surrounding region or due to symmetry by considering a series of symmetric flow domains.

2.3.3 A top boundary at constant pressure and temperature.

An implication of dealing mathematically with an unconfined aquifer is that the position of the top boundary, the water table, in general is unknown and therefore a part of the solution. Furthermore, the position of the water table depends on the net accretion to the water table as well as the flow conditions in the fractured rock mass under consideration. This means that the the position of the water table is time dependent. As a consequence, a transient non-linear boundary conditions applies for the upper boundary of the flow domain, making the flow problem difficult to solve.

As already mentioned above the water table and the ground surface are assumed to coincide. This is considered a relatively good approximation to the groundwater conditions in Sweden, where the water table generally is accompanying the ground surface because of the abundant precipitation. The assumption also means, that the water in the outflow areas runs off or evaporates instantaneously and that there is a continuous supply of water in the inflow areas. Thus, the present assumption, that the water table coincides with the topography, may usually be considered to be a conservative one. However, the assumption might lead to exaggerated piezometric gradients when dealing with hilly areas, where the water table is likely to be situated below the ground surface at the crests of the hills and above the ground surface at the bot-

toms of the valleys. Under such circumstances a phreatic boundary condition should be applied.

The assumption of constant temperature at this boundary means that seasonal variations in temperature are being neglected. This condition gives, together with the prescribed temperature at the bottom of the flow domain, the natural geothermal gradient, which herein is assumed to be 30°C/km.

2.3.4 Vertical fracture zones

A number of examples were carried out assuming that the repository is located between two major vertical fracture zones. It is assumed that the hydraulic gradient in the lateral fracture planes is low enough to allow Dupuit's assumption to be made. Furthermore, the flow through the fractures is asssumed at steady state. Thus, the fractures may be treated as hydrostatic boundaries. Since the velocity of the water in the fractures is significantly higher than the velocity of the water in the rock, it is assumed that the heat transferred from the rock to the fractures is instantaneously transported by the water in the fracture planes. Therefore, the temperature distribution in the fractures is assumed to follow the geothermal gradient.

3. INPUT DATA

This chapter deals with the parameters used in the flow model. The relative significance of the various parameters to the present flow problem is discussed. Furthermore, the characteristics of the radioactive waste repository and the considered flow domain are described.

The flow model includes the following parameters:

(i) Fluid flow equation

porosity
fluid density
fluid viscosity
permeability
fluid compressibility
rock compressibility
thermal volume expansion of the fluid
gravity

(ii) Heat flow equations

porosity
fluid density
specific heat capacity of the fluid
thermal conductivity of the fluid
rock compressibility
rock density
specific heat capacity of the rock
thermal conductivity of the rock
equivalent block radius
heat transfer coefficient

Some of the model parameters such as the thermal volume expansion of the fluid, the density and viscosity of the fluid, may be determined in the laboratory and they are not expected to significantly vary from place to place. Other model parameters, such as porosity and permeability may, however, only be determined by field experiments. Data obtained from field measurements are often related to large uncertainties because of shortcomings in

the measuring techniques as well as difficulties in the interpretation of the data, expecially when using them for mathematical flow models, which in general are based on the continuum approach.

3.1 Hydraulic properties

3.1.1 Permeability and hydraulic conductivity

Hydraulic conductivity is defined as

$$K = \frac{k\rho g}{\mu} \tag{3.1}$$

where k is the intrinsic permeability, μ is the dynamic viscosity, ρ is the fluid density and g is the acceleration of gravity. Fluid density and viscosity are functions of pressure and temperature. Permeability is an intrinsic property of the rock medium.

The permeability of an individual fracture may be estimated using the solution for viscous creeping flow between parallel plates. Then the resulting equivalent permeability becomes

$$k = \frac{b^2}{12} \tag{3.2}$$

where b is the fracture width. To envision how permeability is related to the fracture spacing and fracture width, one may consider a simple conceptual model consisting of three sets of parallel fracture planes intersecting at right angles. Using this approach the average permeability of the bulk volume is approximately

$$k = \frac{b^3}{6L} \tag{3.3}$$

where L represents the characteristic block size and b is the mean fracture width.

Hydraulic conductivity has been determined by field tests in boreholes at Finnsjön, Kråkemåla and Stjärnö. In most cases double packer tests were performed with a spacing of 2 metres between the packers. The results of the tests were interpreted using solutions for the flow through isotropic porous media. The measured values of the hydraulic conductivity vary several orders of magnitude, in the range between 10^{-10} and 10^{-5} , from borehole to borehole, but also within the boreholes themselves. The test intervals fall in quasi-impervious blocks, which sometimes comprise one or several dominating fractures and sometimes not. This makes it difficult to determine the hydraulic conductivity as a space average using the discrete measuring points at the boreholes.

In several boreholes there seems to be a trend of decreasing permeability with depth. It was therefore considered to be of significant interest to examine the effect of decreasing permeability with depth in comparison with constant permeability over the flow domain. In the calculations with decreasing permeability an exponential decrease is assumed and the following relationship is used between permeability and depth

$$k = k^o \, e^{\gamma z} \tag{3.4}$$

where k^o is the permeability at a given reference level (in the present calculations the ground surface is used as reference level), γ is a coefficient that determines how rapid the permeability decreases with depth and z is the elevation.

3.1.2 Porosity

Porosity is of great significance for the determination of travel times for water particles from the repository to the ground surface or to major fracture zones. In the calculation of flow times the fluid velocity is computed according to

$$v_i = \frac{k_{ij}}{\phi\mu} (p_{,j} - \rho^f g_j) \qquad (3.5)$$

where v is the fluid velocity, ϕ is porosity, k is the permeability, p is pressure, ρ^f is the fluid density and g is the acceleration of gravity.

Generally, rock porosity varies with pressure changes and the thermal volume expansion of the rock. In the used model the latter dependence is neglected and porosity is only related to pressure by the rock compressibility. In the calculations, porosity is assumed either constant or exponentially decreasing with depth analogous to the permeability.

The determination of porosity, using tracer injection between two boreholes, drill core samples and electrical resistivity measurements, indicates that the value of porosity is between 0.001 and 0.005. In the calculations with constant permeability a value of 0.003 is used for porosity. The same value is also used as a reference value at the ground surface when porosity is assumed to decrease exponentially with depth.

To envision how porosity is related to the fracture spacing and fracture width, the same concept as for permeability may be used.

Then porosity may be approximated by

$$\phi = \frac{3b}{L} \tag{3.6}$$

where b is the mean fracture width and L is the mean spacing between the fracture planes.

The previous concept used to relate permeability and porosity to fracture width and spacing may also be used to study the relationship between porosity and permeability. Using (3.6) and (3.3) to form the ratio of porosity and permeability, we obtain

$$\phi = \frac{18k}{b^2} \tag{3.7}$$

Rearranging and substituting (3.3) into (3.7), we obtain

$$\phi = 3 \left(\frac{6k}{L^2}\right)^{\frac{1}{3}} \tag{3.8}$$

This means that the assumption of a linear relationship between porosity and permeability may be considered to be conservative, resulting in too short travel times in the calculations, if the decrease in permeability with depth is due to a decrease in fracture width rather than fracture spacing.

3.1.3 Fluid and rock compressibilities

Compressibility was previously defined as the sum of the fluid and rock matrix compressibilities. The fluid compressiblility is considered a known parameter that may be determined in the laboratory. The rock compressibility, on the other hand, must be determined by in situ measurements and there are rather few such measurements reported for hard rocks. However, if the compressiblity of the rock is not significantly higher than that of the fluid, then the effect of compressibility becomes practically negligible in the present problem, implying that pressure transients decay much faster than temperature transients.

3.1.4 Fluid density

Fluid density is a function of pressure and temperature and the function is illustrated in figure 3.1

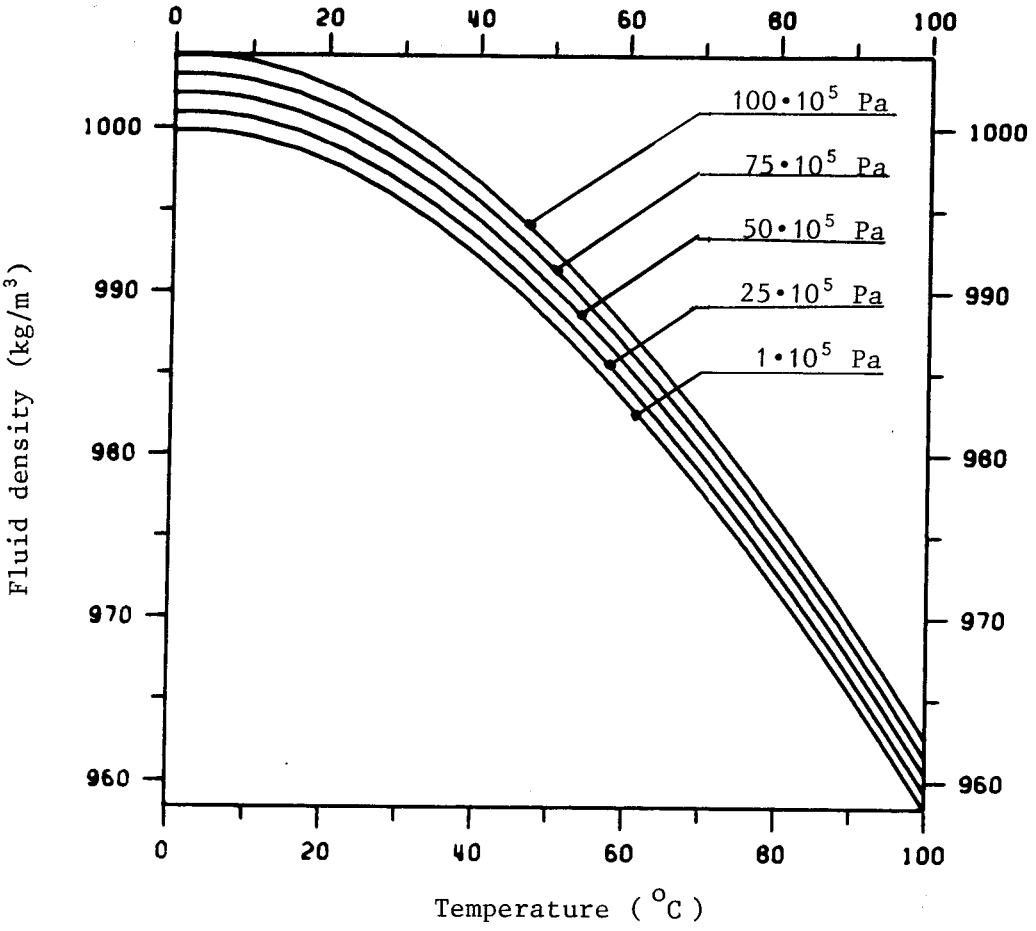

Figure 3.1 Fluid density as a function of pressure and temperature

3.1.5 Dynamic viscosity of the fluid

Dynamic viscosity of the fluid is considered a function of temperature as illustrated in figure 3.2

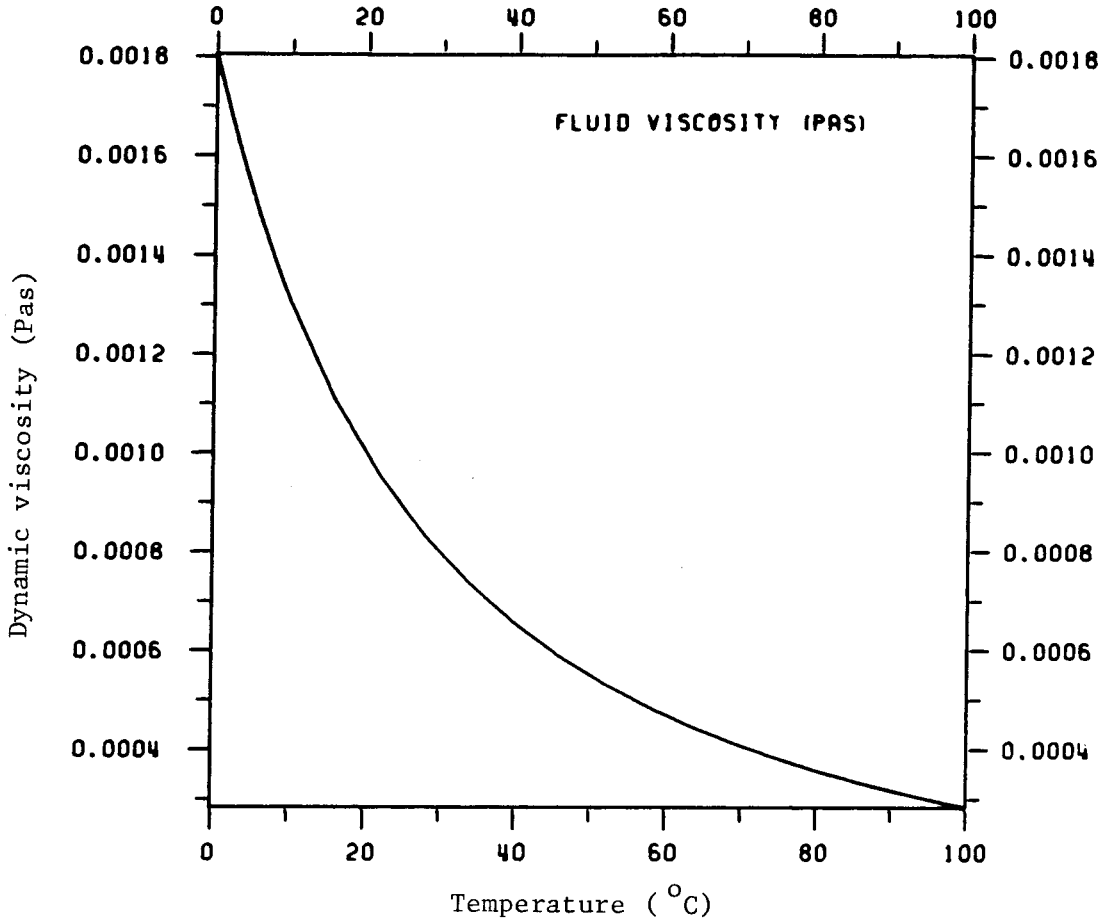

Figure 3.2 Dynamic viscosity of the fluid as a function of temperature

3.2 Thermal properties

Generally, the thermal properties of rock are temperature dependent. The thermal properties of the rock at the Stripa mine have been determined by laboratory and in situ experiments. In the heater experiments at Stripa the following relationship between thermal conductivity and temperature was obtained

$$\lambda = 3.60 - 0.003745\ T \tag{3.9}$$

where λ is the thermal conductivity of the rock and T is the temperature in centigrades. In the present study thermal conductivity as well as the other thermal properties are assumed constant. The following thermal properties are used in the calculations:

Thermal conductivity of the rock	3.5	W/(mK)
Rock density	2700	kg/m^3
Specific heat capacity of the rock	800	J/(kgK)
Thermal conductivity of the fluid	0.6	W/(mK)
Specific heat capacity of the fluid	4180	J/(kgK)
Thermal volume expansion of the fluid	0.0018	1/K

The equivalent thermal conductivity representing both fluid and rock is computed as

$$\lambda^* = \phi\lambda^f + (1-\phi)\lambda^r \tag{3.10}$$

and the equivalent volumetric heat capacity is calculated as

$$(\rho C)^* = \phi\rho^f C^f + (1-\phi)\rho^r C^r \tag{3.11}$$

where the asterisks are used to denote equivalent medium properties, ϕ porosity, λ^f the thermal conductivity of the fluid, λ^r the thermal conductivity of the rock, ρ^f the fluid density being a function of pressure and temperature, C^f is the specific heat capacity of the fluid, ρ^r the rock density, and C^r is the specific heat capacity of the rock. The heat transfer coefficient and the equivalent block radius need only be considered when treating the fluid and rock as separate media.

3.1 The repository

The repository is assumed to be located at a depth of 500 metres. The lateral extent of the repository is assumed to be about 1 km. The repository consists of a single level system of parallel tunnels, with a spacing of 25 metres between the centres of the tunnels. The study area is a cross-section perpendicular to the longitudinal tunnel axes. Thus, a repository with a lateral extent of 1 km comprises 41 tunnels. In the two-dimensional analysis the length of the tunnel system cannot be taken into account, but this will be done in forthcoming three dimensional solutions. The waste canisters are stored in drill holes at the bottom of the tunnels. The distance between the drillholes along each tunnel is about 4 metres.

The heat released from the repository is assumed to be generated by 40 year old high level waste. The decay was interpolated using the following formula

$$\frac{Q(t)}{Q(0)} = a_1 e^{-\alpha_1 t} + a_2 e^{-\alpha_2 t} \qquad (3.12)$$

where Q denotes heat generated by the radioactive waste. The coefficients α_1 and α_2 were selected so that they represent 30 and 500 year half-lives, and a_1 and a_2 were equal to 0.882 and 0.118 respectively.

The thermal load per canister at the moment of the disposal is assumed 525 W, resulting in a uniformly distributed load of 5.25 W/sqm over the area of the repository. For simplicity, it is assumed in the calculations, that all the waste is disposed of at

the same time. The assumed decay of the thermal load is illustrated in figure 3.3.

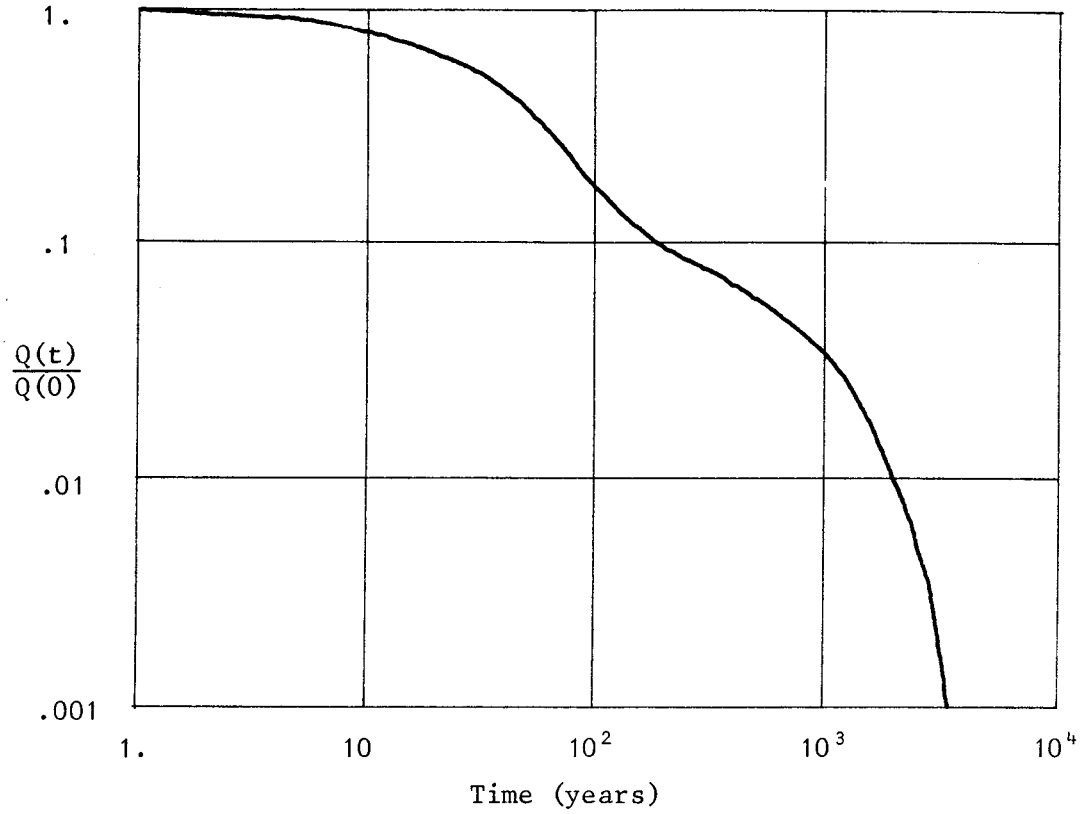

Figure 3.3 Decay of the thermal load

The drill holes with the canisters will be filled with a buffer material composed of 90 per cent quarz sand and 10 per cent bentonite. Eventually, the entire tunnel space will be filled with such a material. The region containing the buffer material will have a very low permeability. The buffer material is considered a safety factor and it is not taken into account in the present study.

3.4 Geometry of the flow domain

The flow domain considered in the calculations represents a two-dimensional cross-section with a lateral extent of 3 km and a depth of 1.5 km. The repository is located at a depth of about 500 metres below the ground surface. Four main cases are considered with regard to the topography or the water table above the repository. The four main cases are:

Case 1 A repository situated in an area with a horizontal ground surface. See figure 3.4.

Case 2 A repository situated below the crest of a hill with linearly sloping sides. See figure 3.5.

Case 3 A repository located below a linearly sloping hillside. See figure 3.6.

Case 4 A repository located between two major vertical fracture zones. See figure 3.7.

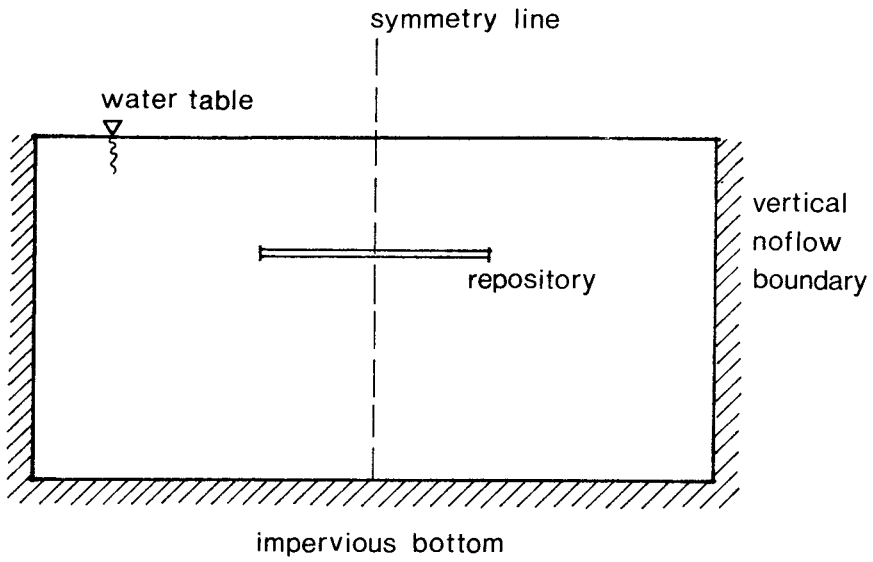

Figure 3.4 Case 1. A repository located in an area where the groundwater is horizontal.

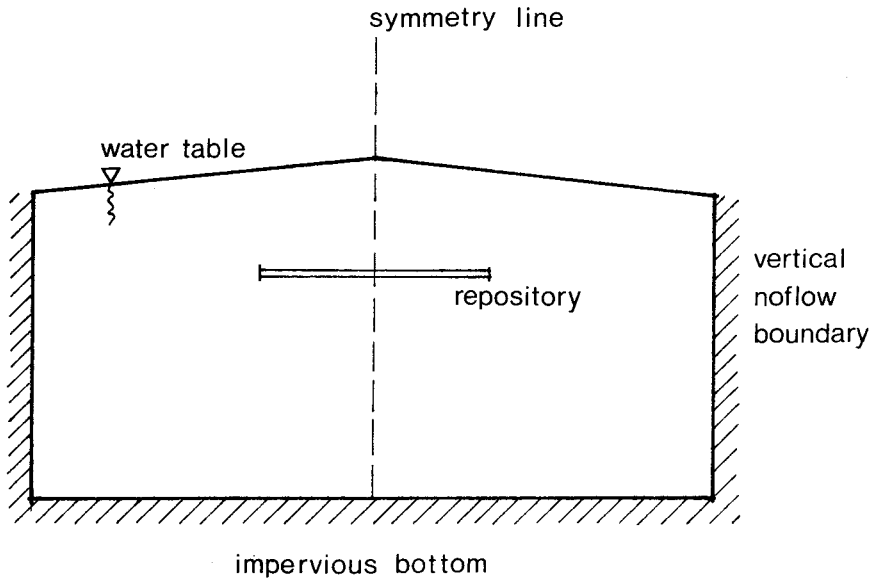

Figure 3.5 Case 2. A repository located below the crest of a hill.

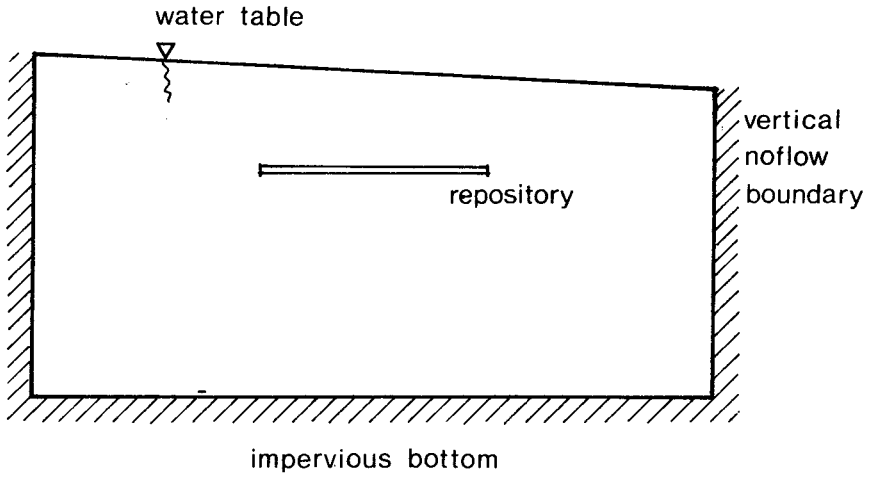

Figure 3.6 Case 3. A repository located below a hillside.

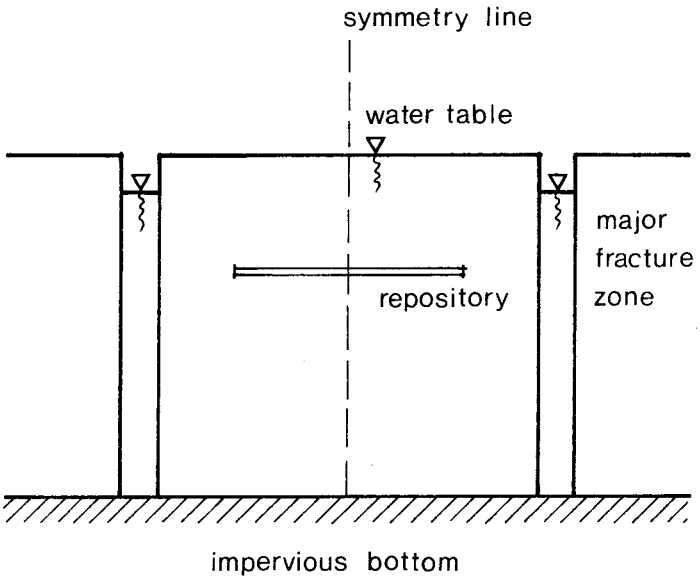

Figure 3.7 Case 4. A repository located between two major vertical fracture zones.

4. NUMERICAL SOLUTIONS

Four main cases are considered for the numerical solutions. Each case is defined by the geometry of the flow domain, boundary conditions and the location of the repository. The four main cases are:

4.1 Repository located below a horizontal ground surface.

4.2 Repository located below the crest of a hill with linearly sloping sides.

4.3 Repository located below a linearly sloping hillside.

4.4 Repository located between two major vertical fracture zones.

Each case is analysed for constant permeability and porosity respectively exponentially decreasing permeability and porosity with depth. The considered flow domain is symmetrical around the vertical centre line through the repository for all cases except for the third case, where the repository is situated below a unidirectionally sloping ground surface. Thus, in the three symmetric cases only one half of the flow domain needs be analysed, reducing the computational work.

The following results from the computations are presented for each case: Exit times (travel times for water particles from the repository to the ground surface, or to a major fracture zone), pathlines from the repository, groundwater fluxes and isotherms.

Flow times from the repository to the ground surface, or alternatively to a major fracture zone, are calculated for water particles spaced out 100 metres apart at the repository. The results are presented in the form of tables of the flow times and graphical display of the pathlines. The calculations are performed for conditions with heat released from the repository as well as for undisturbed conditions, taking into account only the effects of topography and the natural geothermal gradient.

Groundwater fluxes are graphically displayed in the form of vector plots. The arrow of a vector indicates the flow direction and the length indicates the relative order of magnitude of the specific discharge. The velocities are logarithmically scaled in such a way that the maximum velocity at a certain instant corresponds to 1 centimetre on the graph.

Isotherms are used to illustrate the temperature distribution over the flow domain. The difference in temperature between each isotherm is $5^{o}C$.

In the solutions the time step was increased by a factor of 1.2 during the first 50 years. Thereafter the time step was increased by 1.5. The time step procedure has been checked against analytical solutions.

In case 1 and 2, an element mesh consisting of 130 elements and 501 nodes corresponding to one symmetric half of the flow domain is used. In case 3, an element mesh of 300 elements and 971 nodes corresponding to the entire flow domain is used. In case 4, an element mesh of 128 elements and 433 nodes is used for the first setting and an element mesh of 160 elements and 533 nodes is used for the second setting. The elements were designed such that smaller elements were generated around the repository and larger elements towards the bottom and the lateral boundaries of the flow domain.

In some of the examples, problems were encountered in the pathline trace due to the large elements towards the flow domain boundaries. The elements at the boundaries appeared to be too coarse to properly describe the sudden variation in the flow direction within these elements. As a consequence, some of the pathlines hit the boundaries. When this occurs, the pathline trace is continued along the boundary until the ground surface or a major fracture zone is reached.

Summary of material properties used in the examples

Porosity at the ground surface	0.003	-
Permeability at the ground surface	10^{-14}	m
Fluid density	998	kg/m^3
Dynamic viscosity	0.001	Pas
Fluid compressibility	10^{-10}	1/Pa
Thermal volume expansion of the fluid	0.0018	1/K
Thermal conductivity of the fluid	0.6	W/(mK)
Specific heat capacity of the fluid	4180	J/(kgK)
Rock density	2700	kg/m^3
Thermal conductivity of the rock	3.5	W/(mK)
Specific heat capacity of the rock	800	J/(kgK)
Rock compressibility	10^{-11}	1/Pa
Gravity	9.81	m/s^2

Fluid density and viscosity are given in the previous table as reference values corresponding to a temperature of 20 ^{o}C . Using these values and a reference value of the permeability of 10^{-14}, then the value of the hydraulic conductivity becomes about 10^{-7} m/s. The exponential decrease in the permeability with depth is in the examples

$$--- \quad k = 10^{-14}\, e^{0.0092 \cdot z} \qquad (4.1)$$

Thus, at an elevation of -500 metres the value of permeability is 10^{-16} and at -1000 metres 10^{-18} and the corresponding values of the hydraulic conductivity are approximately 10^{-9} respectively 10^{-11} m/s.

4.1 Repository located below a horizontal ground surface

This case illustrates a situation where the groundwater flow is only induced by heat released from the radioactive waste repository. In the initial stage the groundwater is in hydrostatic equilibrium, assuming that the pressure gradient is vertical and parallel to the geothermal gradient over the entire flow domain.

Two examples are presented for this case. In the first example permeability and porosity are constant and in the second example permeability and porosity decrease exponentially with depth over the flow domain. In the example with constant permeability the shortest exit time was about 650 years, while in the example with exponentially decreasing permeability, the initial hydrostatic equilibrium was reestablished before any water particles could reach the ground surface.

4.1.1 Repository located below a horizontal ground surface. Permeability and porosity are constant over the flow domain.

Exit time: > 650 years

No exit without the influence of a repository

The results of the pathline trace are presented in table 4.1.1.

Pathlines are displayed in figure 4.1.1

Groundwater fluxes and isotherms are displayed in figures 4.1.2 - 4.1.4

In this example, the flow pattern remains qualitatively the same within the considered solution period. The flow pattern is characterized by a region of upward movements at the centre of the repository, a region of rotative movements at the edge of the repository, and a region of downward movements at some distance from the repository.

The shortest exit time is obtained for water particles starting at the centre of the repository. Local convection cells are formed around the edges of the repository. As a consequence, water particles starting at a distance of about 300 metres and further away from the centre towards the edges of the repository will be included in these convection cells, which means that these water particles are not going to reach the ground surface.

In the present exemple the calculations were carried out for a period of about 1900 years. Thus, the pathlines obtained in the this example were obtained by extrapolation, using the most recent flow pattern, that is to say the solution after about 1900 years.

Therefore in fact, the convection cells being created at the edges of the repository are actually going to vanish within the 15000 years, as was the period for the pathline trace.

Table 4.1.1 Coordinates of the starting respectively end points and the corresponding travel times in years of pathlines traced from a radioactive waste repository situated below a horizontal ground surface. Permeability and porosity are constant over the flow domain.

No	Starting point		End point		Travel time
1	0	-500	5	0	650
2	100	-500	160	0	670
3	200	-500	365	0	810
4	300	-500	-	-	No exit
5	400	-500	-	-	No exit
6	500	-500	-	-	No exit

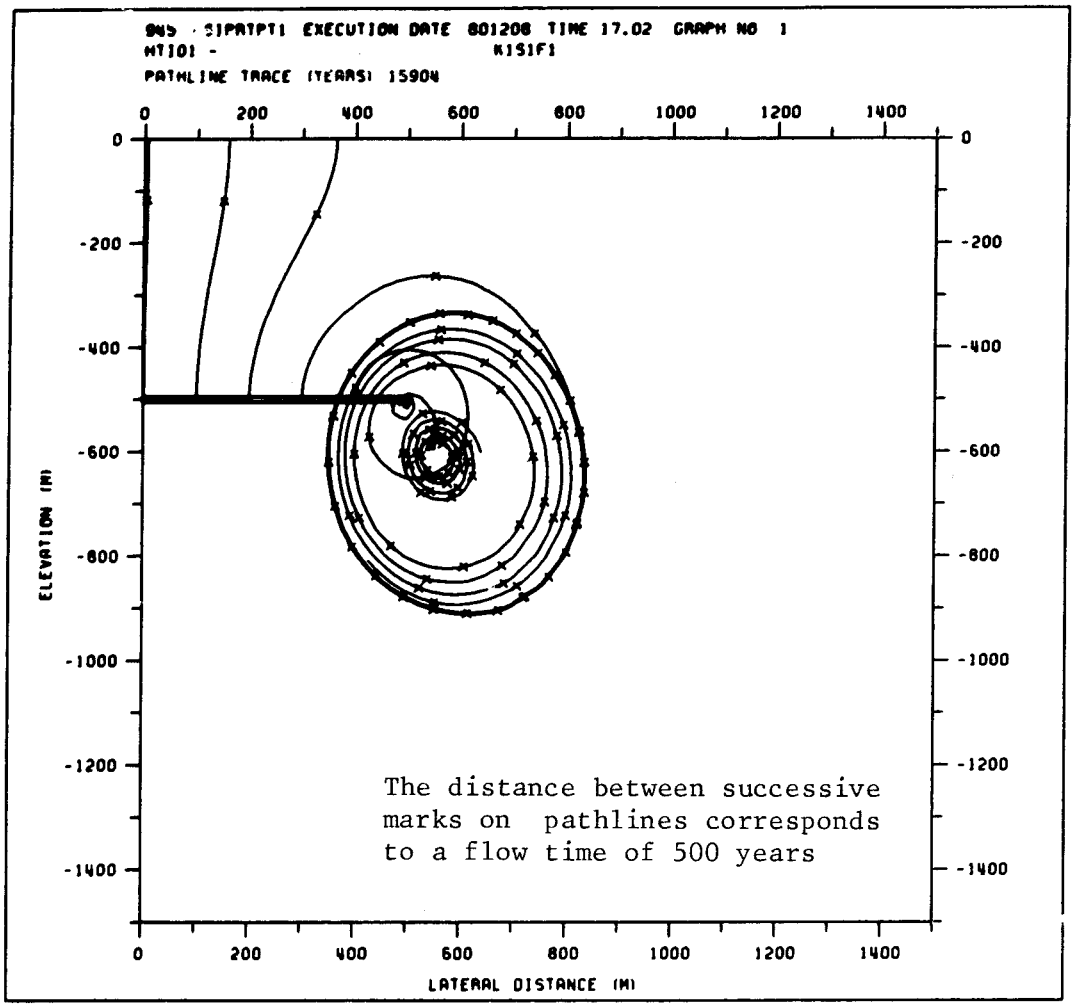

Figure 4.1.1 Pathlines for the fluid flow induced by a radioactive waste repository located below a horizontal ground surface. Permeability and porosity are constant.

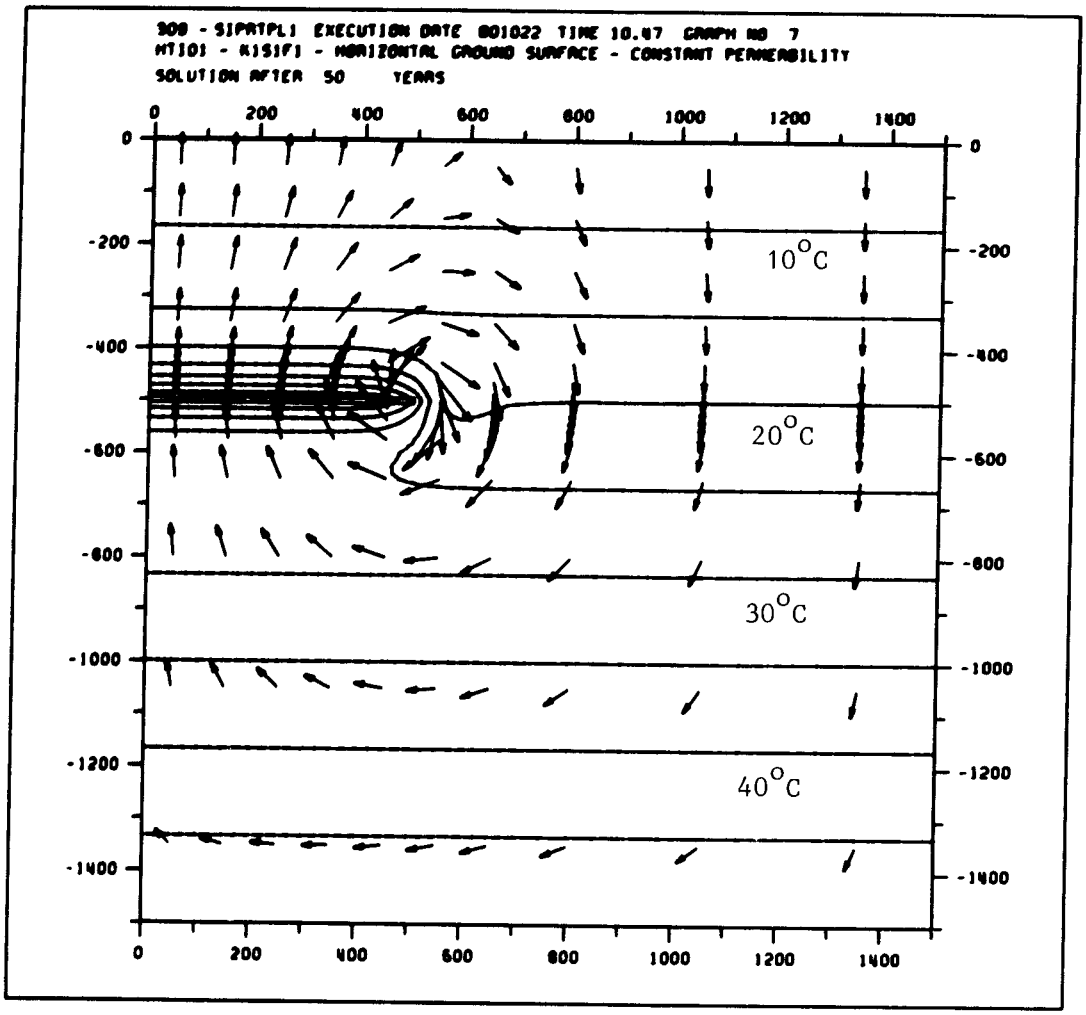

Figure 4.1.2 Groundwater fluxes and isotherms illustrating the hydrothermal flow conditions around a radioactive waste repository situated below a horizontal ground surface. Permeability and porosity are constant. Release time: 50 years.

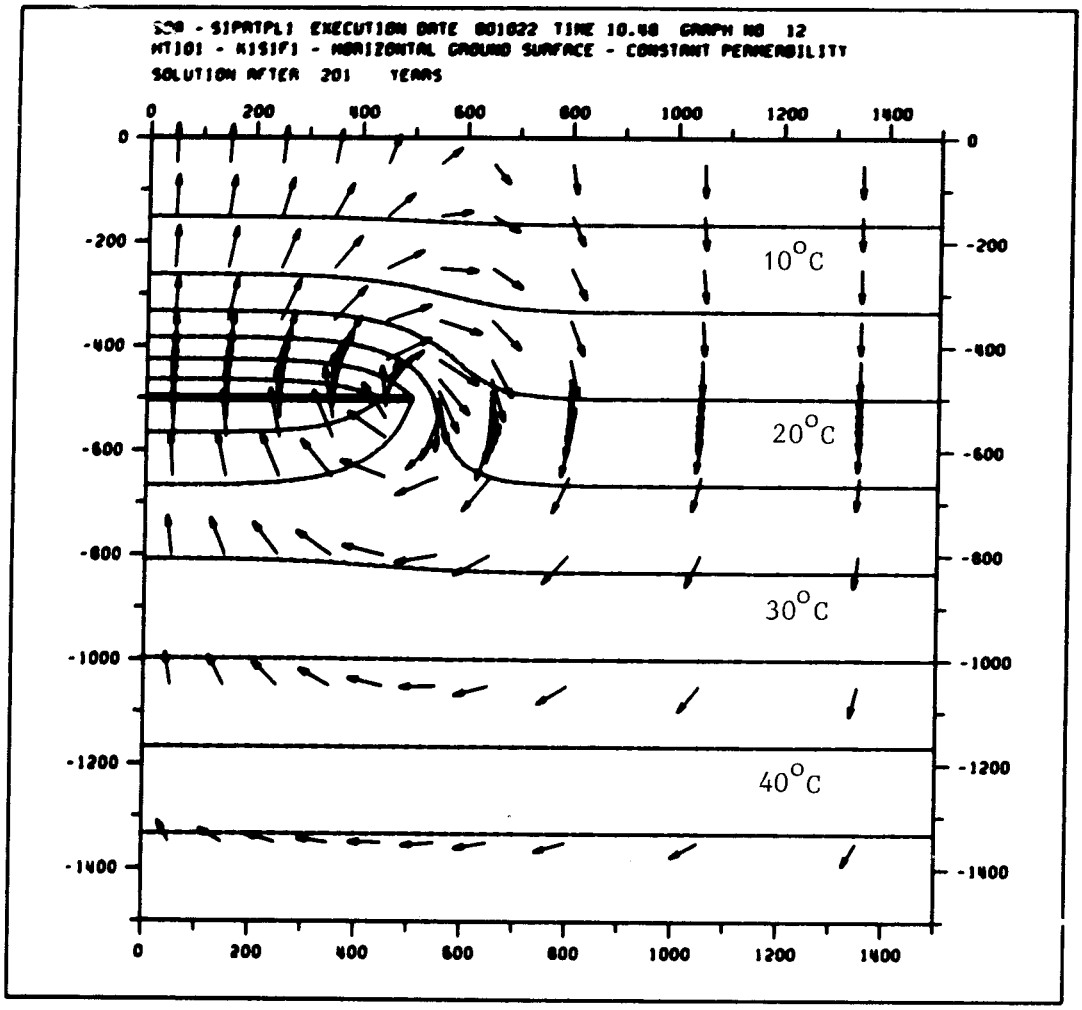

Figure 4.1.3 Groundwater fluxes and isotherms illustrating the hydrothermal flow conditions around a radioactive waste repository situated below a horizontal ground surface. Permeability and porosity are constant. Release time: 201 years.

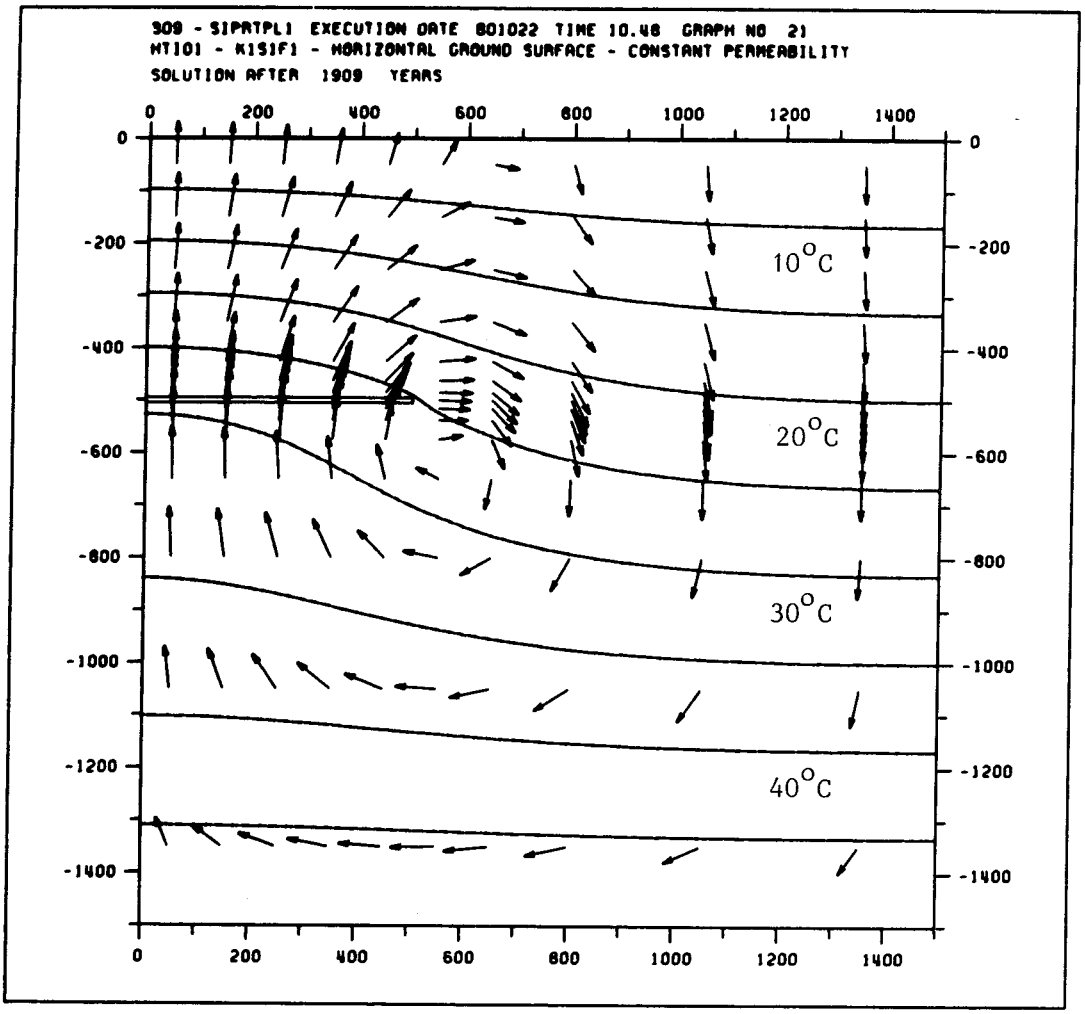

Figure 4.1.4 Groundwater fluxes and isotherms illustrating the hydrothermal flow conditions around a radioactive waste repository situated below a horizontal ground surface. Permeability and porosity are constant. Release time: 1909 years.

4.1.2 Repository located below a horizontal ground surface. Permeability and porosity are exponentially decreasing with depth.

Exit time: No exit

No exit without the influence of a repository

The results of the pathline trace are presented in table 4.1.2.

Pathlines are displayed in figure 4.1.5

Groundwater fluxes and isotherms are displayed in figures 4.1.6 - 4.1.8

A comparison between the flow patterns in this example and the the flow patterns obtained in the previous example, in which peremeability and porosity were constant, shows a notable difference between the two solutions, especially when comparing the most recent solutions. In the present example, the flow at the repository is mainly horizontal and directed towards the centre of the repository, whereas in the previous example the flow at the repository is mainly vertical and directed upwards. Moreover, the assumed exponential decrease of the permeability substantially reduces the fluxes, increasing the travel times from the repository to the ground surface.

In consequence of the very low fluid velocities in this example the initial hydrostatic equilibrium will be reestablished before any fluid particles reach the ground surface. This seems to occur after about 7500 years and the water particles starting from the repository will discontinue at a depth of about 175 metres below the ground surface.

A local convection cell is also formed in this example, but its centre is located in an area above the edge of the repository, fairly close to the ground surface. However, none of the water particles starting from the repository seem to be involved in this convection cell.

The exponential decrease in permeability with depth particularly reduces the magnitude of the vertical flux component. The reason for the bend of the pathlines towards the vertical centre line through the repository is that in the area around the repository, the magnitude of the vertical flux component is reduced to the same order of magnitude as the horizontal one, which is directed towards the centre of the repository. This is due to the minor increase in temperature towards the centre of the repository.

Table 4.1.2 Coordinates of the starting respectively end points and the corresponding travel times in years of pathlines traced from a radioactive waste repository situated below a horizontal ground surface. Permeability and porosity are exponentially decreasing with depth.

No	Starting point		End point		Travel time
0	-175	-500	0	-175	No exit
2	100	-500	35	-175	No exit
3	200	-500	75	-175	No exit
4	300	-500	132	-175	No exit
5	400	-500	200	-175	No exit
6	500	-500	200	-175	No exit

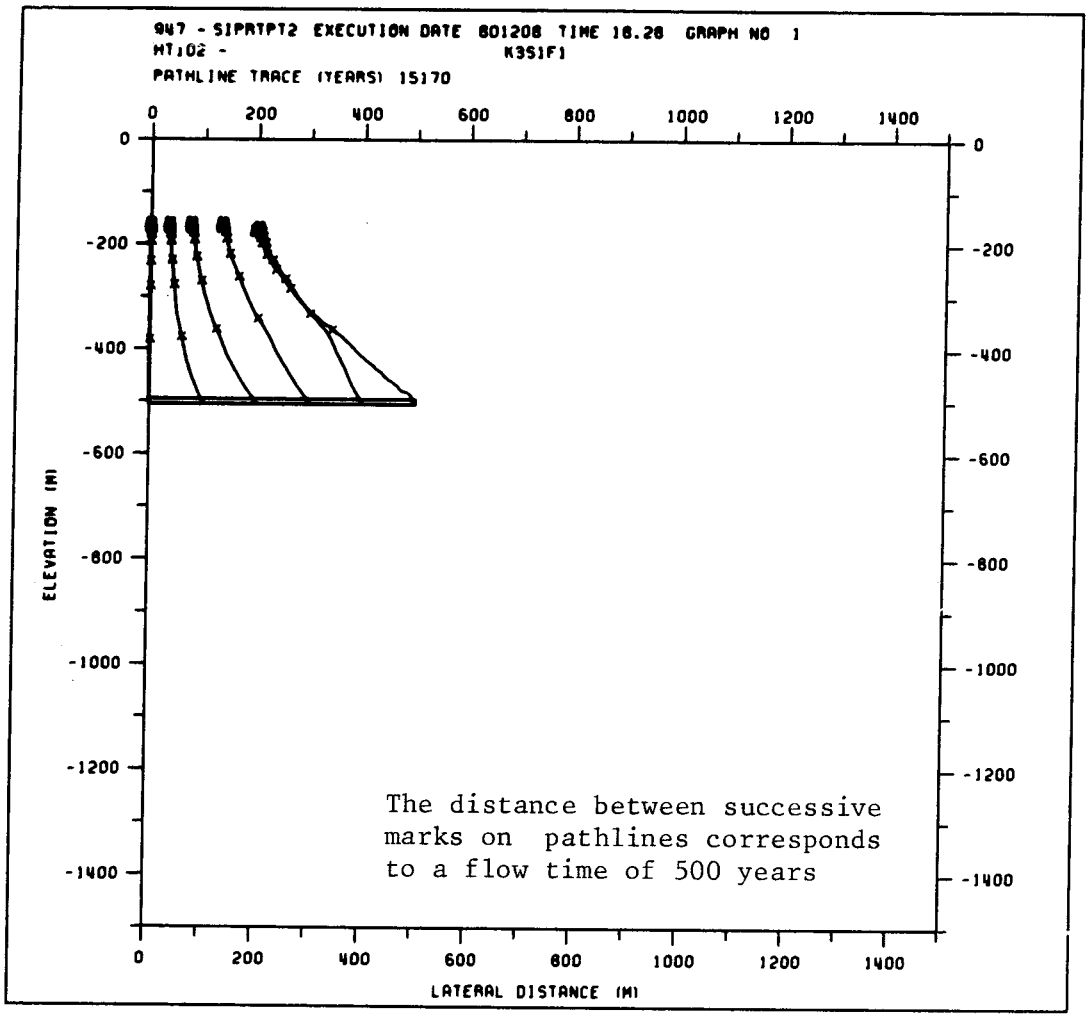

Figure 4.1.5 Pathlines for the fluid flow induced by a radioactive waste repository located below a horizontal ground surface. Permeability and porosity are exponentially decreasing with depth.

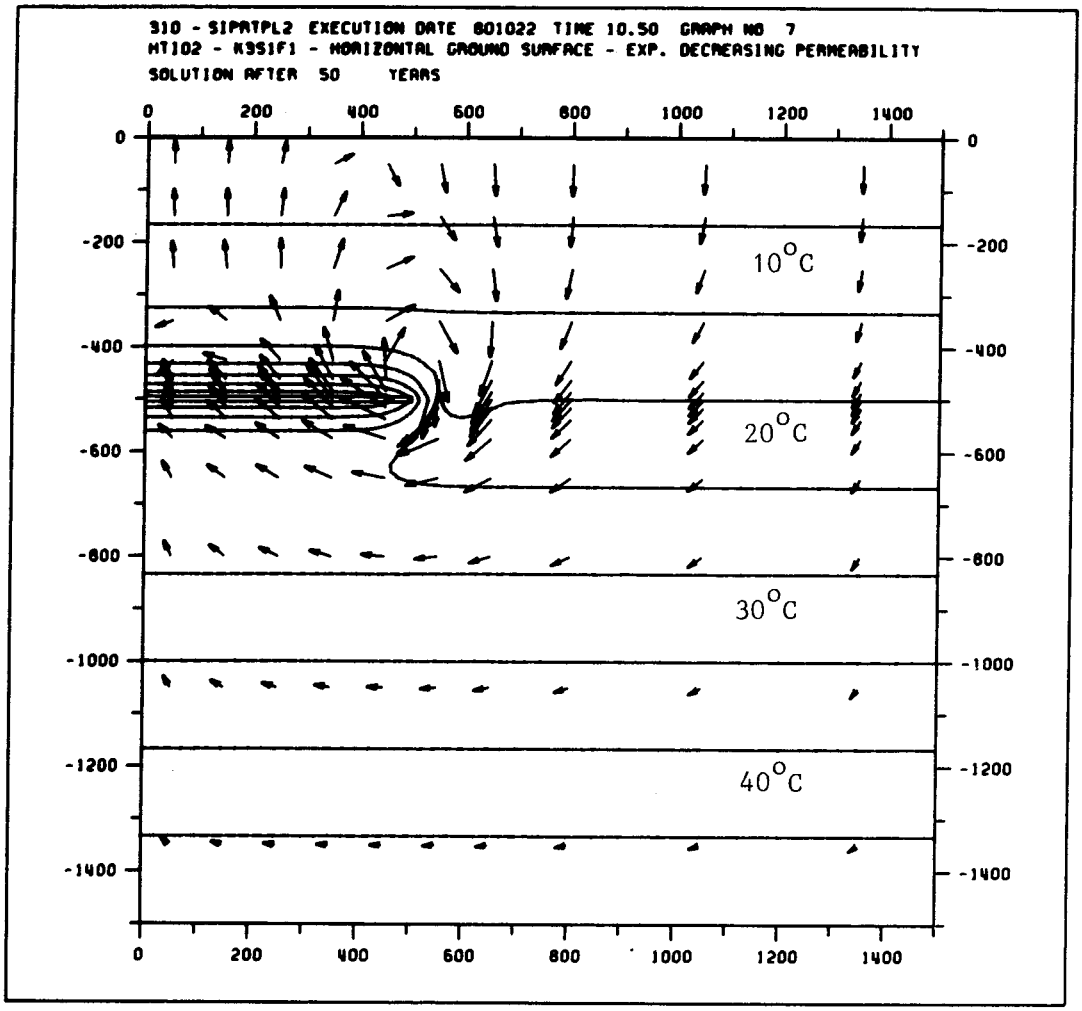

Figure 4.1.6 Groundwater fluxes and isotherms illustrating the hydrothermal flow conditions around a radioactive waste repository situated below a horizontal ground surface. Permeability and porosity are exponentially decreasing with depth. Release time: 50 years.

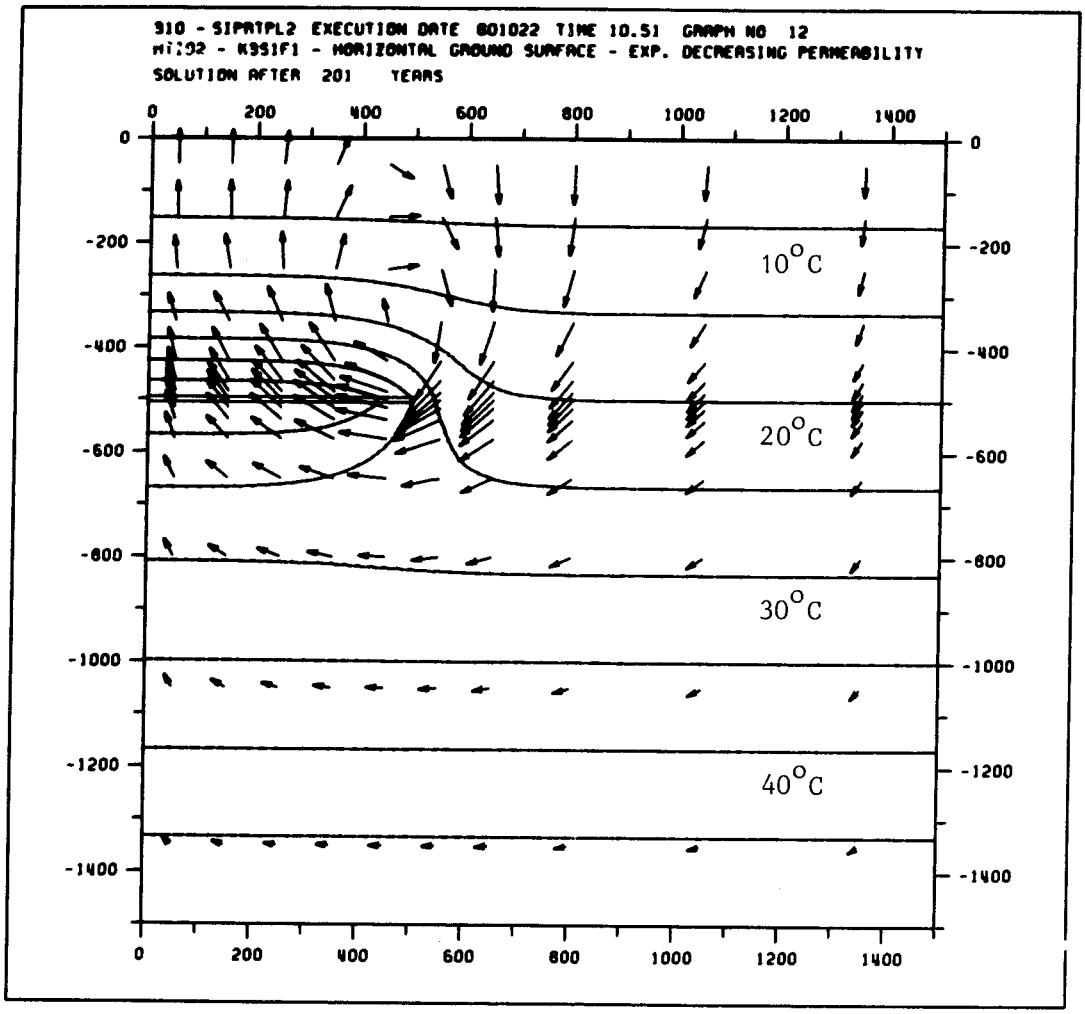

Figure 4.1.7 Groundwater fluxes and isotherms illustrating the hydrothermal flow conditions around a radioactive waste repository situated below a horizontal ground surface. Permeability and porosity are exponentially decreasing with depth. Release time: 201 years.

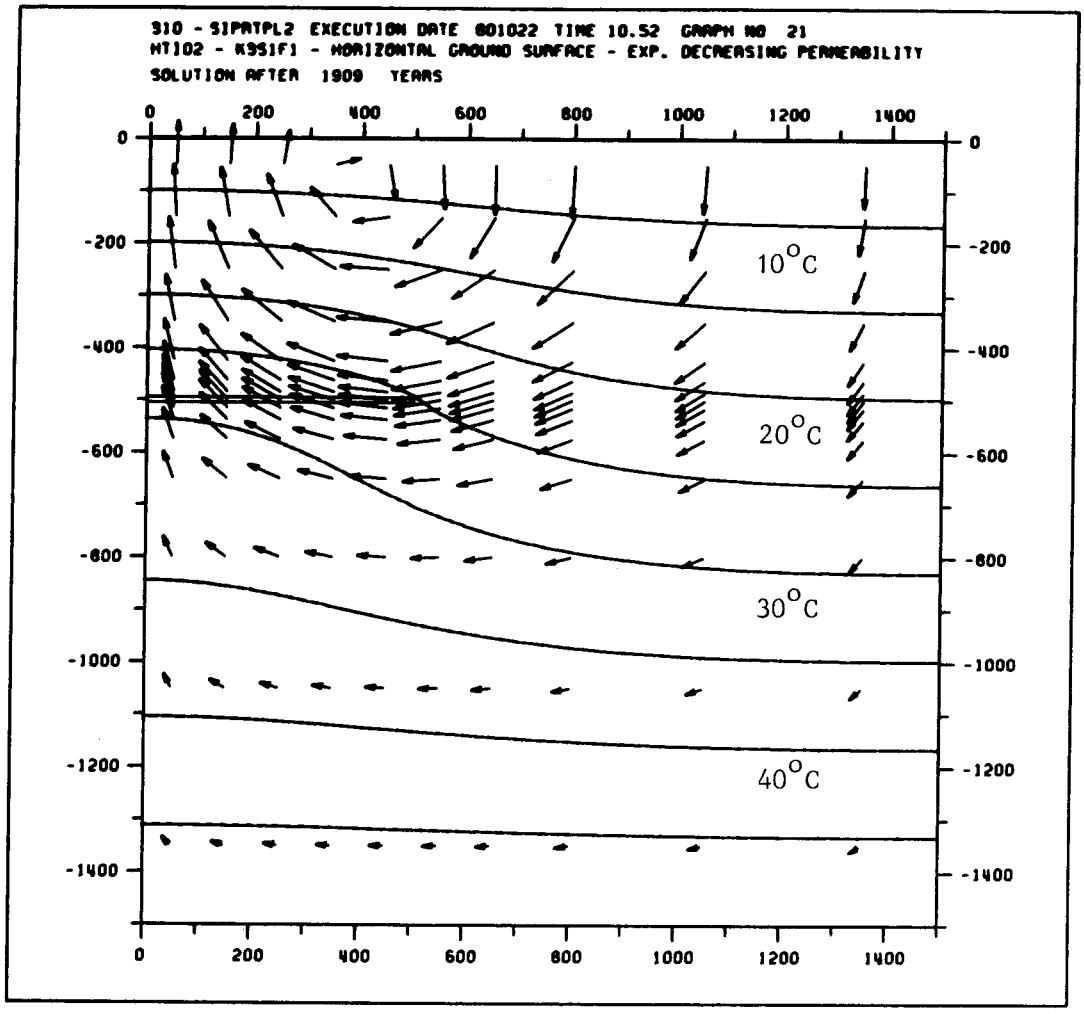

Figure 4.1.8 Groundwater fluxes and isotherms illustrating the hydrothermal flow conditions around a radioactive waste repository situated below a horizontal ground surface. Permeability and porosity are exponentially decreasing with depth. Release time: 1909 years.

4.2 Repository located below the crest of a hill

The repository is symmetrically located below the crest of the hill. In this case the groundwater flow is induced both by the slope of the ground surface and by the heat released from the repository.

This case is of great interest since it implies long flow times from the repository to the ground surface if the groundwater flow is only governed by topography. The longer flow times are expected because the repository is situated below an inflow area, with downward groundwater movements at the repository.

Four examples were worked out for this case. Two examples have a slope of one per mille and constant respectively exponentially decreasing permeability with depth. Two examples have a slope of one per cent and constant respectively exponentially decreasing permeability with depth.

Pathlines are also presented for the natural steady flow conditions, corresponding to the flow conditions without the influence of a radioactive waste repository.

The four examples are organized as follows:

4.2.1 Repository located below the crest of a hill with a slope of one per mille. Constant permeability and porosity.

4.2.2 Repository located below the crest of a hill with a slope of one per mille. Exponentially decreasing permeability and porosity

with depth.

4.2.3 Repository located below the crest of a hill with a slope of one per cent. Constant permeabililty and porosity.

4.2.4 Repository located below the crest of a hill with a slope of one per cent. Exponentially decreasing permeability and porosity with depth.

4.2.1 Repository located below the crest of a hill with a slope of one per mille Permeability and porosity are constant.

Exit time: > 3800 years

> 2550 years without the influence of a repository

The results of the pathline trace are presented in tables 4.2.1 and 4.2.2.

Pathlines for the flow conditions with the influence of a repository are displayed in figure 4.2.1

Pathlines for the natural flow conditions without the influence of a repository are displayed in figure 4.2.2

Groundwater fluxes and isotherms are displayed in figures 4.2.3 - 4.2.6

In the initial stage the flow pattern is dominated by the effect of the topography. The flow is directed downwards around the repository and upwards when approaching the lateral boundary.

As time goes on a rotative movement of the groundwater is formed near the edge of the repository. After about 50 years the downward movement at the centre of the repository is balanced by the upward movement caused by the heat from the repository.

It is interesting to see the creation of a horizontal water divide above the repository. This water divide separates water, flowing from the crest of the hill towards the repository, from water surrounding the repository.

In this example, the heat released from the repository has a sig-

nificant effect on the flow pattern and subsequently also on the flow times. The effect of the heat released from the repository is to create convection currents, which after a certain period of time turn some of the water particles back towards the repository in wide circular paths, prolonging the flow times. Because of the decay in the heat generation by the waste in the repository, the effect of the heat becomes too small to maintain the rotational movement of the groundwater around the repository. Thus, after some thousand years the groundwater is again governed essentially by topography. The result of the influence exerted by the heat from the repository is to prolong the travel times for most of the water particles starting at the repository. However, at points close to the centre of the repository, the travel times are significantly reduced due to the heat from the repository.

Table 4.2.1 Coordinates of the starting respectively end points and the corresponding travel times in years of pathlines traced from a radioactive repository located below the crest of a hill with a slope of one per mille. Permeability and porosity are constant over the flow domain.

No	Starting point		End point		Travel time
1	0	-500	1399	0	3863
2	100	-500	1500	0	4255
3	200	-500	1497	0	12305
4	300	-500	1473	0	8615
5	400	-500	1494	0	7749
6	500	-500	1484	0	8520

Table 4.2.2 Coordinates of the starting respectively end points and the corresponding travel times in years of pathlines traced from a repository located below the crest of a hill with a slope of one per mille. Permeability and porosity are constant over the flow domain. No heat is released from the repository.

No	Starting point		End point		Travel time
1	0	-500	-	-	-
2	100	-500	1487	0	11700
3	200	-500	1449	0	6540
4	300	-500	1427	0	4550
5	400	-500	1401	0	3220
6	500	-500	1382	0	2550

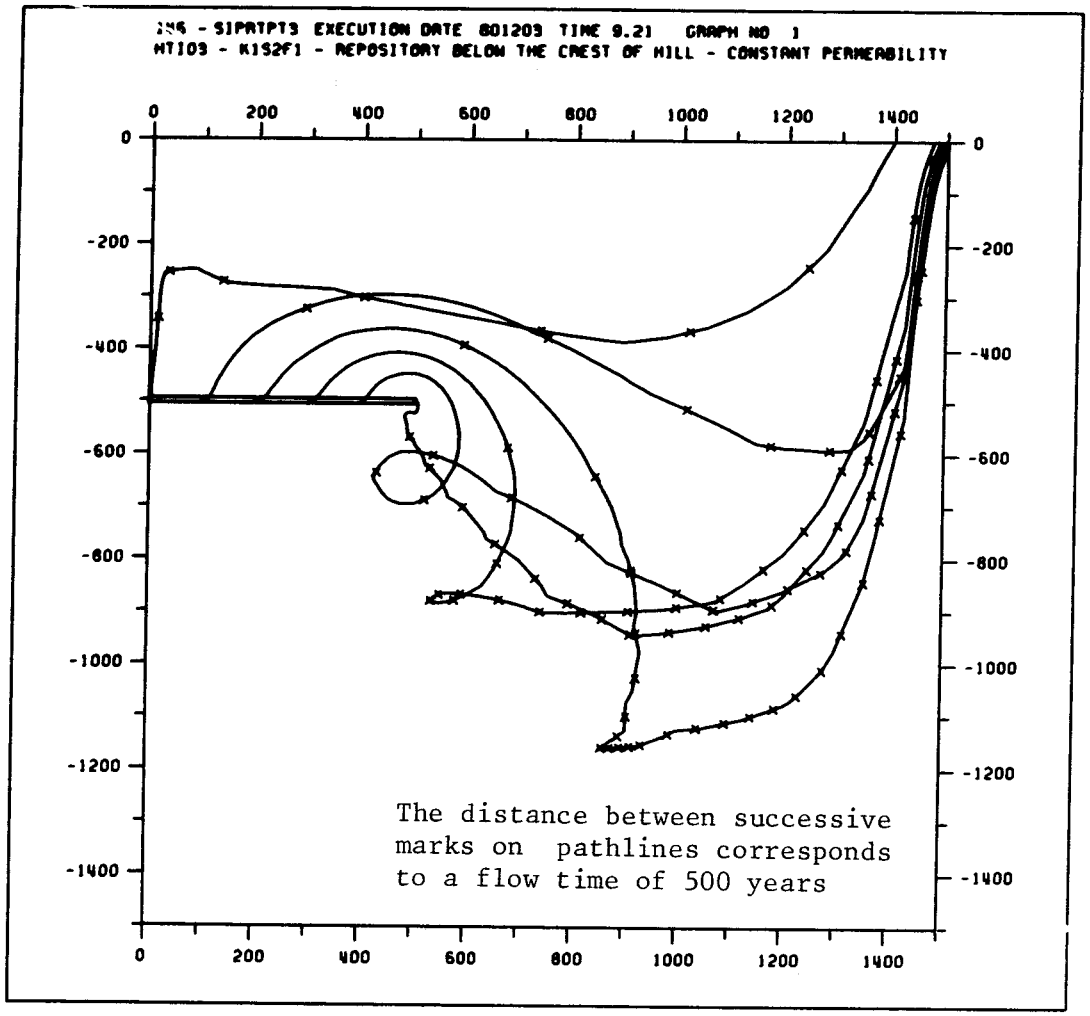

Figure 4.2.1 Pathlines for the flow conditions with the influence of a repository located below the crest of a hill with a slope of the hillsides of one per mille. Permeability and porosity are constant.

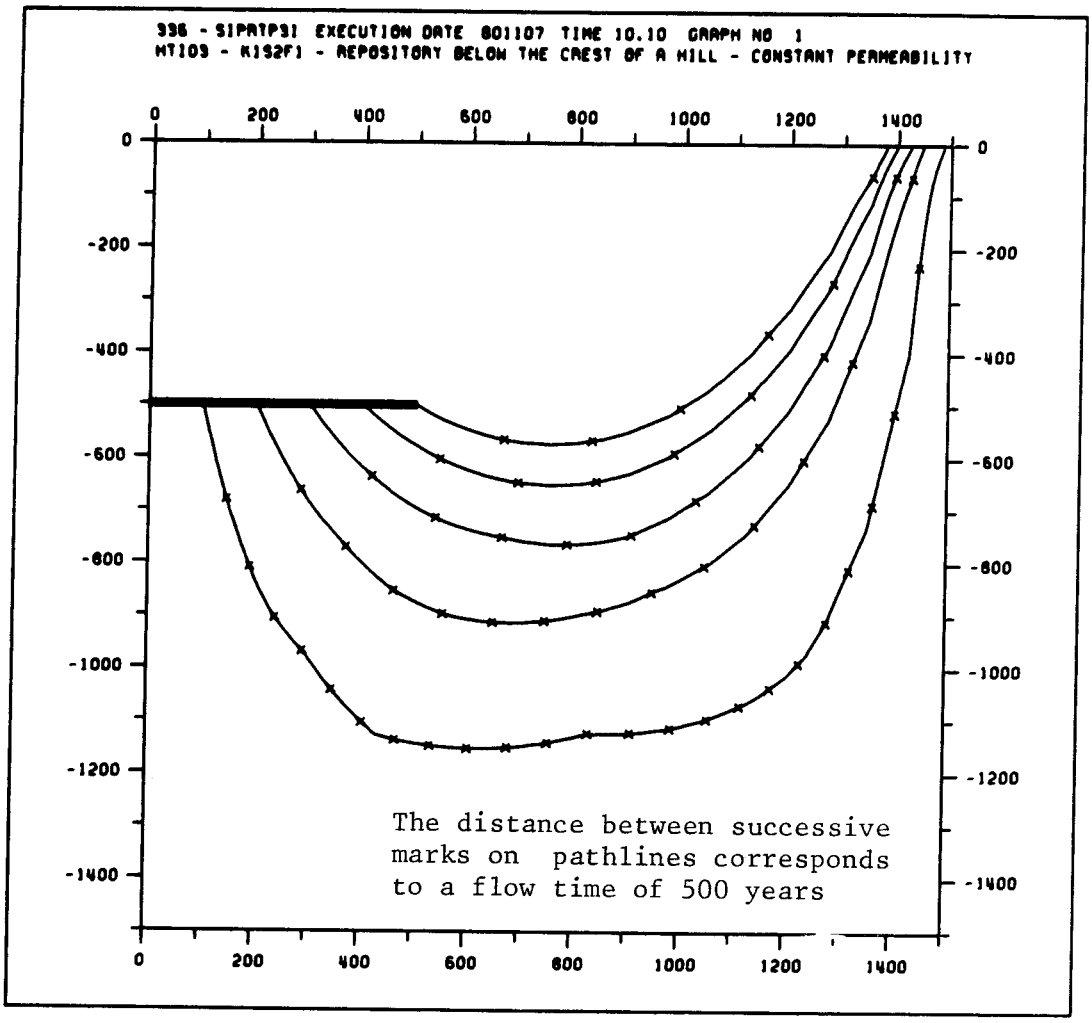

Figure 4.2.2 Pathlines for the natural flow conditions below the crest of a hill with a slope of one per mille. Permeability and porosity are constant.

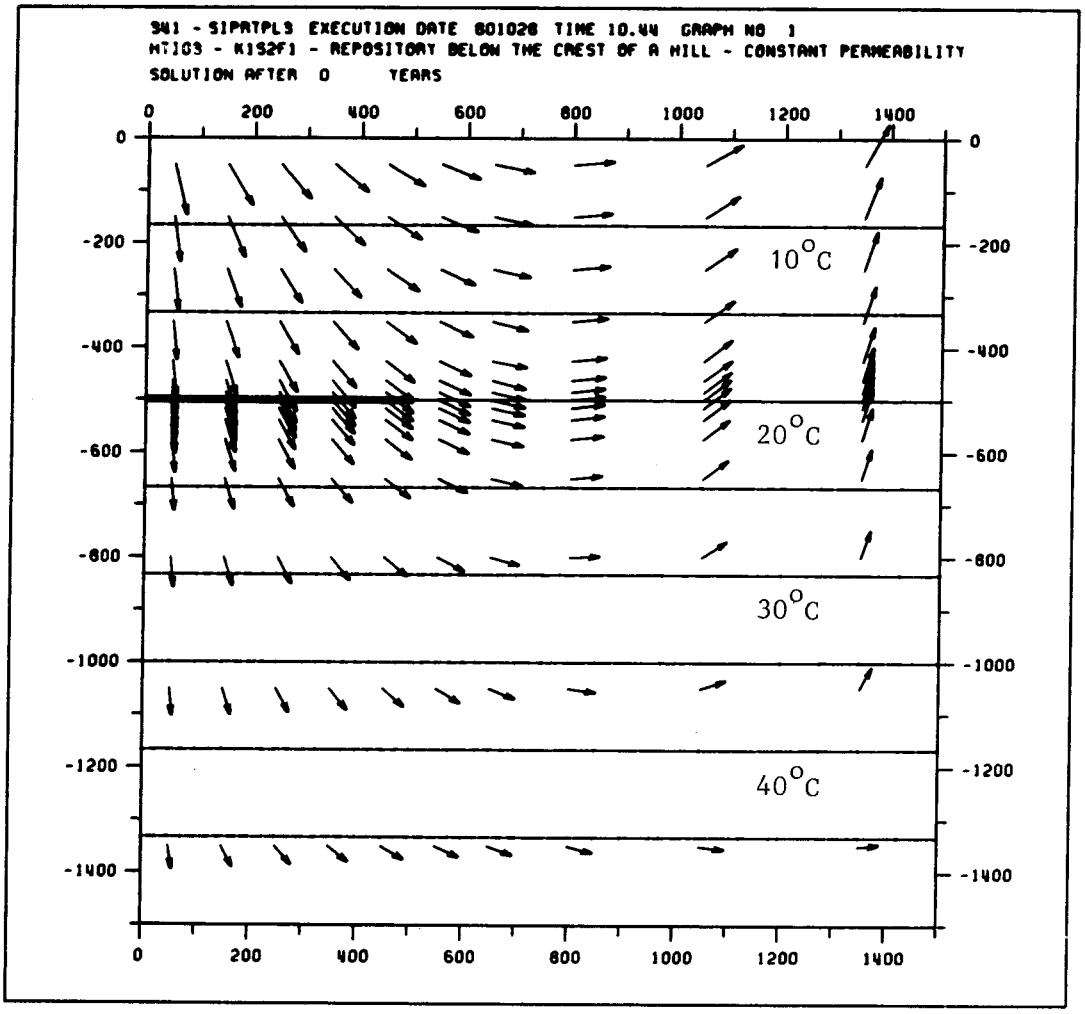

Figure 4.2.3 Groundwater fluxes and isotherms illustrating the hydrothermal flow conditions around a radioactive waste repository situated below the crest of a hill with a slope of one per mille. Permeability and porosity are constant. Release time: 0 years.

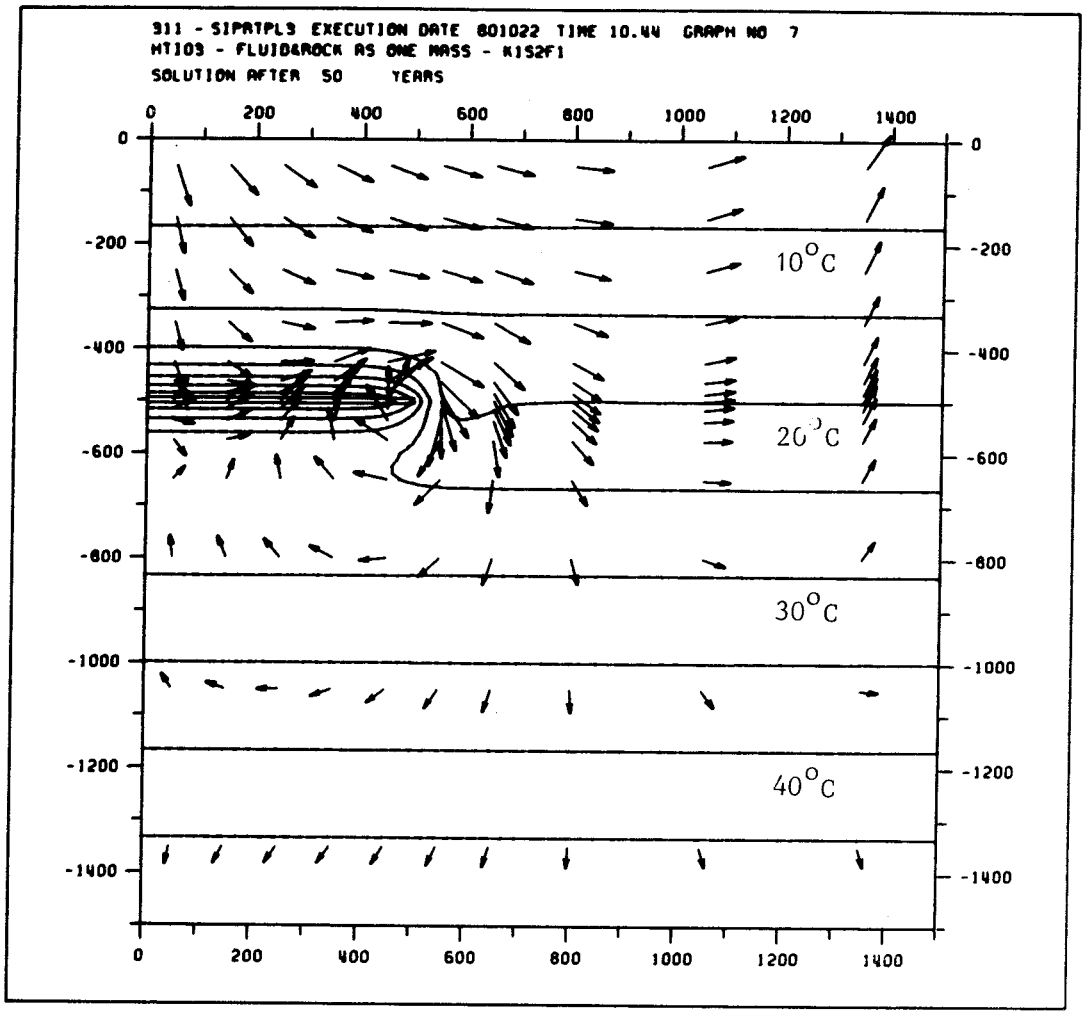

Figure 4.2.4 Groundwater fluxes and isotherms illustrating the hydrothermal flow conditions around a radioactive waste repository situated below the crest of a hill with a slope of one per mille. Permeability and porosity are constant. Release time: 50 years.

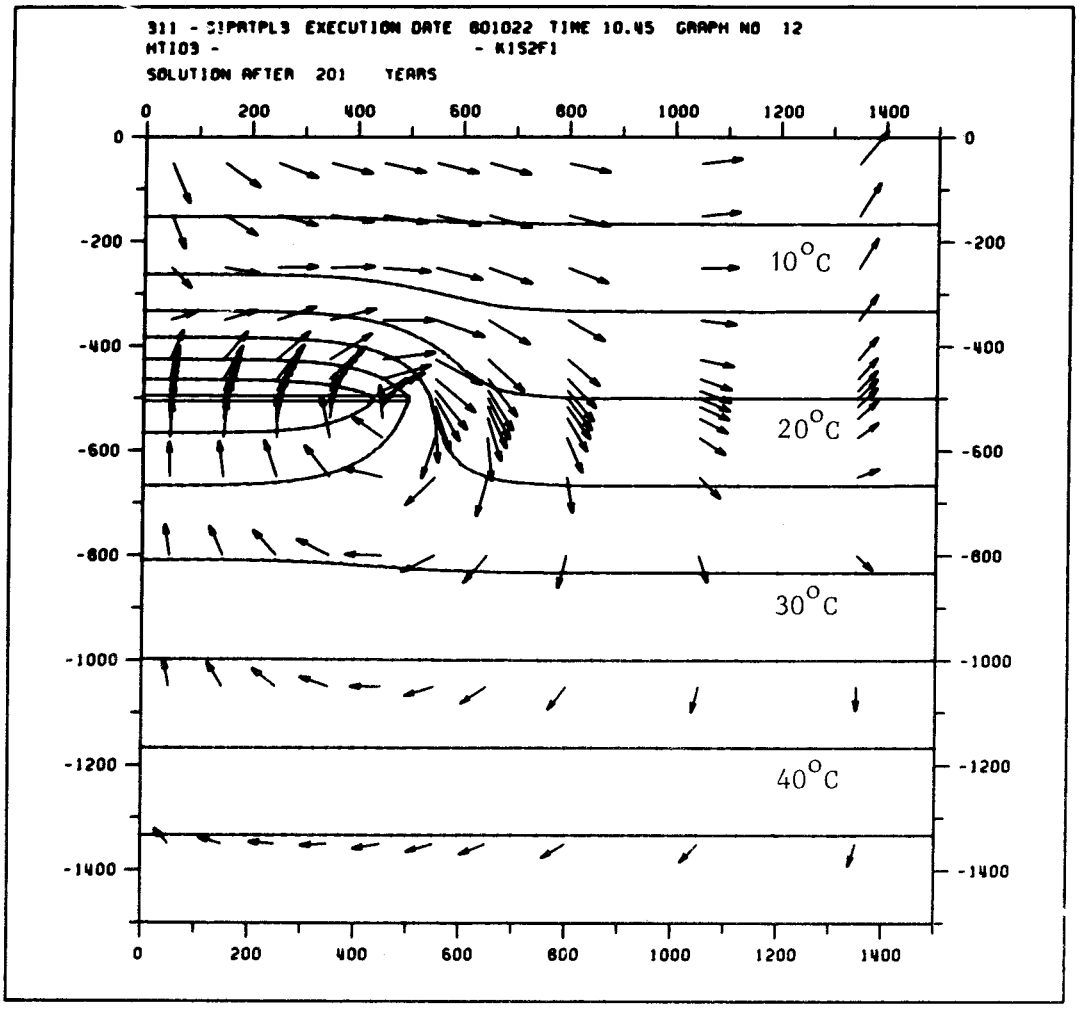

Figure 4.2.5 Groundwater fluxes and isotherms illustrating the hydrothermal flow conditions around a radioactive waste repository situated below the crest of a hill with a slope of one per mille. Permeability and porosity are constant. Release time: 201 years.

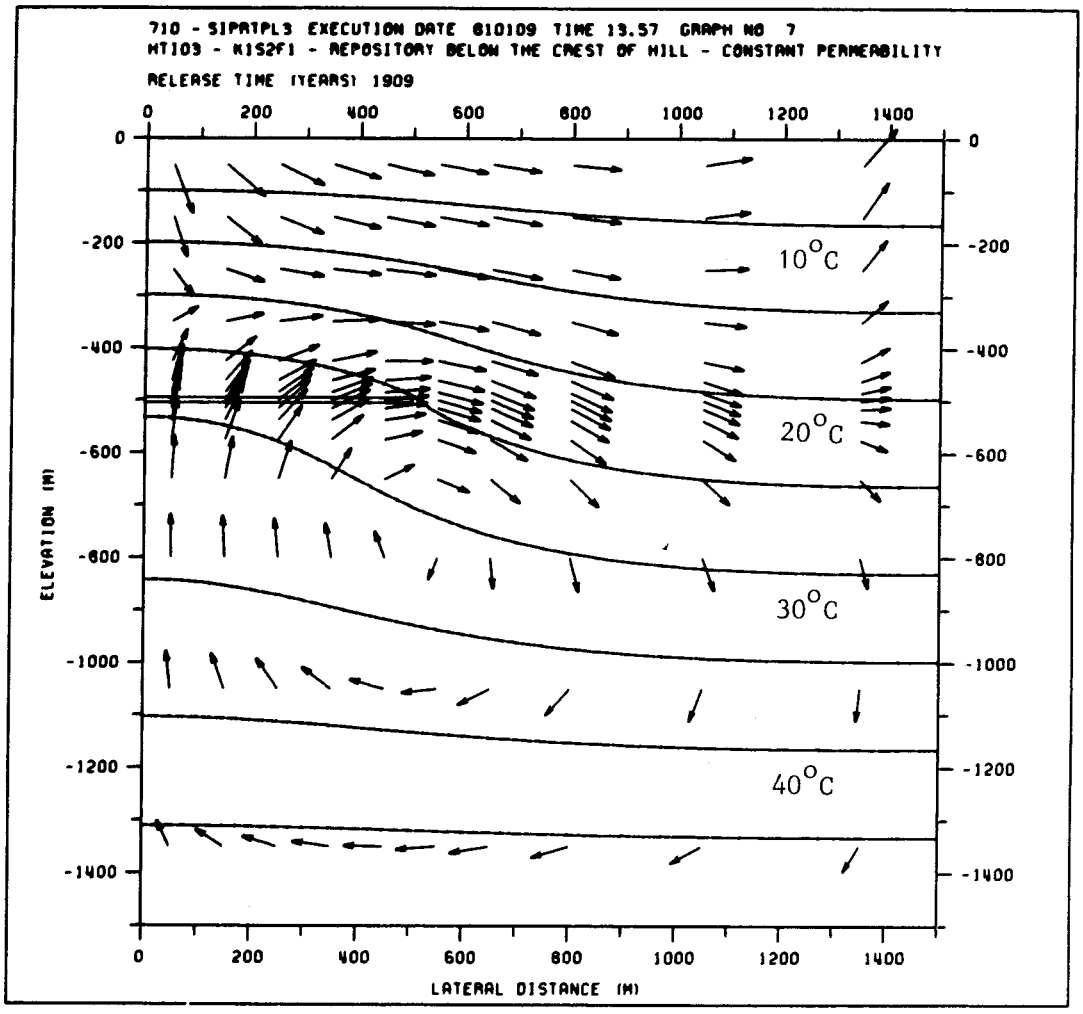

Figure 4.2.6 Groundwater fluxes and isotherms illustrating the hydrothermal flow conditions around a radioactive waste repository situated below the crest of a hill with a slope of one per mille. Permeability and porosity are constant. Release time: 1909 years.

4.2.2 Repository located below the crest of a hill with a slope of one per mille. Permeability and porosity are exponentially decreasing with depth.

Exit time: > 3900 years

> 2200 years without the influence of a repository

The results of the pathline trace are presented in tables 4.2.3 and 4.2.4.

Pathlines for the flow conditions with the influence of a repository are presented in figure 4.2.7.

Pathlines for the natural flow conditions without the influence of a repository are displayed in figure 4.2.8.

Groundwater fluxes and isotherms are displayed in figures 4.2.9 - 4.2.12.

In the initial stage the groundwater flow is largely governed by the topographical gradient. Owing to the decrease in permeability with depth, the groundwater flow is mainly horizontal and below the location depth of the repository the velocities are very small. At the centre of the repository the flow is directded downwards. A water particle starting from this point in the beginning downwards at very low velocity. Then it moves upwards through the repository until it reaches a point above the repository, from where it again goes downwards through the repository, following a mainly horizontal path.

Eventually, as for the previous case with constant permeability, a horizontal water divide is formed above the repository. In comparison with the previous example, in which permeability and porosity were constant over the flow domain, the water divide is situated more closely to the repository. In this example, the effect of the heat is less drastic compared with that of the previous case. The exponential decrease in permeability significantly reduces the fluxes at depth. The heat from the repository affects the flow times notwithstanding. All of the traced pathlines resulted in longer travel times. The shortest exit time was obtained for the water particles starting at a distance of 100 metres from the centre of the repository and the longest flow time was obtained for water particles starting at the edge of the repository. The longer flow times towards the edge of the repository are due to the convection cell created in this area.

Table 4.2.3 Coordinates of the starting respectively end points and the corresponding travel times in years of pathlines traced from a radioactive repository located below the crest of a hill with a slope of one per mille. Permeability and porosity are exponentially decreasing with depth.

No	Starting point		End point		Travel time
1	0	-500	1500	0	5394
2	100	-500	1500	0	3917
3	200	-500	1500	0	4444
4	300	-500	1500	0	4833
5	400	-500	1500	0	4437
6	500	-500	1500	0	5411

Table 4.2.4 Coordinates of the starting respectively end points and the corresponding travel times in years of pathlines traced from a repository located below the crest of a hill with a slope of one per mille. Permeability and porosity are exponentially decreasing with depth. No heat is released from the repository.

No	Starting point		End point		Travel time
1	0	-500	1500	0	5580
2	100	-500	1500	0	3290
3	200	-500	1500	0	2860
4	300	-500	1500	0	2610
5	400	-500	1500	0	2420
6	500	-500	1500	0	2240

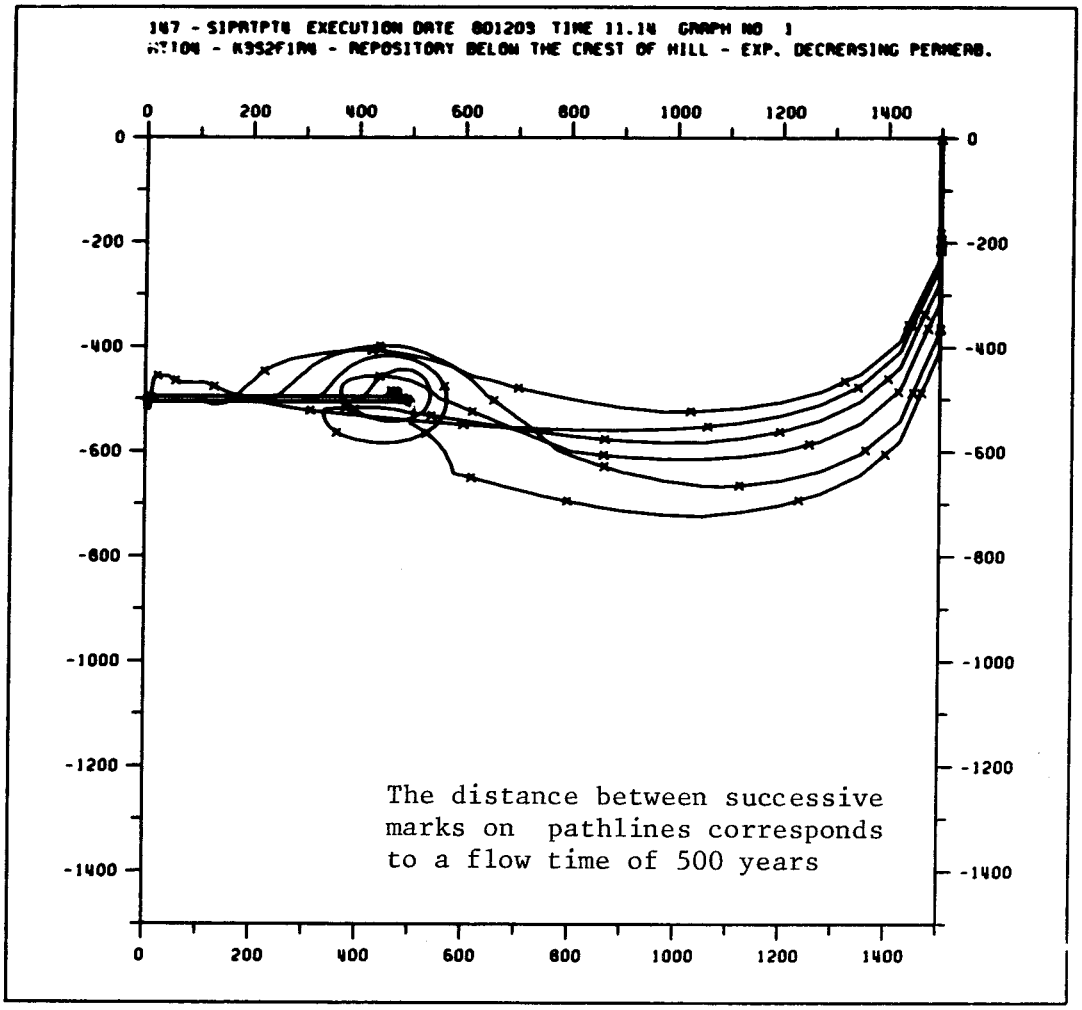

Figure 4.2.7 Pathlines for the flow conditions with the influence of a repository located below the crest of a hill with a slope of one per mille. Permeability and porosity are exponentially decreasing with depth.

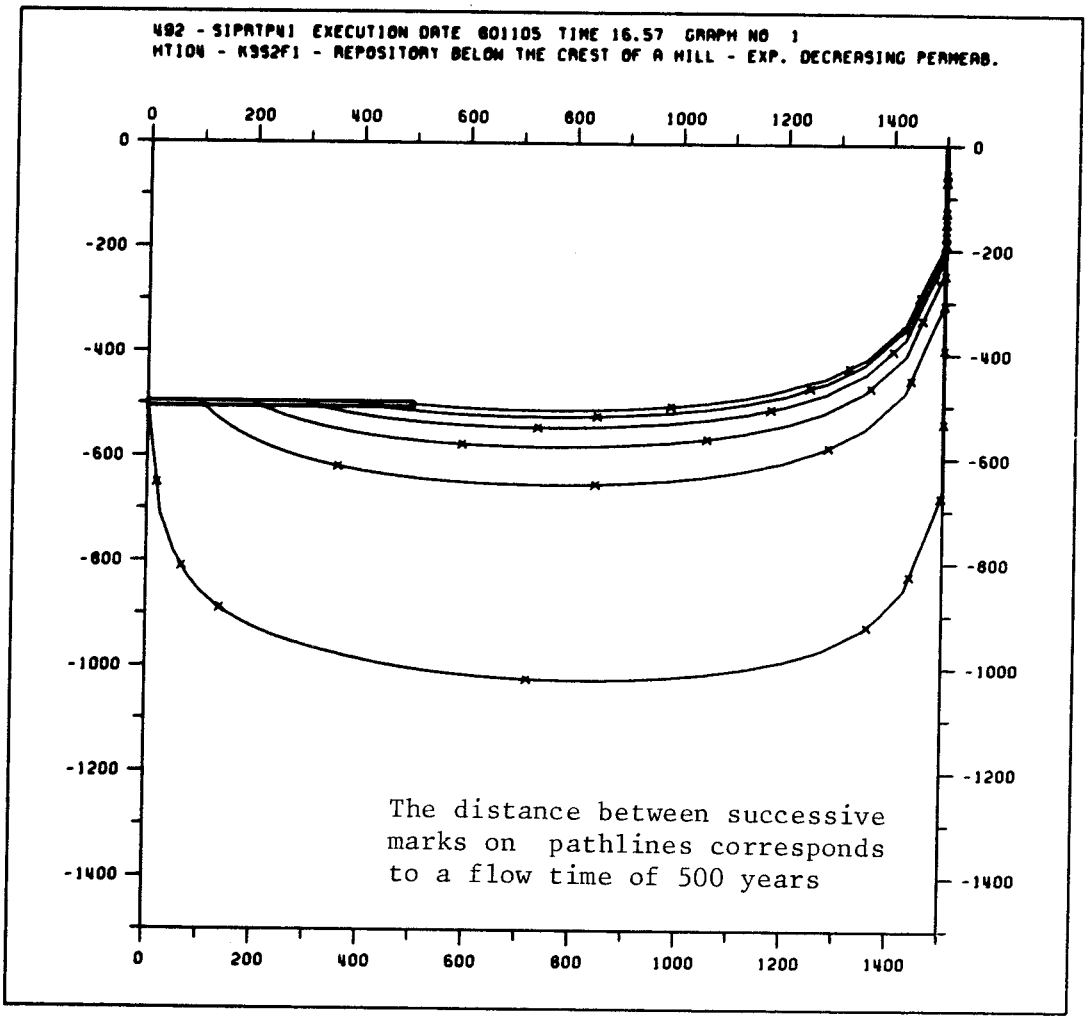

Figure 4.2.8 Pathlines for the natural flow conditions below the crest of a hill with a slope of one per mille. Permeability and porosity are exponentially decreasing with depth.

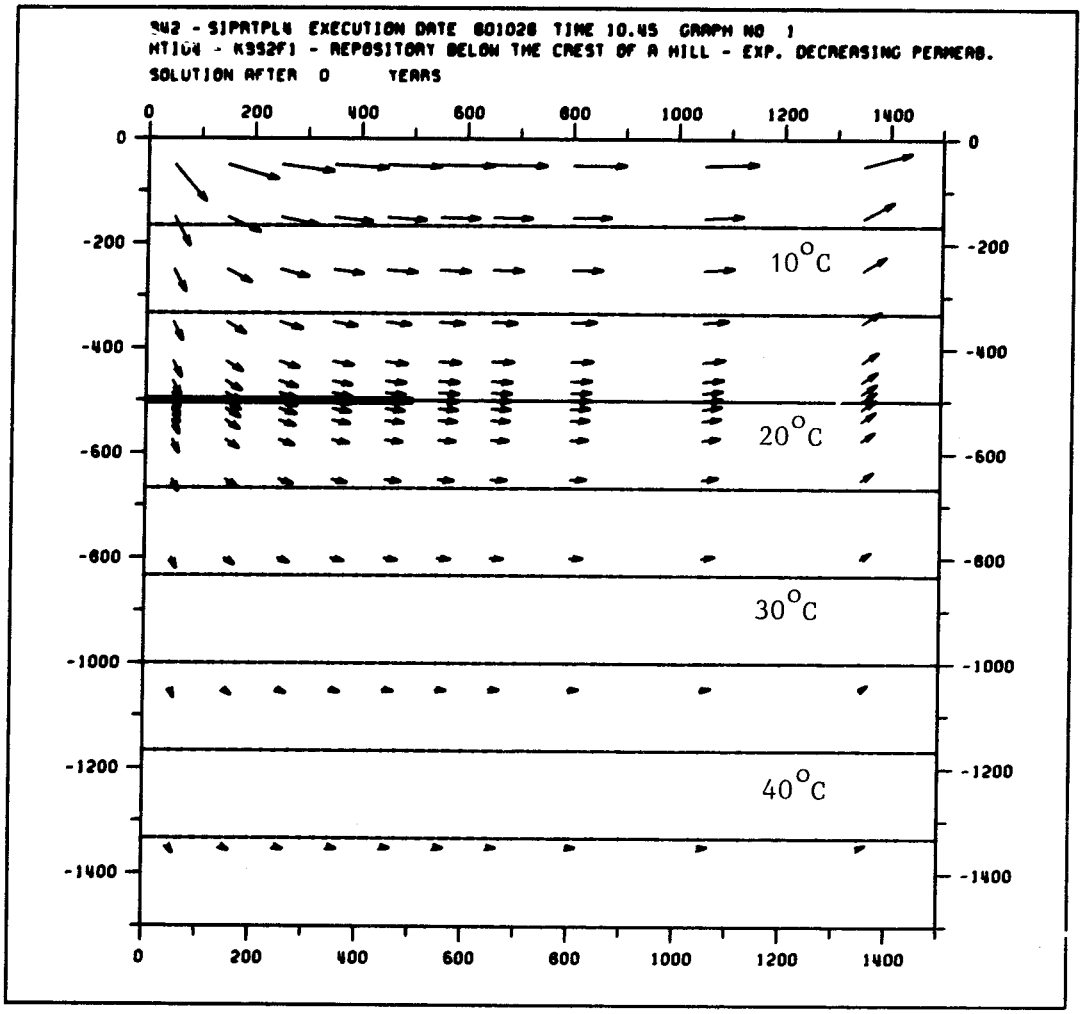

Figure 4.2.9 Groundwater fluxes and isotherms illustrating the hydrothermal flow conditions around a radioactive waste repository situated below the crest of a hill with a slope of one per mille. Permeability and porosity are exponentially decreasing with depth. Release time: 0 years.

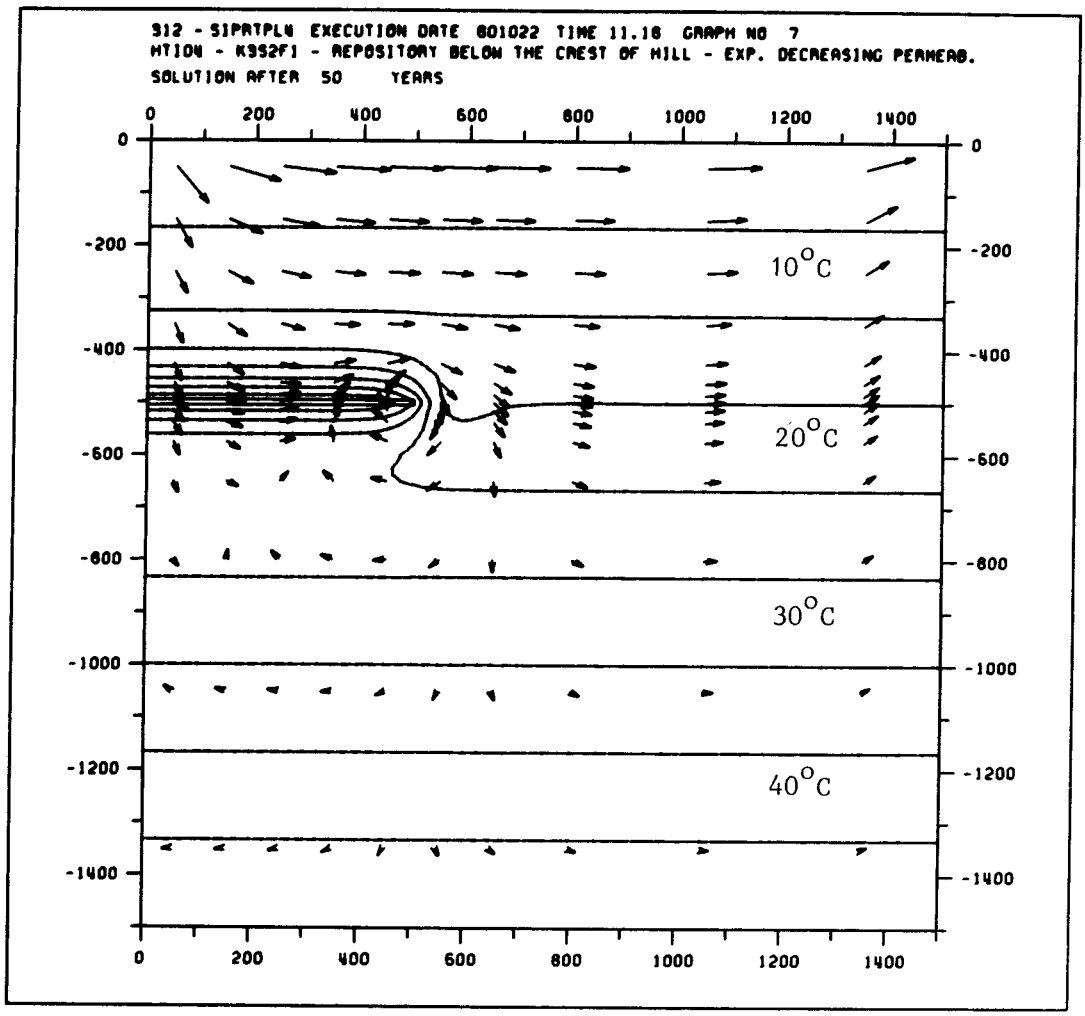

Figure 4.2.10 Groundwater fluxes and isotherms illustrating the hydrothermal flow conditions around a radioactive waste repository situated below the crest of a hill with a slope of one per mille. Permeability and porosity are exponentially decreasing with depth. Release time: 50 years.

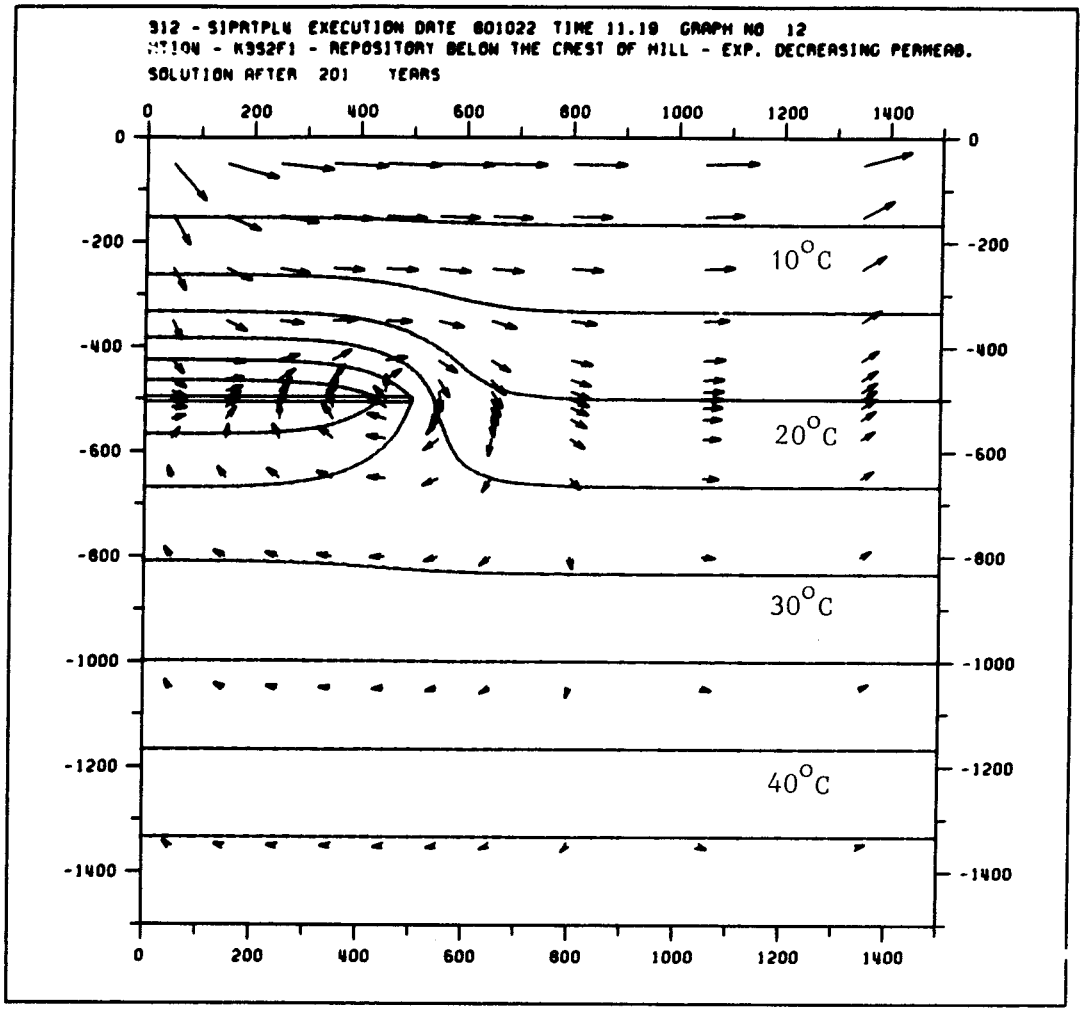

Figure 4.2.11 Groundwater fluxes and isotherms illustrating the hydrothermal flow conditions around a radioactive waste repository situated below the crest of a hill with a slope of one per mille. Permeability and porosity are exponentially decreasing with depth. Release time: 201 years.

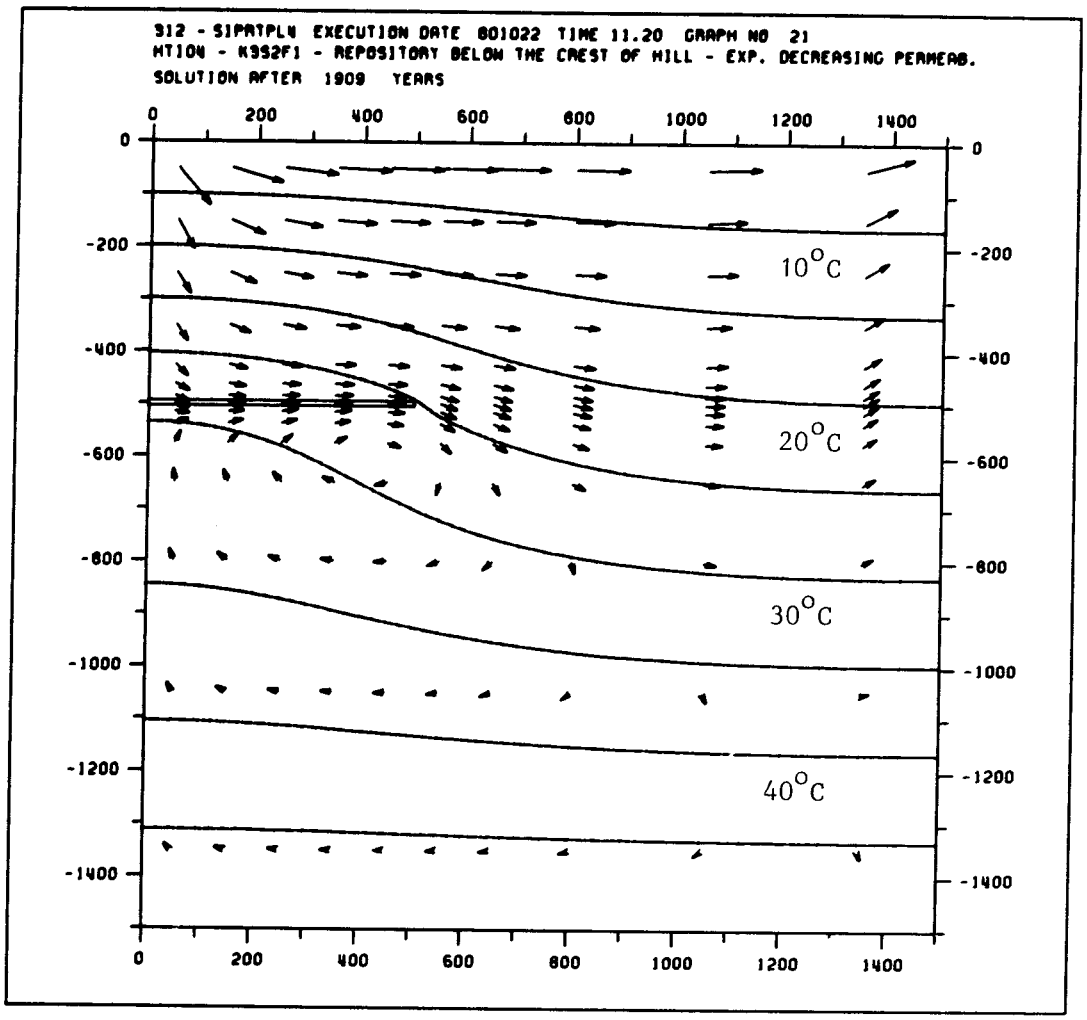

Figure 4.2.12 Groundwater fluxes and isotherms illustrating the hydrothermal flow conditions around a radioactive waste repository situated below the crest of a hill with a slope of one per mille. Permeability and porosity are exponentially decreasing with depth. Release time: 1909 years.

4.2.3 Repository located below the crest of a hill with a slope of one per cent. Constant permeability and porosity.

Exit time: > 292 years

> 250 years without the influence of a repository

The results of the pathline trace are presented in tables 4.2.5 and 4.2.6.

Pathlines for the flow conditions with the influence of a repository are displayed in figure 4.2.13.

Pathlines for the natural flow conditions without the influence of a repository are displayed in figure 4.2.14.

Groundwater fluxes and isotherms are displayed in figures 4.2.15 - 4.2.17.

In this example the slope of the hill is 10 times higher than that of the previous examples, as for the rest the assumptions are the same. The effect of the topography is the dominating one and the flow pattern is hardly affected by the heat released from the repository. However, the heat has a slight effect on the flow times, prolonging them by about 30 per cent.

Table 4.2.5 Coordinates of the starting respectively end points and the corresponding travel times in years of pathlines traced from a repository located below the crest of a hill with a slope of one per cent. Permeability and porosity are constant over the flow domain.

No	Starting point		End point		Travel time
1	0	-500	-	-	-
2	100	-500	1500	0	1510
3	200	-500	1471	0	869
4	300	-500	1450	0	567
5	400	-500	1430	0	404
6	500	-500	1408	0	292

Table 4.2.6 Coordinates of the starting respectively end points and the corresponding travel times in years of pathlines traced from a repository located below the crest of a hill with a slope of one per cent. Permeability and porosity are constant over the flow domain. No heat is released from the repository.

No	Starting point		End point		Travel time
1	0	-500	-	-	-
2	100	-500	1485	0	1150
3	200	-500	1452	0	666
4	300	-500	1426	0	448
5	400	-500	1400	0	325
6	500	-500	1381	0	250

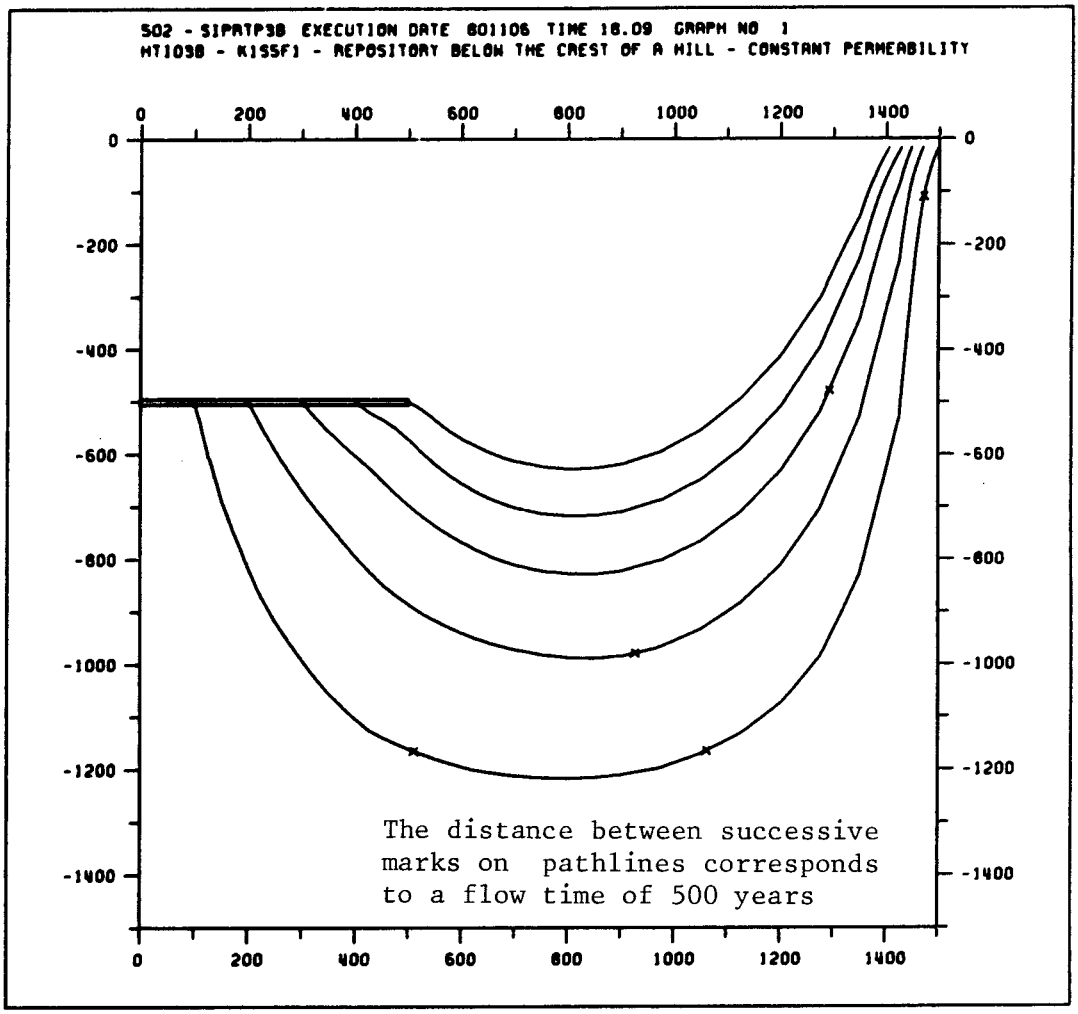

Figure 4.2.13 Pathlines for the flow conditions with the influence of a repository located below the crest of a hill with a slope of the hillsides of one per cent. Permeability and porosity are constant.

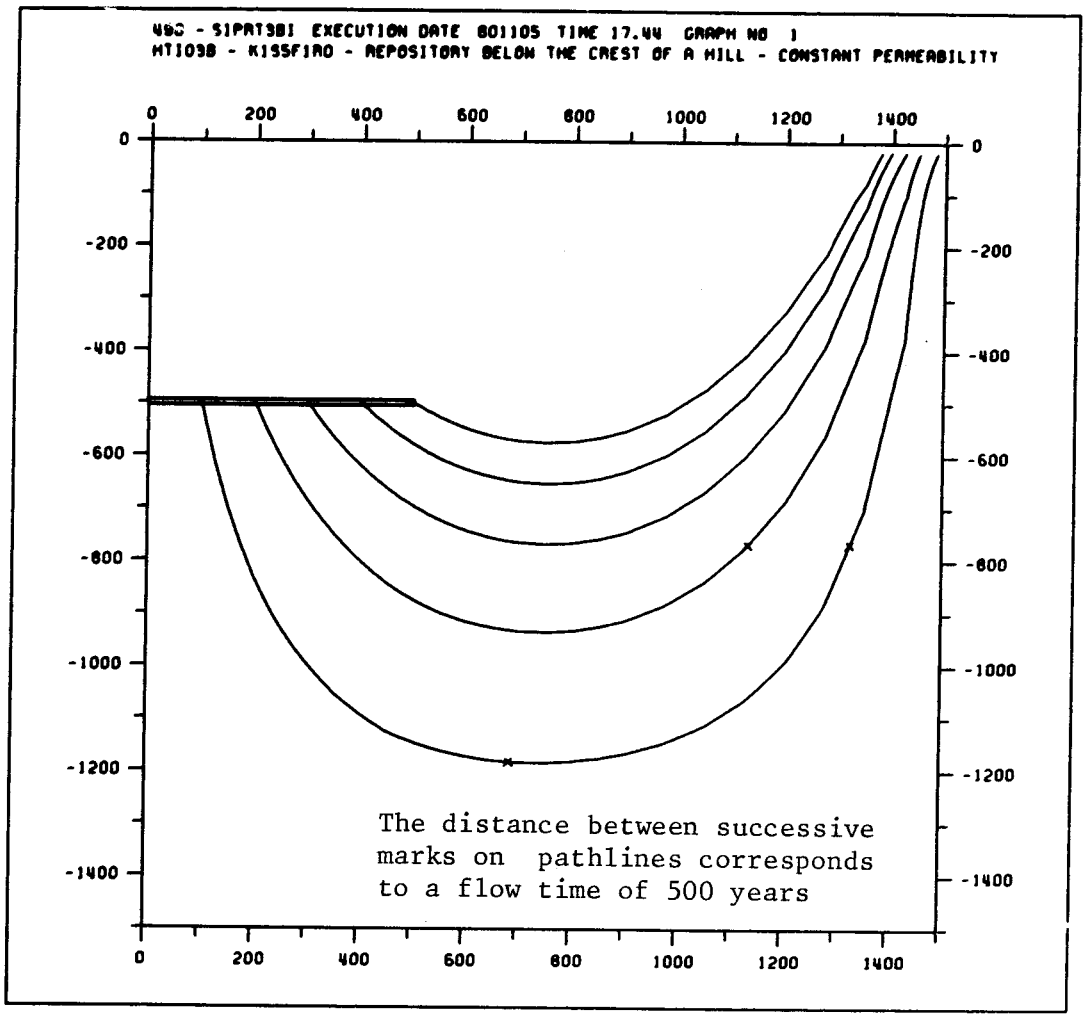

Figure 4.2.14 Pathlines for the natural flow conditons below the crest of a hill with a slope of one per cent. Permeability and porosity are constant.

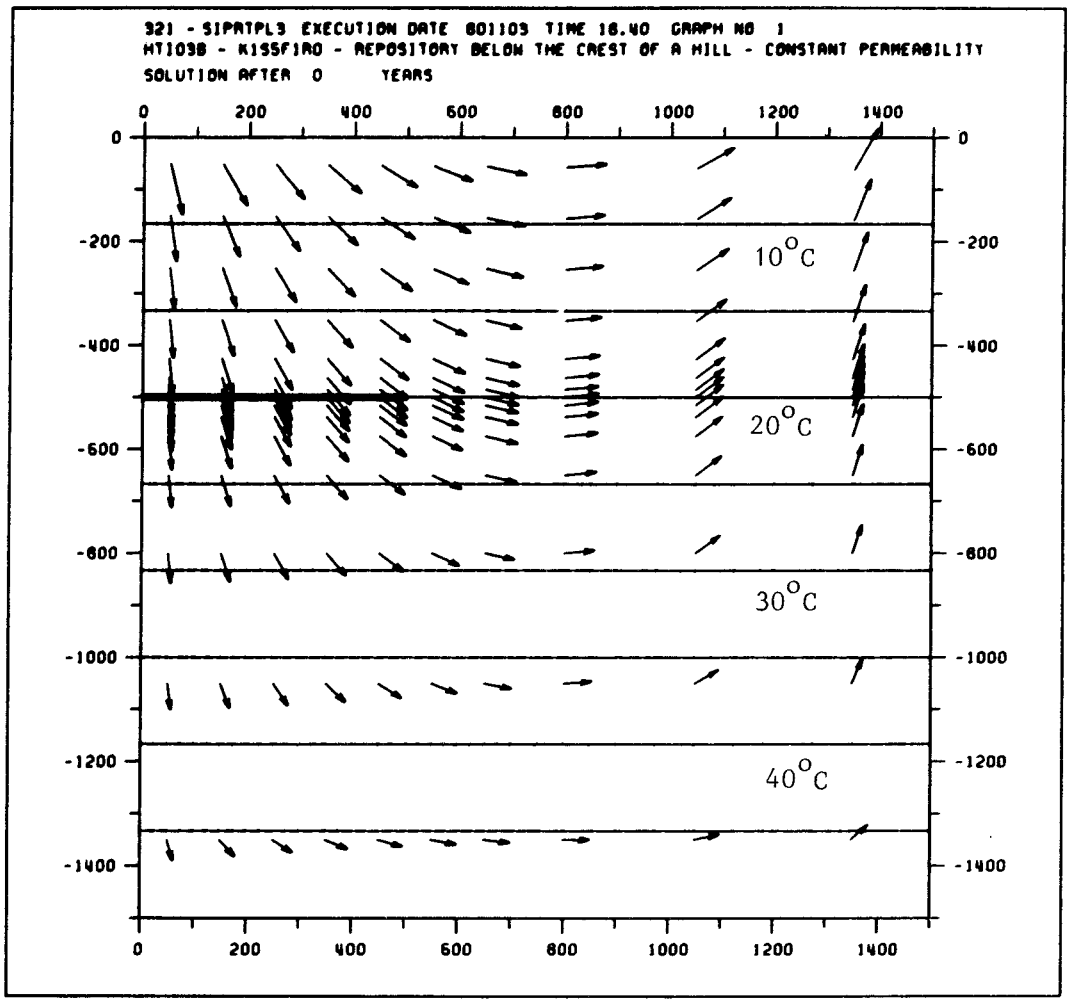

Figure 4.2.15 Groundwater fluxes and isotherms illustrating the hydrothermal flow conditions around a radioactive waste repository situated below the crest of a hill with a slope of one per cent. Permeability and porosity are constant over the flow domain. Release time: 0 years.

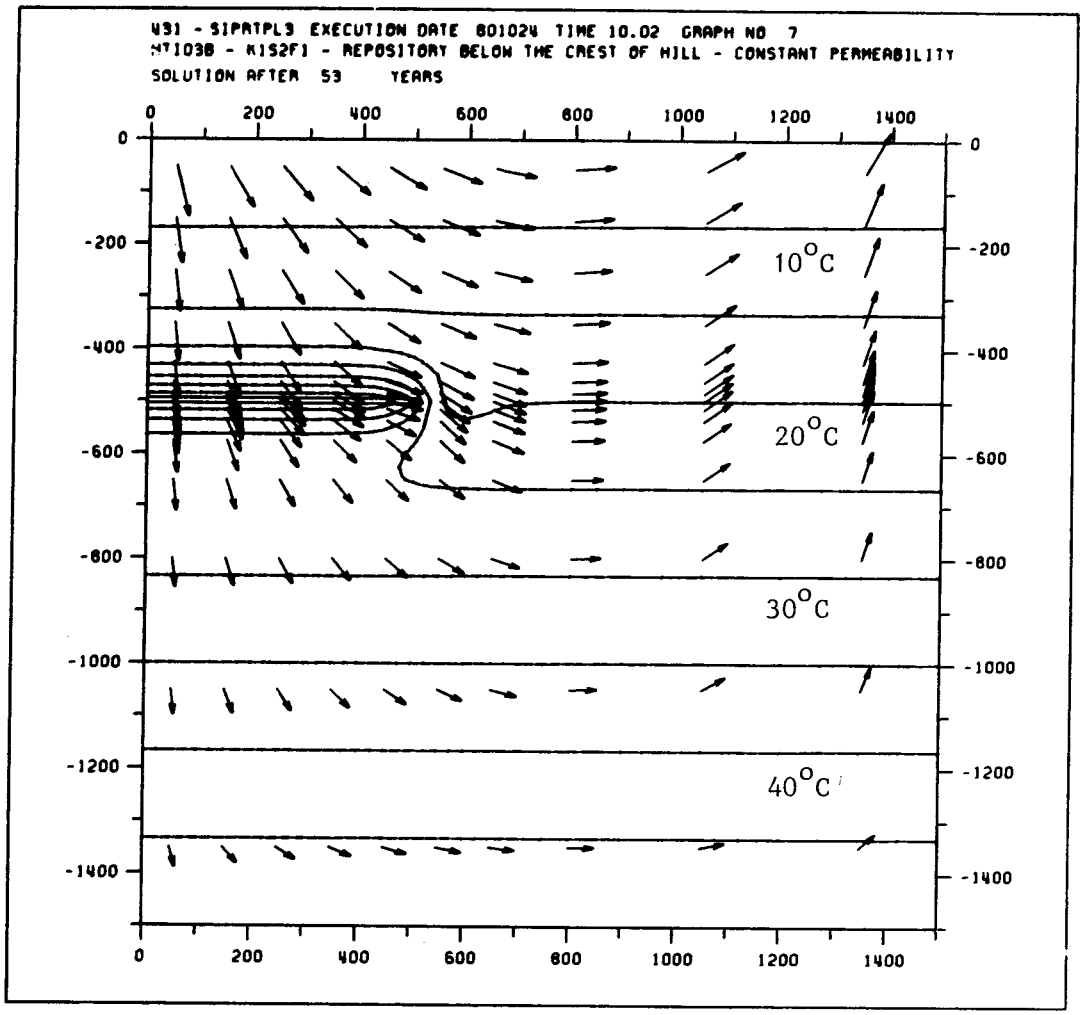

Figure 4.2.16 Groundwater fluxes and isotherms illustrating the hydrothermal flow conditions around a radioactive waste repository situated below the crest of a hill with a slope of one per cent. Permeability and porosity are constant over the flow domain. Release time: 53 years.

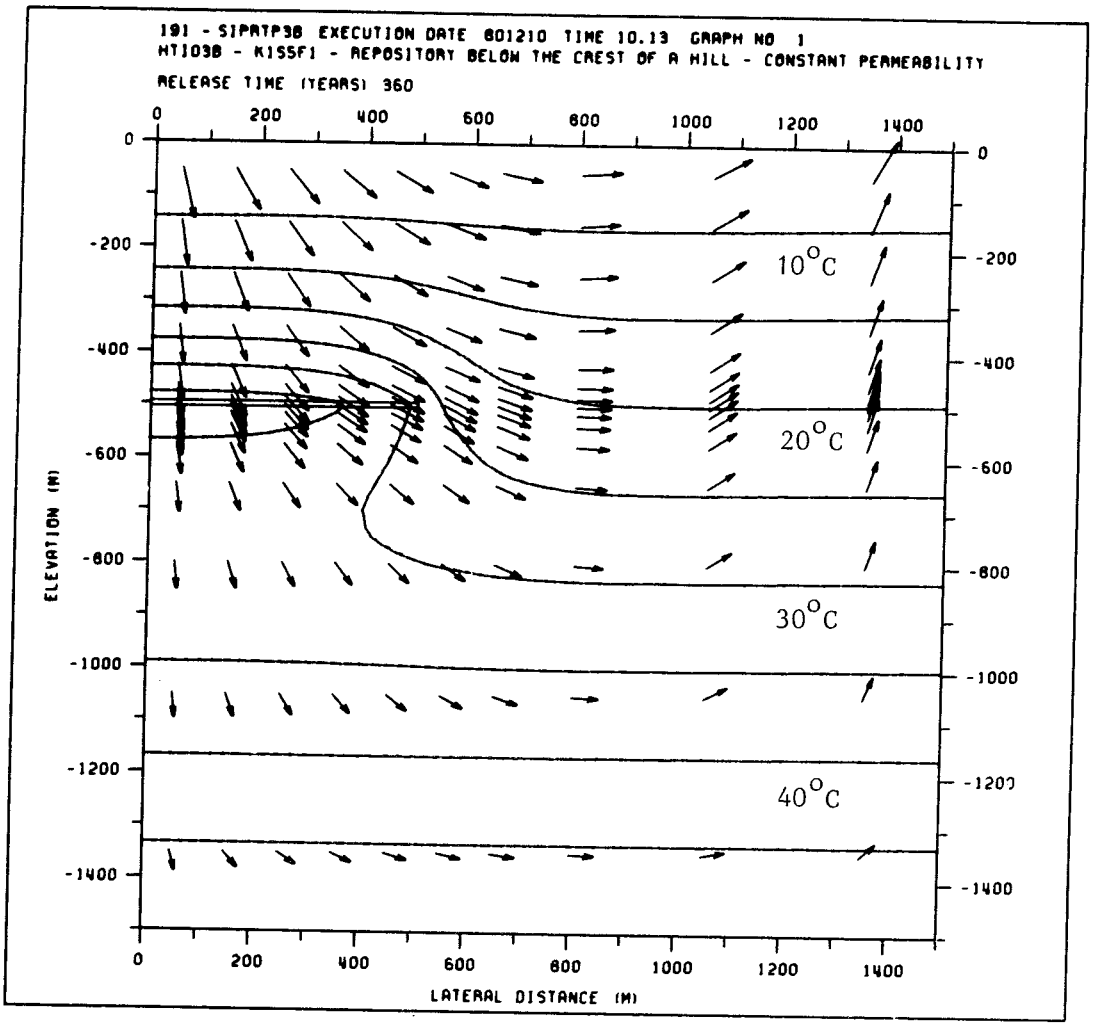

Figure 4.2.17 Groundwater fluxes and isotherms illustrating the hydrothermal flow conditions around a radioactive waste repository situated below the crest of a hill with a slope of one per cent. Permeability and porosity are constant over the flow domain. Release time: 360 years.

4.2.4 Repository located below the crest of a hill with a slope of one per cent. Permeability and porosity are exponentially decreasing with depth.

Exit time: > 222 years

> 218 years without the influence of a repository

The results of the pathline trace are presented in tables 4.2.7 and 4.2.8.

Pathlines for the flow conditions with the influence of a repository are presented in figure 4.2.18.

Pathlines for the natural flow conditions with the influence of a repository are presented in figure 4.2.19.

Groundwater fluxes and isotherms are displayed in figures 4.2.20 - 4.2.22.

In this example, the slope of the hill is the same as in the previous one, that is to say one per cent, but permeability and porosity are exponentially decreasing with depth. The effect of the heat released from the repository is practically negligible. A very small increase in the flow times can be observed. The effect of the exponential decrease in permeability and porosity with depth is that the flow times from the repository to the ground surface become less.

Table 4.2.7 Coordinates of the starting respectively end points and the corresponding travel times in years of path-lines traced from a radioactive repository located below the crest of a hill with a slope of one per cent. Permeability and porosity are exponentially decreasing with depth.

No	Starting point		End point		Travel time
1	0	-500	1500	0	579
2	100	-500	1500	0	325
3	200	-500	1500	0	284
4	300	-500	1500	0	258
5	400	-500	1500	0	234
6	500	-500	1500	0	222

Table 4.2.8 Coordinates of the starting respectively end points and the corresponding travel times in years of path-lines traced from a repository located below the crest of a hill with a slope of one per cent. Permeability and porosity are exponentially decreasing with depth. No heat is released from the repository.

No	Starting point		End point		Travel time
1	0	-500	1500	0	546
2	100	-500	1500	0	322
3	200	-500	1500	0	281
4	300	-500	1500	0	255
5	400	-500	1500	0	237
6	500	-500	1500	0	218

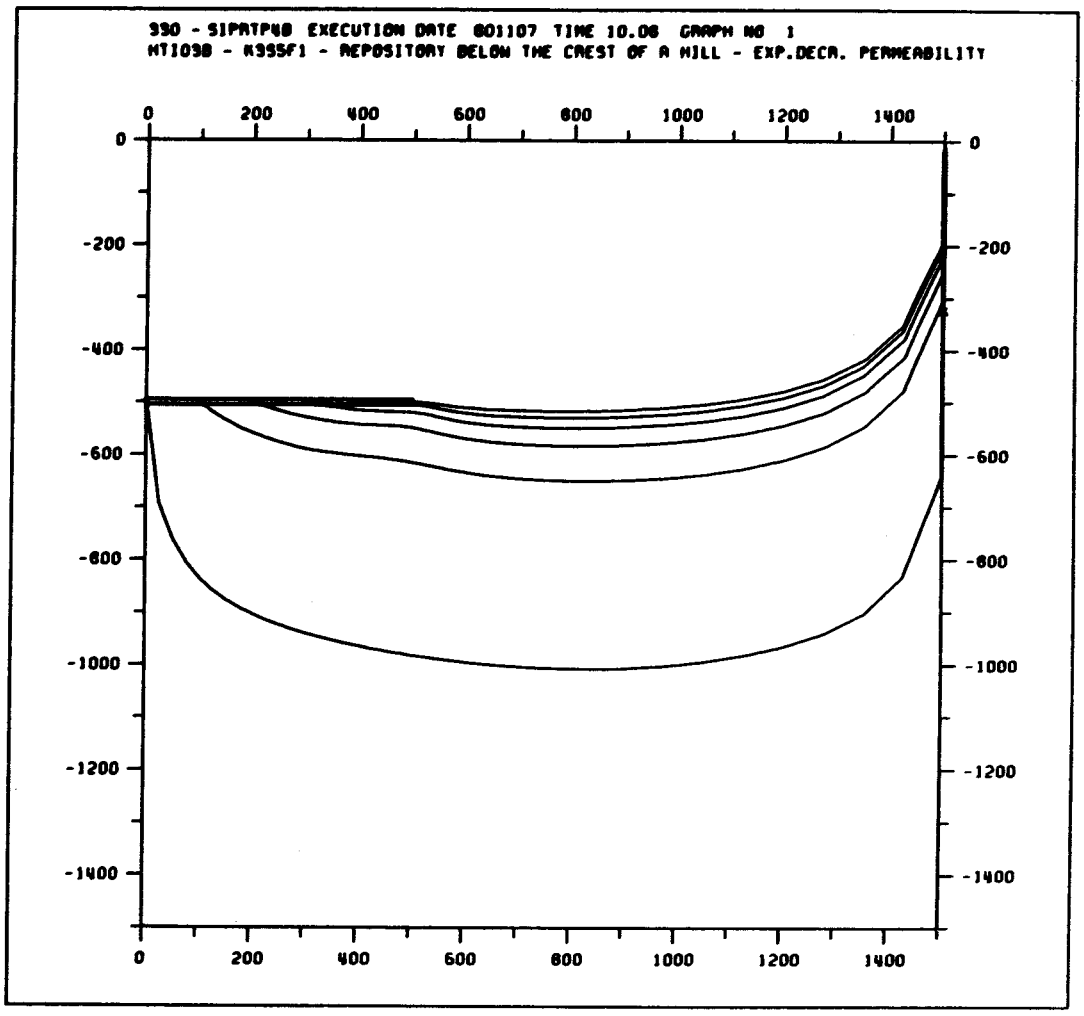

Figure 4.2.18 Pathlines for the flow conditions with the influence of a repository located below the crest of a hill with a slope of one per cent. Permeability and porosity are exponentially decreasing with depth.

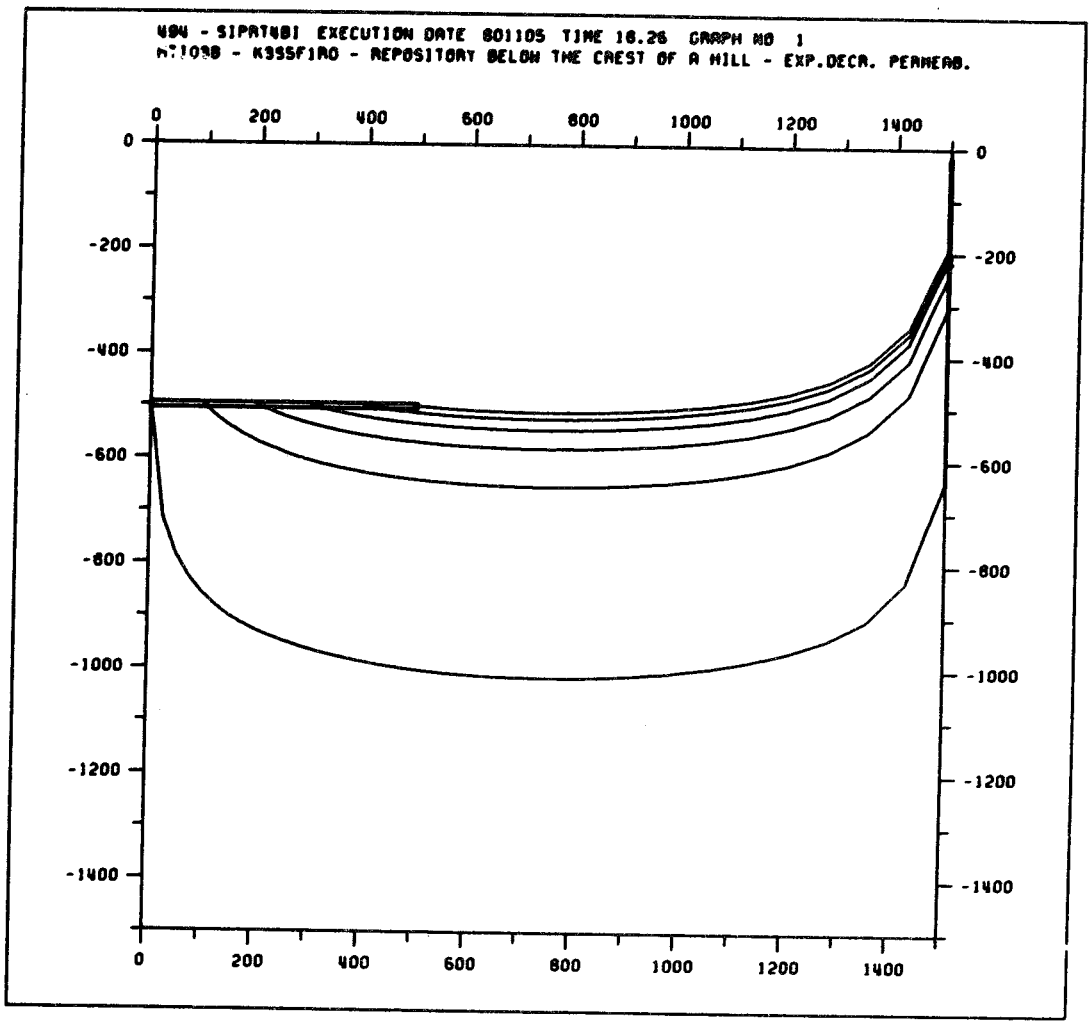

Figure 4.2.19 Pathlines for the natural flow conditions below the crest of a hill with a slope of one per cent. Permeability and porosity are exponentially decreasing with depth.

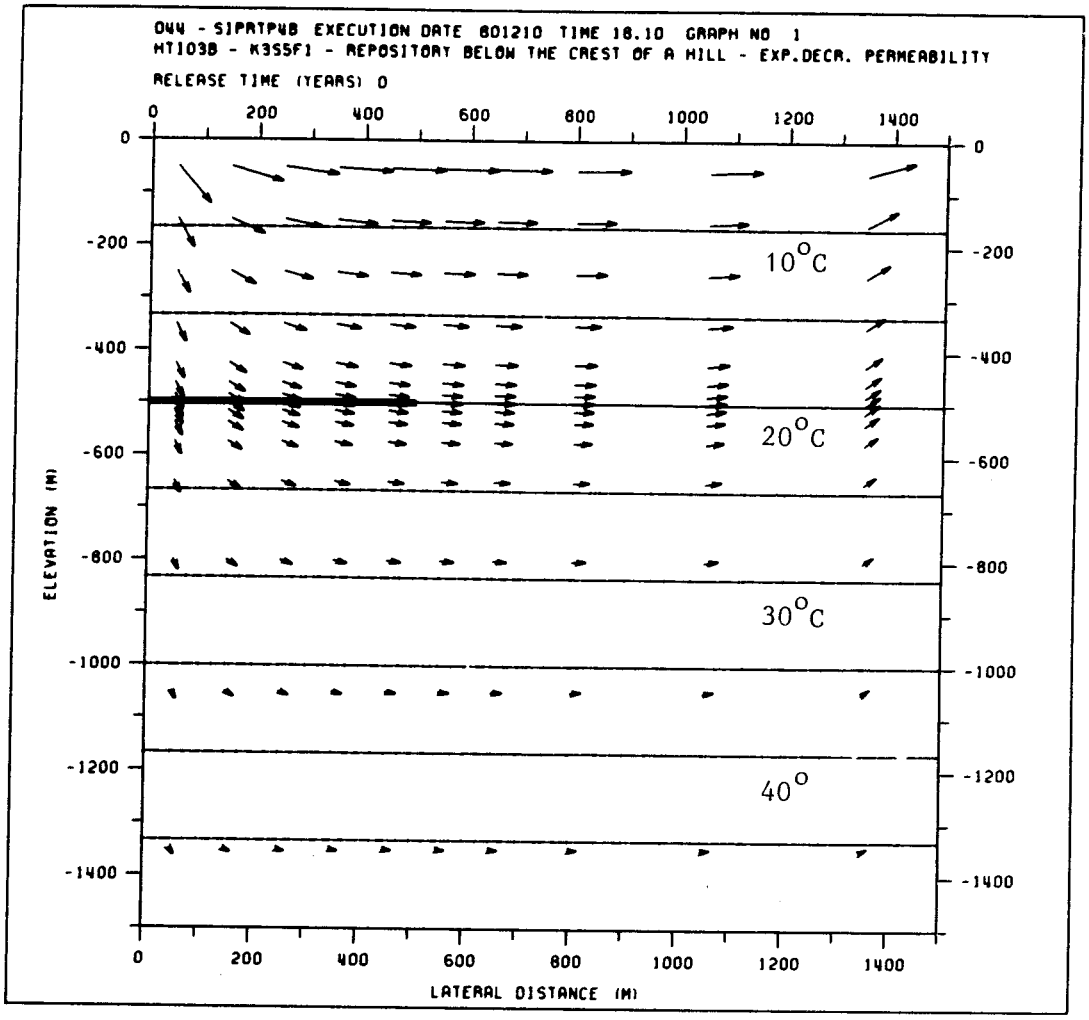

Figure 4.2.20 Groundwater fluxes and isotherms illustrating the hydrothermal flow conditions around a radioactive waste repository situated below the crest of a hill with a slope of one per cent. Permeability and porosity are exponentially decreasing with depth. Release time: 0 years.

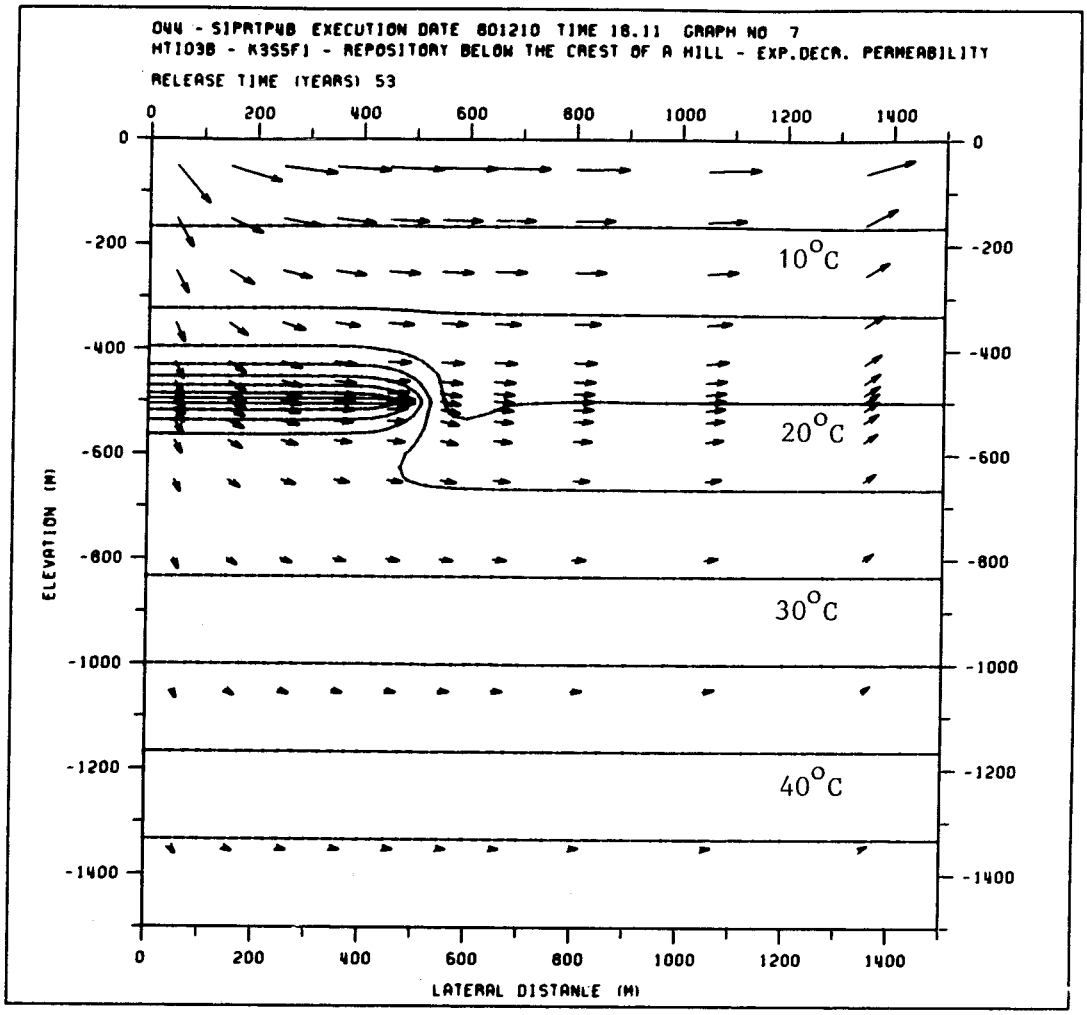

Figure 4.2.21 Groundwater fluxes and isotherms illustrating the hydrothermal flow conditions around a radioactive waste repository situated below the crest of a hill with a slope of one per cent. Permeability and porosity are exponentially decreasing with depth. Release time: 53 years.

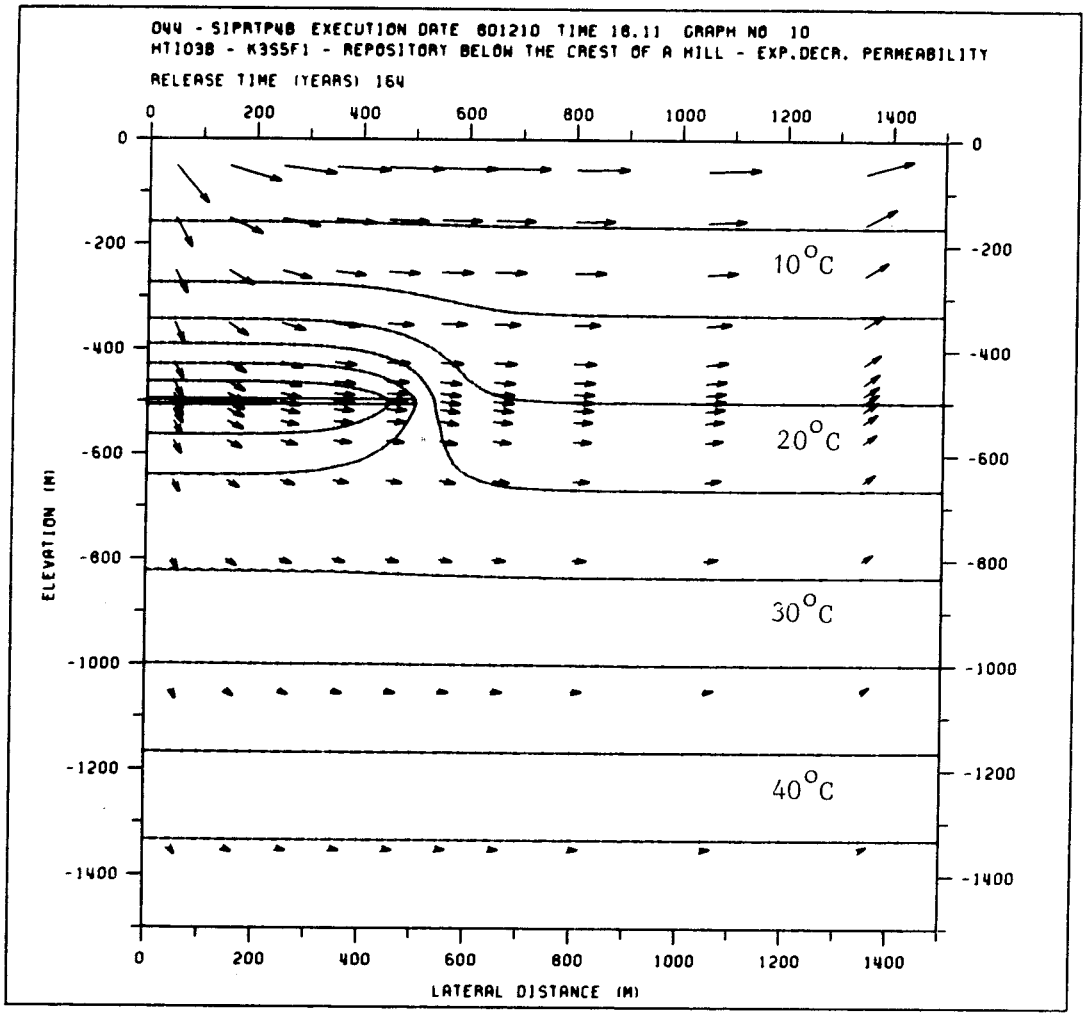

Figure 4.2.22 Groundwater fluxes and isotherms illustrating the hydrothermal flow conditions around a radioactive waste repository situated below the crest of a hill with a slope of one per cent. Permeability and porosity are exponentially decreasing with depth. Release time: 164 years.

4.3 Repository located below a hillside

This case deals with a repository located below a hillside with a slope of one per mille. Two examples have been worked out.

In the first example, permeability and porosity are constant over the flow domain. In the initial stage in this example, the repository is subject to downward groundwater movements in one part of the repository and upward movements in another part. Convective currents are created at both edges of the repository as a result of the heat released from it.

In the second example permeability and porosity are exponentially decreasing with depth over the flow domain. In this example, the initial groundwater flow pattern is characterized by horizontal groundwater flow in most parts of the flow domain. Convective currents are formed only at the downstream edge of the repository.

4.3.1 Repository located below a hillside with a slope of one per mille. Constant permeability and porosity.

Exit time: > 625 years

> 900 years without the influence of a repository

The results of the pathline trace are presented in tables 4.3.1 and 4.3.2.

Pathlines for the flow conditions with the influence of a repository are displayed in figure 4.3.1.

Pathlines for the natural flow conditions without the influence of a repository are presented in figure 4.3.2.

Groundwater fluxes and isotherms are displayed in figures 4.3.3 - 4.3.6.

In this example, the flow pattern is significantly modified by the heat particularly in the vicinity of the repository. The groundwater is being pushed up around the repository by the heat, reducing the flow times to the ground surface. Under undisturbed conditions the shortest flow time from the repository to the ground surface is obtained starting at the dowstream edge of the repository. With the effect of the heat released from the repository, the longest flow time is obtained at this point. This is due to the convection cell being created at the downstream edge of the repository. A convection cell is also formed at the upstream edge of the repository, resulting in longer flow times for water particles starting in this area. The effect of the heat is most obvious for water particles starting upstream and at the centre of the repository. In this region the flow times are reduced to about half the flow times under undisturbed conditions. The shortest

exit time from the repository to the ground surface is about 30 per cent less owing to the heat released from the repository.

Table 4.3.1 Coordinates of the starting respectively end points and the corresponding travel times in years of pathlines traced from a repository located below a hillside with a slope of one per mille. Permeability and porosity are constant over the flow domain.

No	Starting point		End point		Travel time
1	-500	-500	-74	0	1475
2	-400	-500	-46	0	850
3	-300	-500	141	0	650
4	-200	-500	298	0	626
4	-100	-500	455	0	637
6	0	-500	650	0	707
7	100	-500	917	0	876
8	200	-500	1143	0	1033
9	300	-500	1321	0	1275
10	400	-500	1419	0	1968
11	500	-500	1485	0	5952

Table 4.3.2 Coordinates of the starting respectively end points and the corresponding travel times in years of pathlines traced from a repository located below a hillside with a slope of one per mille. Permeability and porosity are constant over the flow domain. No heat is released from the repository.

No	Starting point		End point		Travel time
1	-500	-500	1071	0	2520
2	-400	-500	1041	0	2280
3	-300	-500	1016	0	2070
4	-100	-500	1005	0	1880
5	-100	-500	995	0	1710
6	0	-500	990	0	1540
7	100	-500	993	0	1400
8	200	-500	1004	0	1270
9	300	-500	1016	0	1140
10	400	-500	1039	0	3220
11	500	-500	1068	0	935

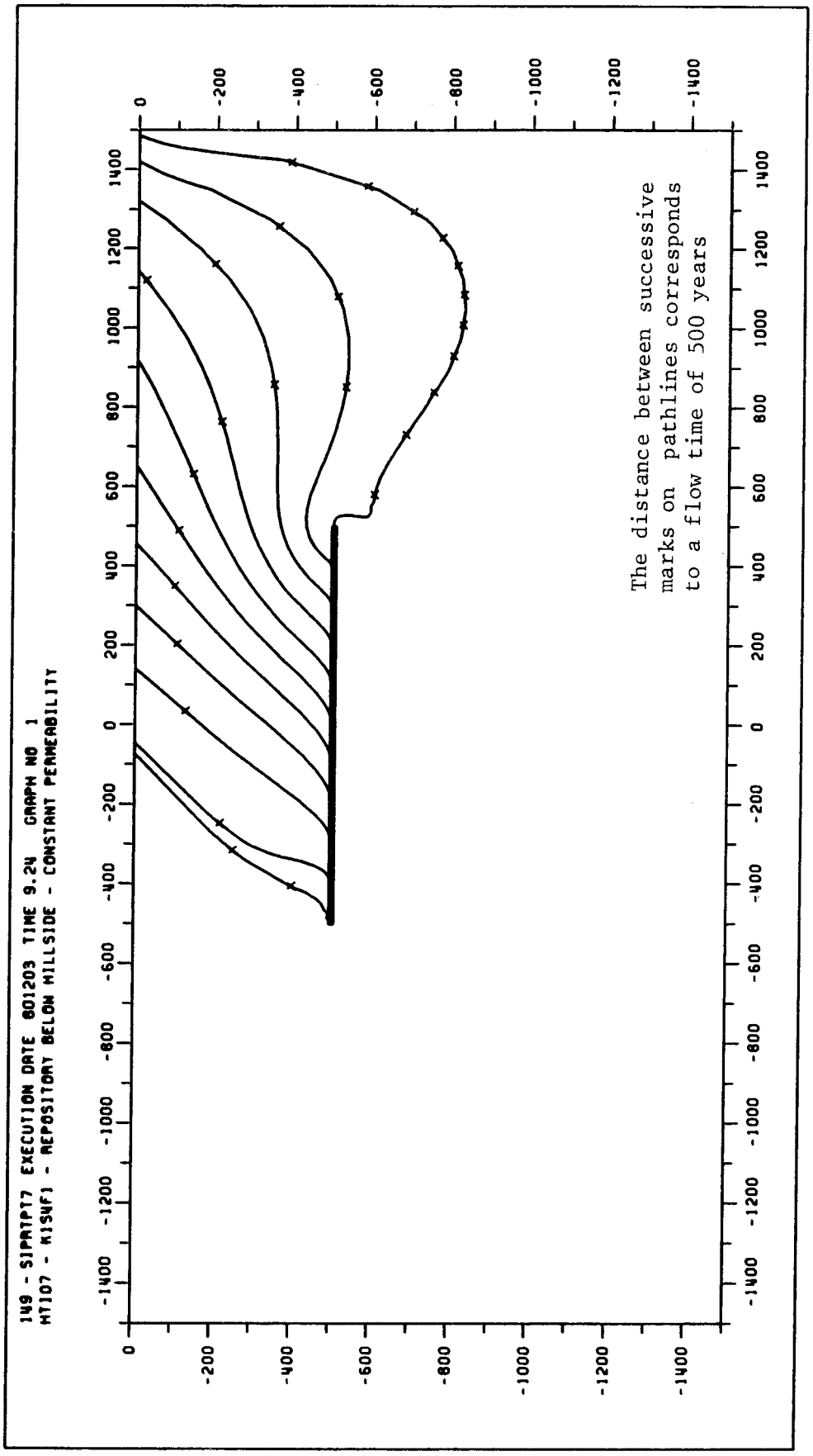

Figure 4.3.1 Pathlines for the flow conditions with the influence of a repository located below a hillside with a slope of one per mille. Permeability and porosity are constant.

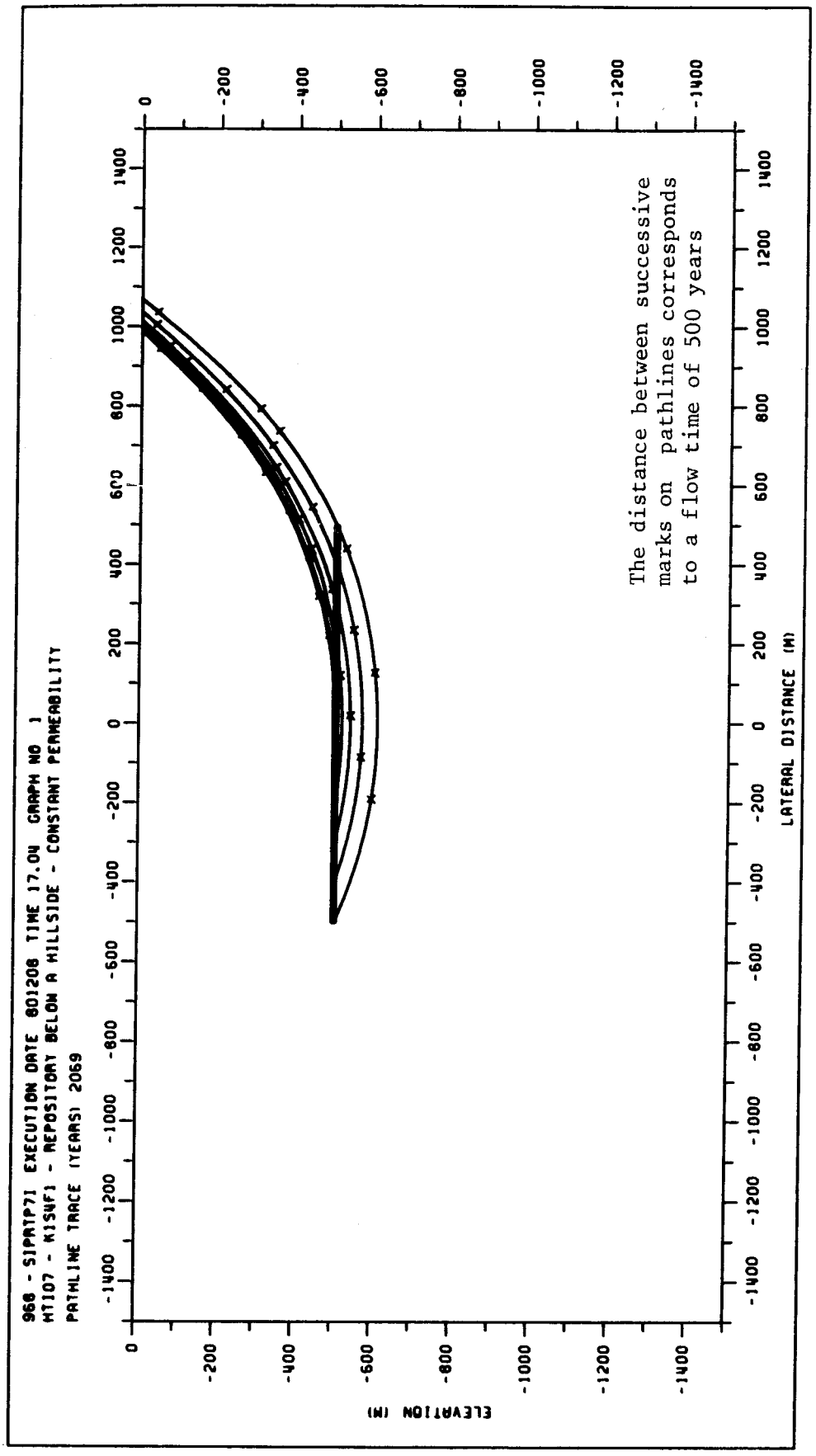

Figure 4.3.2 Pathlines for the natural flow conditions below a hillside with a slope of one per mille. Peremability and porosity are constant.

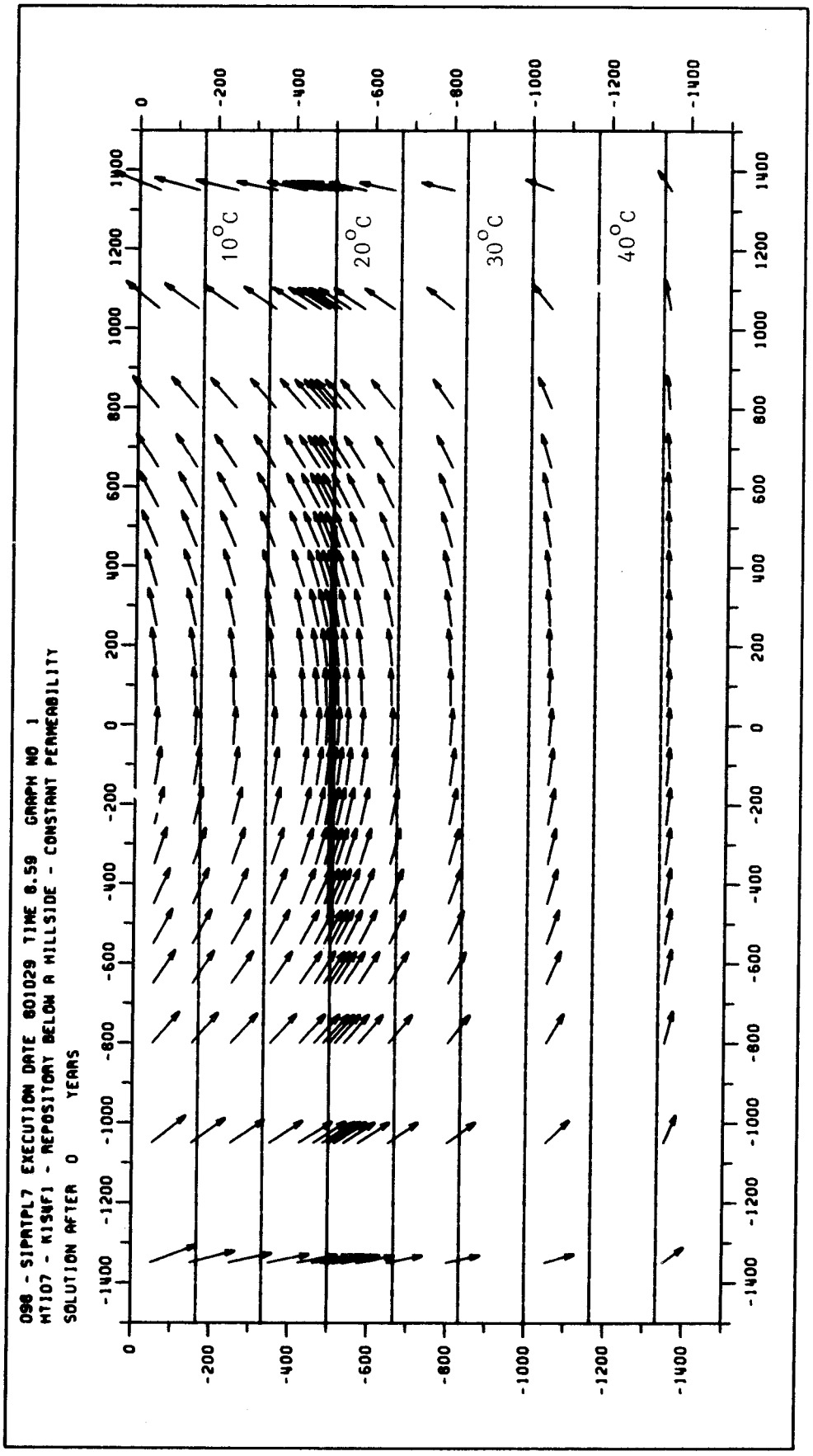

Figure 4.3.3 Groundwater fluxes and isotherms illustrating the hydrothermal flow conditions around a radioactive waste repository located below a hillside with a slope of one per mille. Peremability and porosity are constant. Release time: 0 years.

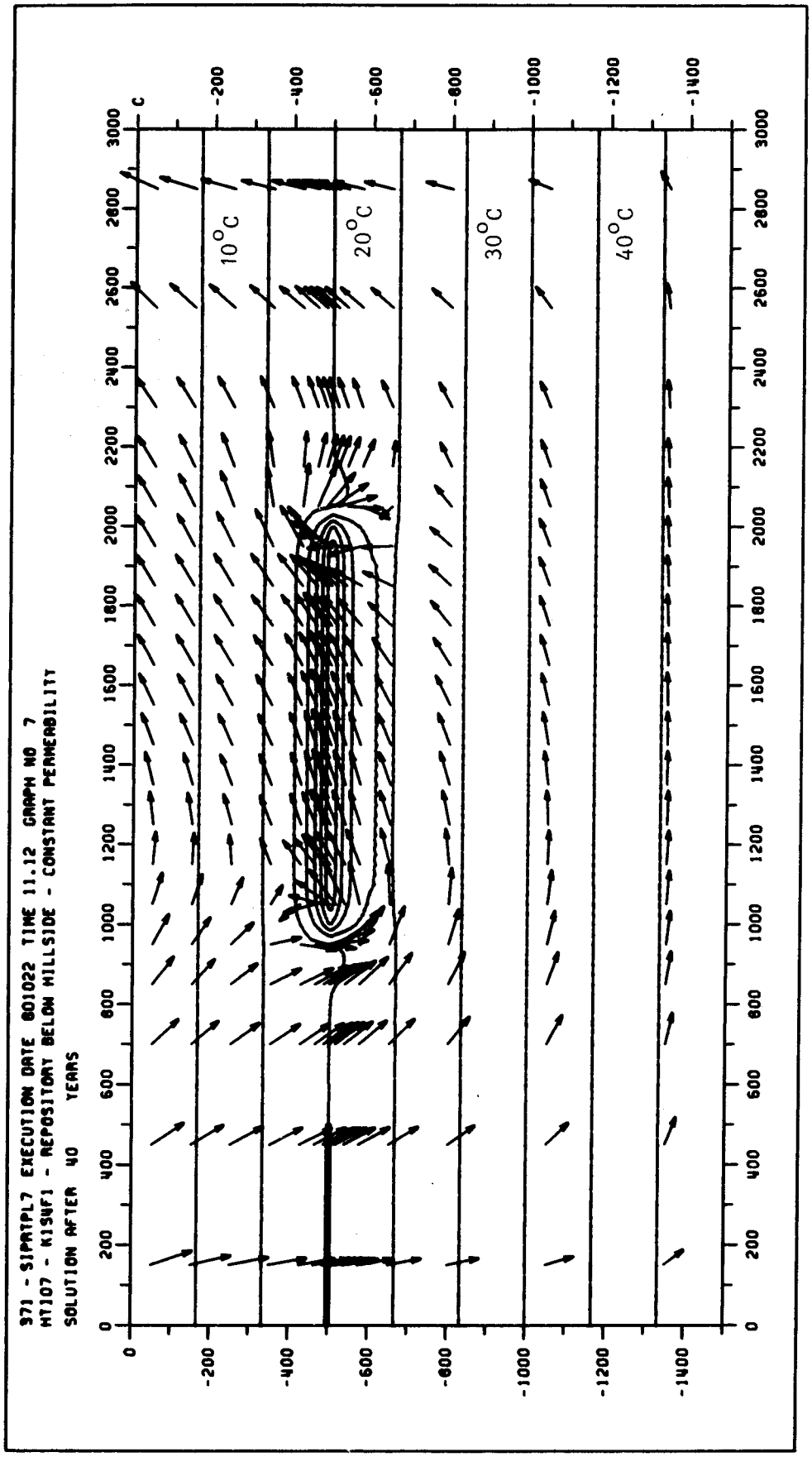

Figure 4.3.4 Groundwater fluxes and isotherms illustrating the hydrothermal flow conditions around a radioactive waste repository located below a hillside with a slope of one per mille. Peremability and porosity are constant. Release time: 40 years.

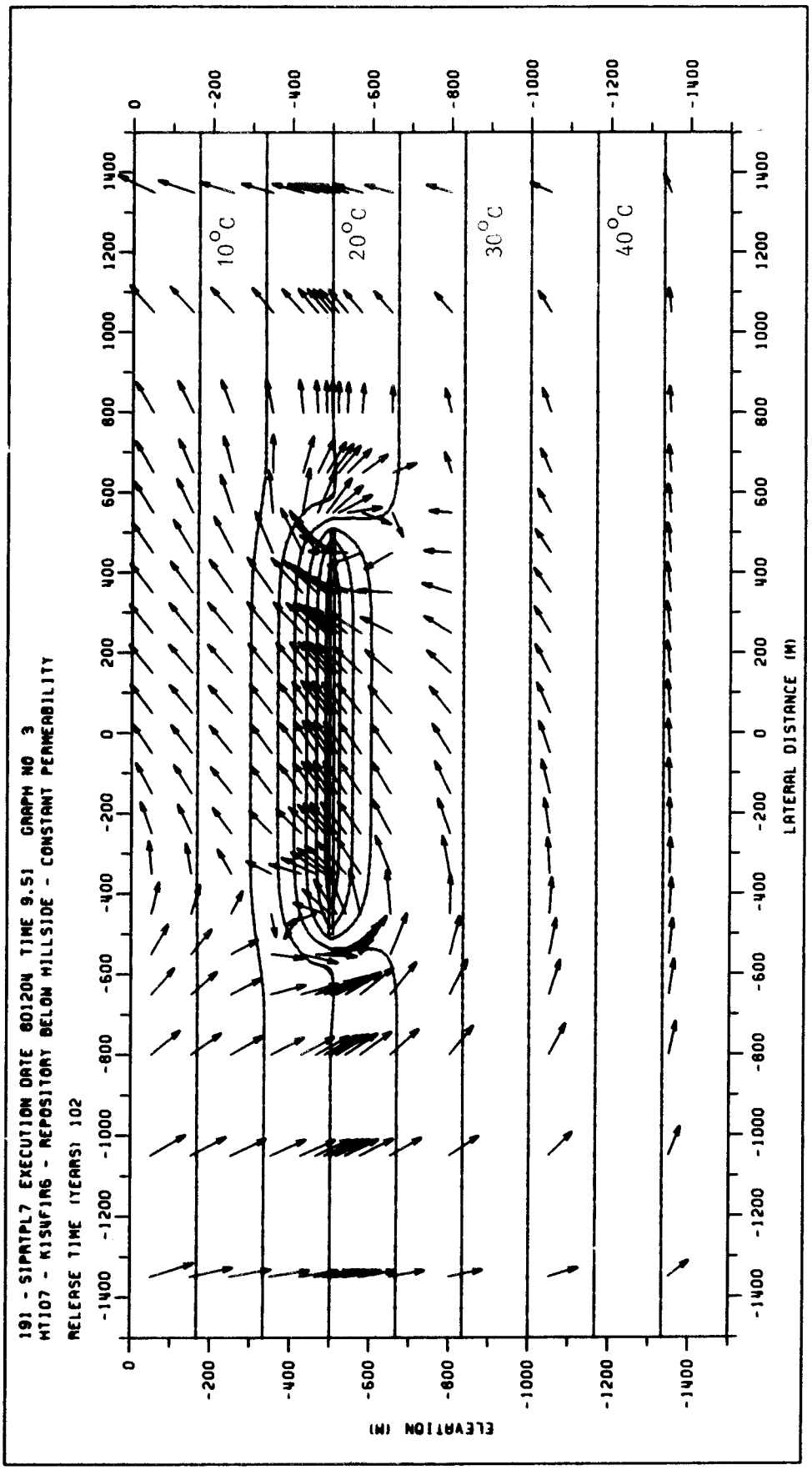

Figure 4.3.5 Groundwater fluxes and isotherms illustrating the hydrothermal flow conditions around a radioactive waste repository located below a hillside with a slope of one per mille. Peremability and porosity are constant. Release time: 102 years.

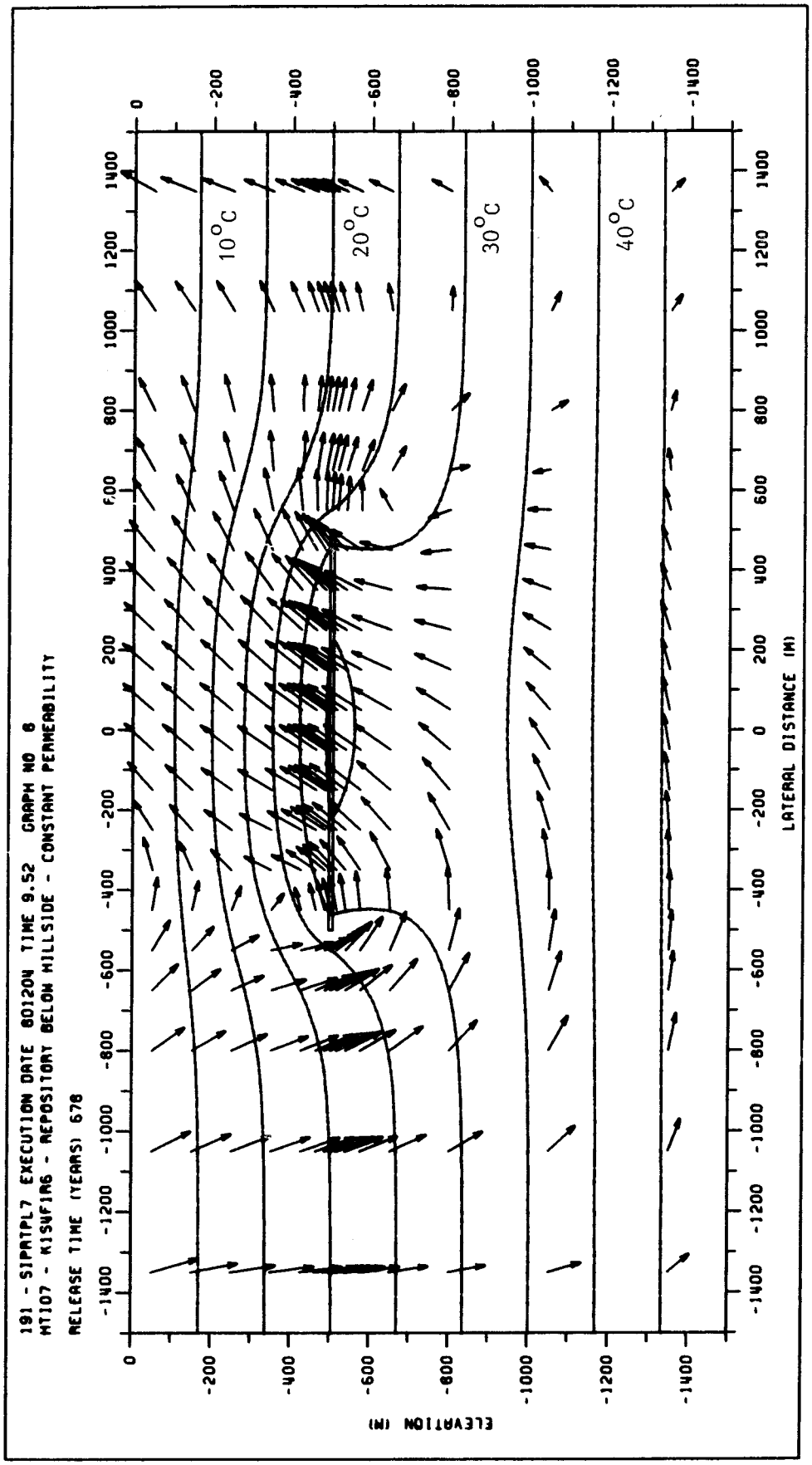

Figure 4.3.6 Groundwater fluxes and isotherms illustrating the hydrothermal flow conditions around a radioactive waste repository located below a hillside with a slope of one per mille. Peremability and porosity are constant. Release time: 678 years.

4.3.2 Repository located below a hillside with a slope of one per mille. Permeability and porosity are exponentially decreasing with depth.

Exit time: > 2500 years

> 2100 years without the influence of a repository

The results of the pathline trace are presented in tables 4.3.3 and 4.3.4.

Pathlines for the flow conditions with the influence of a repository are displayed in figure 4.3.7.

Pathlines for the natural flow conditions without the influence of a repository are displayed in figure 4.3.8.

Groundwater fluxes and isotherms are displayed in figures 4.3.9 - 4.3.12.

In this example, the effect of the heat is less apparent than in the previous example, in which permeability and porosity were constant over the flow domain. At the repository the effect of the heat is to uplift the water particles. Downstream the repository, there is a tendency to draw down the pathlines when aproaching the lateral boundary, before turing up at the ground surface. The effect of the heat on the flow times is very small, with the xception of the flow times for water particles starting at the downstream edge, where local convection currents are induced, approximately doubling the flow times.

Table 4.3.3 Coordinates of the starting respectively end points and the corresponding travel times in years of pathlines traced from a repository located below a hillside with a slope of one per mille. Permeability and porosity are exponentially decreasing with depth.

No	Starting point		End point		Travel time
1	-500	-500	1500	0	2907
2	-400	-500	1500	0	2483
3	-300	-500	1500	0	2803
4	-200	-500	1500	0	3016
5	-100	-500	1500	0	2908
6	0	-500	1500	0	2985
7	100	-500	1500	0	3077
8	200	-500	1500	0	3324
9	300	-500	1500	0	5075
10	400	-500	1500	0	4188
11	500	-500	1500	0	4948

Table 4.3.4 Coordinates of the starting respectively end points and the corresponding travel times in years of pathlines traced from a repository located below a hillside with a slope of one per mille. Permeability and porosity are exponentially decreasing with depth. No heat is released from the repository.

No	Starting point		End point		Travel time
1	-500	-500	155	0	3160
2	-400	-500	209	0	3050
3	-300	-500	385	0	2960
4	-200	-500	641	0	2840
5	-100	-500	1000	0	2750
6	0	-500	1500	0	2630
7	100	-500	1500	0	2550
8	200	-500	1500	0	2450
9	300	-500	1500	0	2360
10	400	-500	1500	0	2260
11	500	-500	1500	0	2170

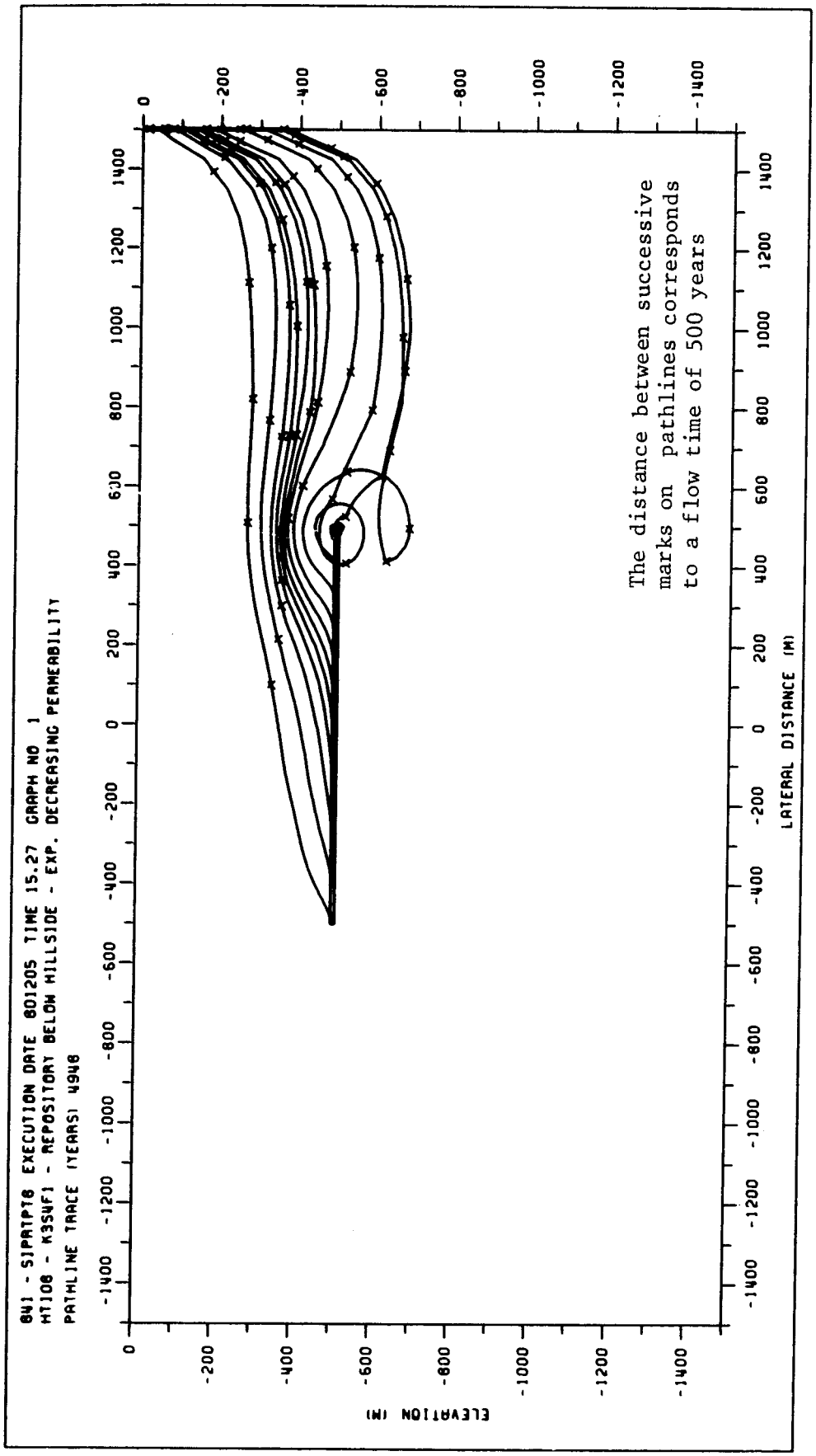

Figure 4.3.7 Pathlines for the flow conditons with the influence of a repository located below a hillside with a slope of one per mille. Permeability and porosity are exponentially decreasing with depth.

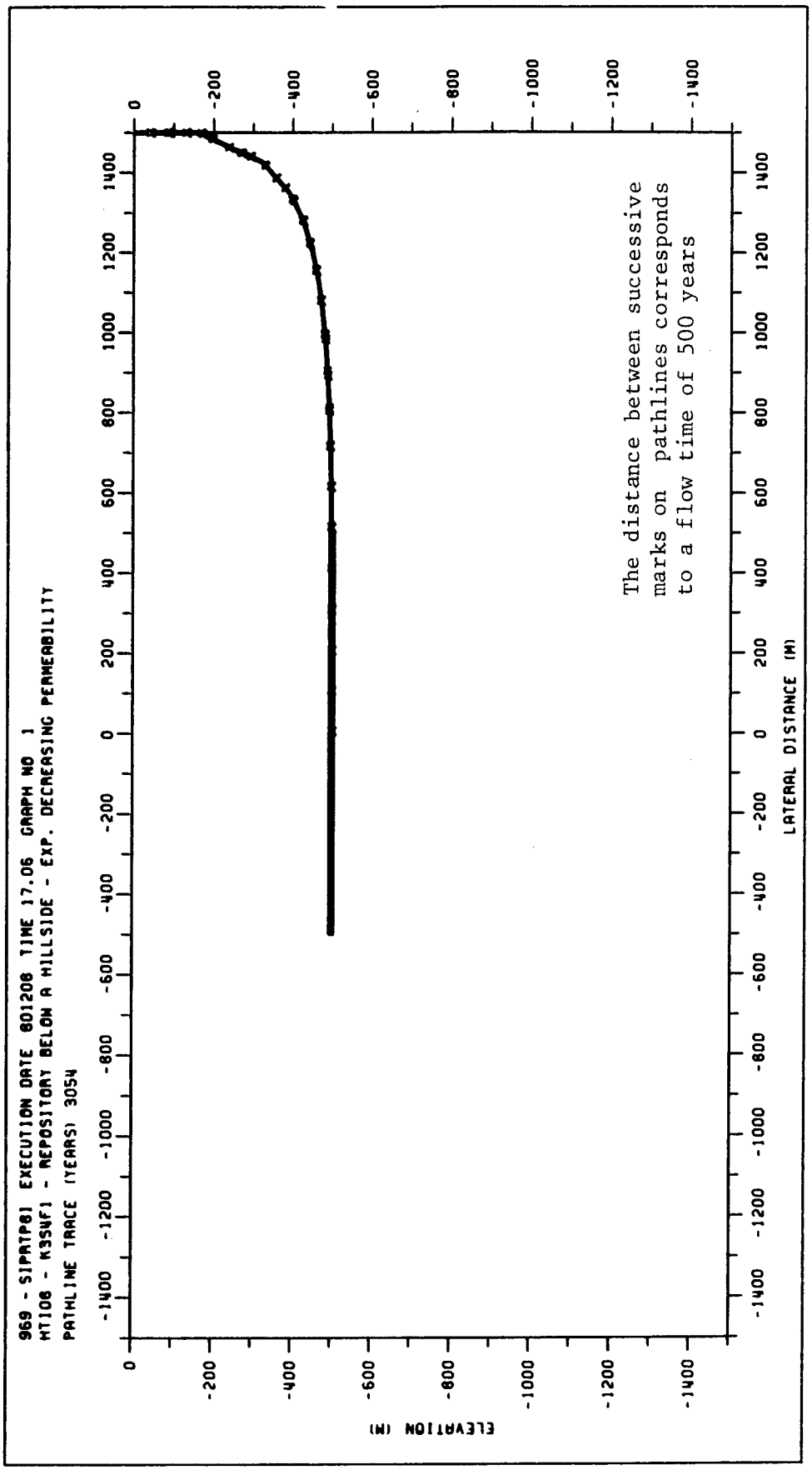

Figure 4.3.8 Pathlines for the natural flow conditons below a hillside with a slope of one per mille. Permeability and porosity are exponentially decreasing with depth.

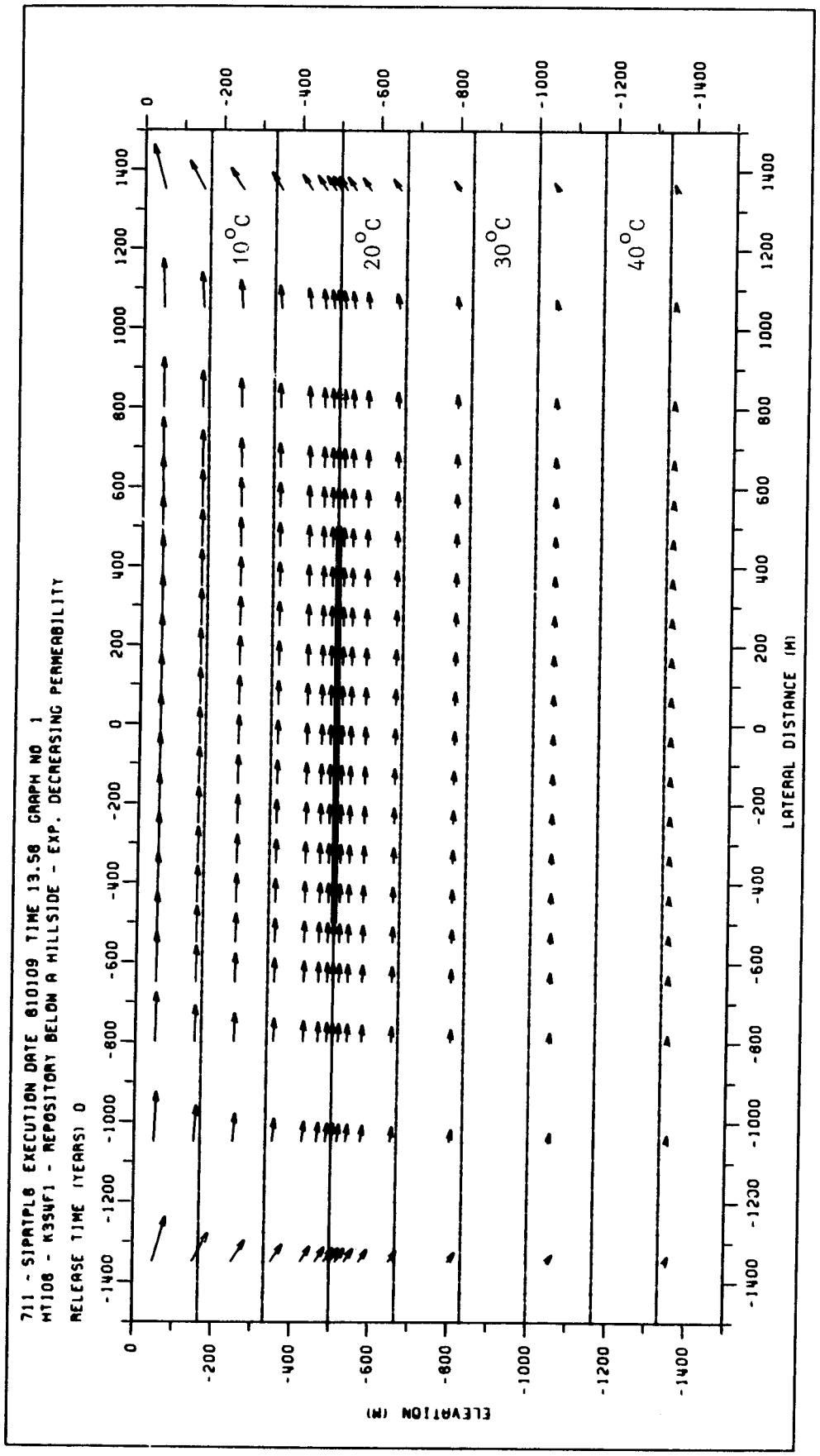

Figure 4.3.9 Groundwater fluxes and isotherms illustrating the hydrothermal flow conditions around a radioactive waste repository located below a hillside with a slope of one per mille. Permeability and porosity are exponentially decreasing with depth. Release time: 0 years.

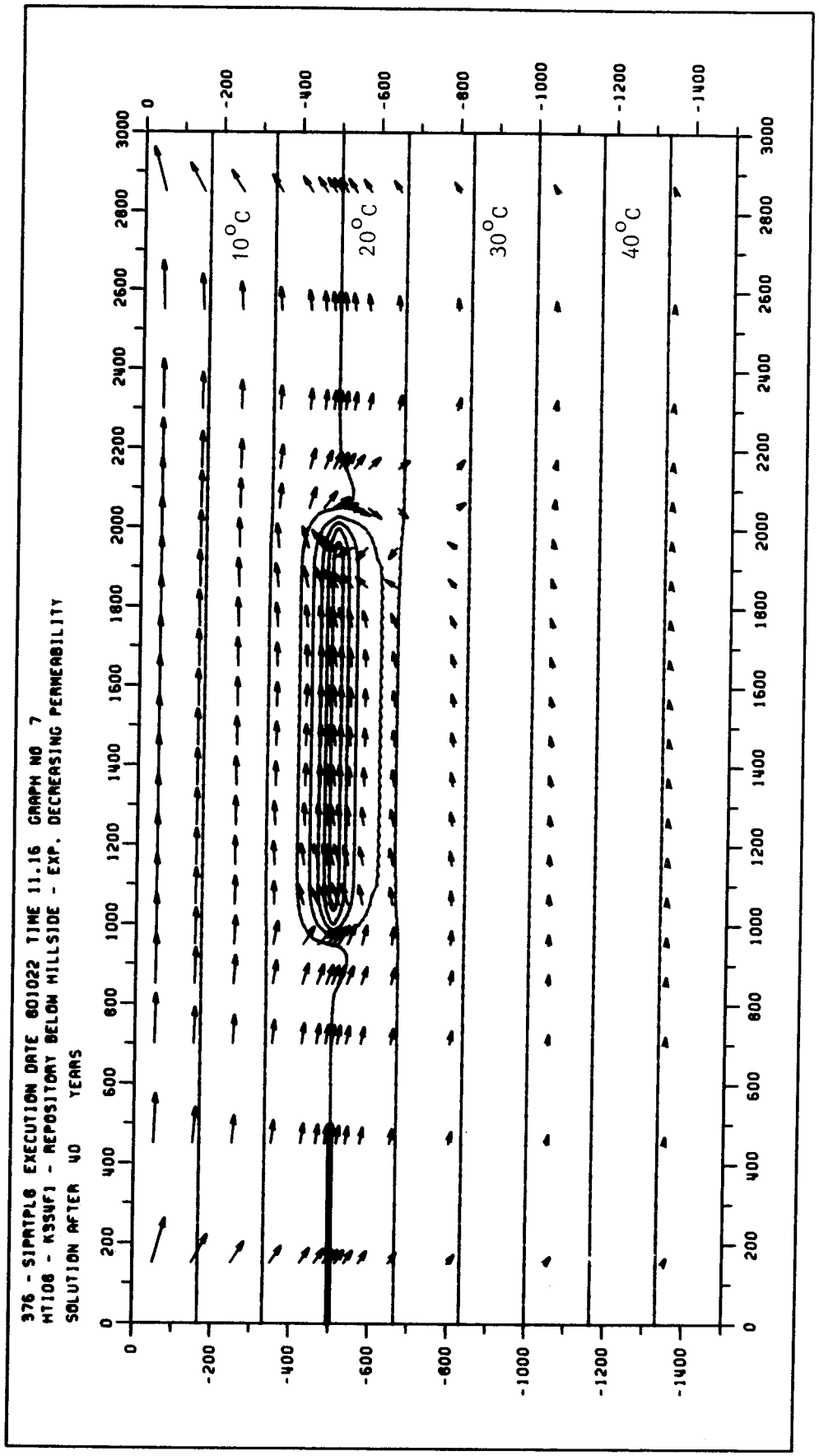

Figure 4.3.10 Groundwater fluxes and isotherms illustrating the hydrothermal flow conditions around a radioactive waste repository located below a hillside with a slope of one per mille. Permeability and porosity are exponentially decreasing with depth. Release time: 40 years.

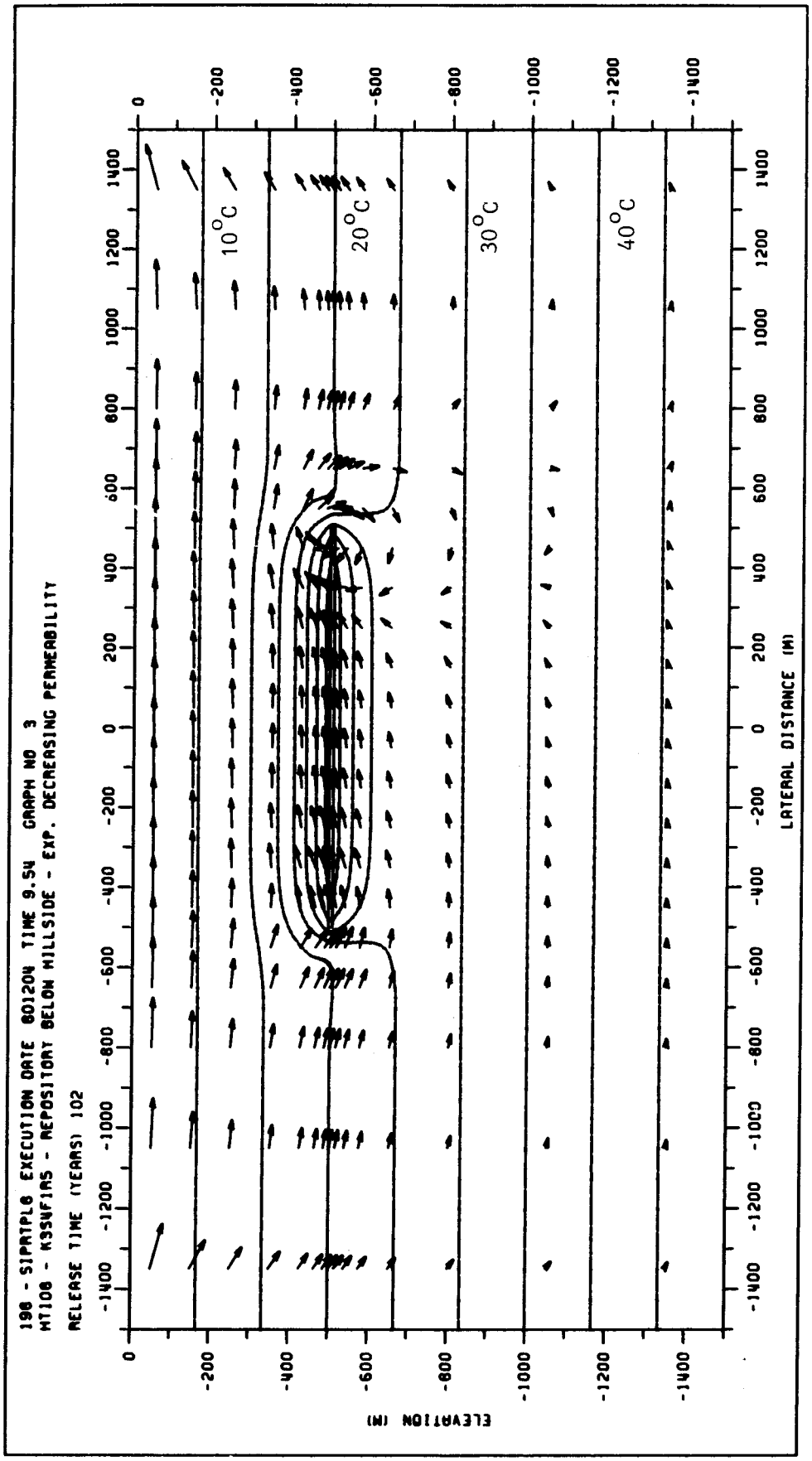

Figure 4.3.11 Groundwater fluxes and isotherms illustrating the hydrothermal flow conditions around a radioactive waste repository located below a hillside with a slope of one per mille. Permeability and porosity are exponentially decreasing with depth. Release time: 102 years.

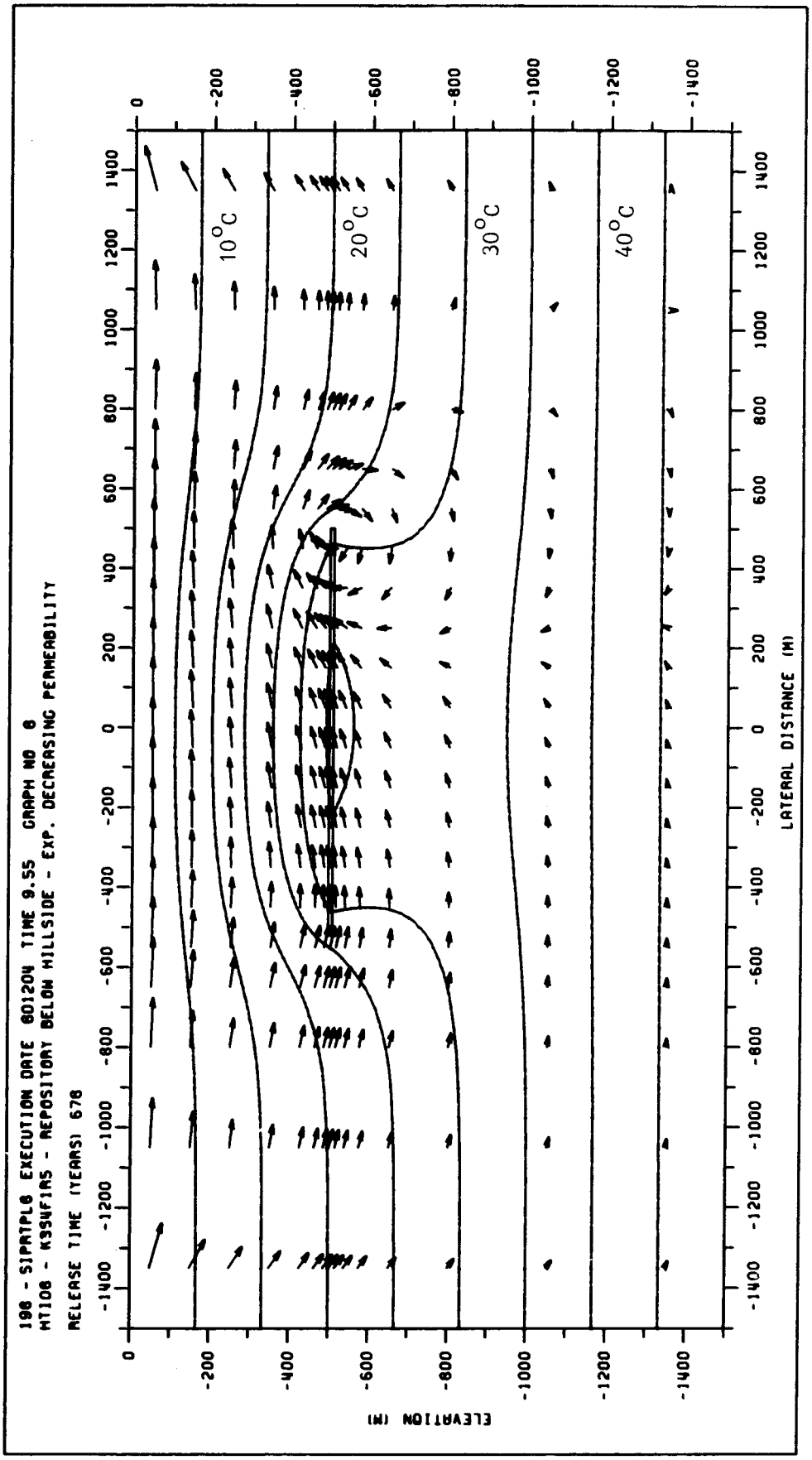

Figure 4.3.12 Groundwater fluxes and isotherms illustrating the hydrothermal flow conditions around a radioactive waste repository located below a hillside with a slope of one per mille. Permeability and porosity are exponentially decreasing with depth. Release time: 678 years.

4.4 Repository located between two major fracture zones

This case illustrates the effect of two major fracture zones of high permeability situated in the vicinity of the repository. The relatively high flow velocity in the fracture planes causes a drawdown of the water level in the fractures. Subsequently, the fractures will drain the adjacent rock.

Two examples are worked out with a distance of 100 metres from the repository to the fracture zones. In one of the two examples permeability and porosity are constant, and in the other permeability and porosity are exponentially decreasing with depth. Furthermore, two examples are considered with a distance of 200 metres from the repository to the fracture zones. In the first one of the latter two examples permeability and porosity are constant, while in the second one permeability while porosity are exponentially decreasing with depth. The drawdown in the fractures is 5 metres in the first two examples and 3 metres in the last two examples.

The presented examples show a similar qualitative behaviour. The effect of the heat released from the repository is to make the flow times from the centre of the repository to the fracture zones longer. The flow times from the edges of the repository to the fracture zones are not influenced by the heat in the examples.

The exit times obtained in the examples are very short. The actual travel times, however, will probably be significantly longer. Firstly, the entry into the fractures takes place at about the same depth as or even deeper than the repository itself. The

flow time in the fracture zones to the ground surface is not accounted for in the computations. Secondly, it is assumed that the water level in the fractures as well as in the surrounding rock is stationary. This is a very conservative assumption, since the drawdown in the fractures is likely to lower the water table in the surrounding rock as well.

4.4.1 Repository located between two major vertical fracture zones at a distance of 100 metres to the fracture zones. Permeability and porosity are constant over the flow domain.

Exit time: > 25 years

> 25 without the influence of a repository

The results of the pathline trace is presented in tables 4.4.1 and 4.4.2.

Pathlines for the flow conditions with the influence of a repository are displayed in figure 4.4.1.

Pathlines for the natural flow conditions without the influence of a repository are displayed in figure 4.4.2.

Groundwater fluxes and isotherms are displayed in figures 4.4.3 - 4.4.4.

Table 4.4.1 Coordinates of the starting respectively end points and the corresponding travel times in years of pathlines traced from a radioactive waste repository located between two major vertical fracture zones. The distance from the repository to respective fracture zone is 100 metres and the drawdown in the fractures is 5 metres. Permeability and porosity are constant over the flow domain.

No	Starting point		End point		Travel time
1	0	-500	600	-1437	2890
2	100	-500	600	-1020	583
3	200	-500	600	-760	257
4	300	-500	600	-625	128
5	400	-500	600	-562	59
6	500	-500	600	-526	25

Table 4.4.2 Coordinates of the starting respectively end points and the corresponding travel times in years of pathlines traced from a radioactive waste repository located between two major vertical fracture zones. The distance from the repository to respective fracture zone is 100 metres and the drawdown in the fractures is 5 metres. Permeability and porosity are constant over the flow domain. No heat is released from the repository.

No	Starting point		End point		Travel time
1	0	-500	600	-1452	2100
2	100	-500	600	-1072	475
3	200	-500	600	-816	213
4	300	-500	600	-664	111
5	400	-500	600	-571	59
6	500	-500	600	-518	25

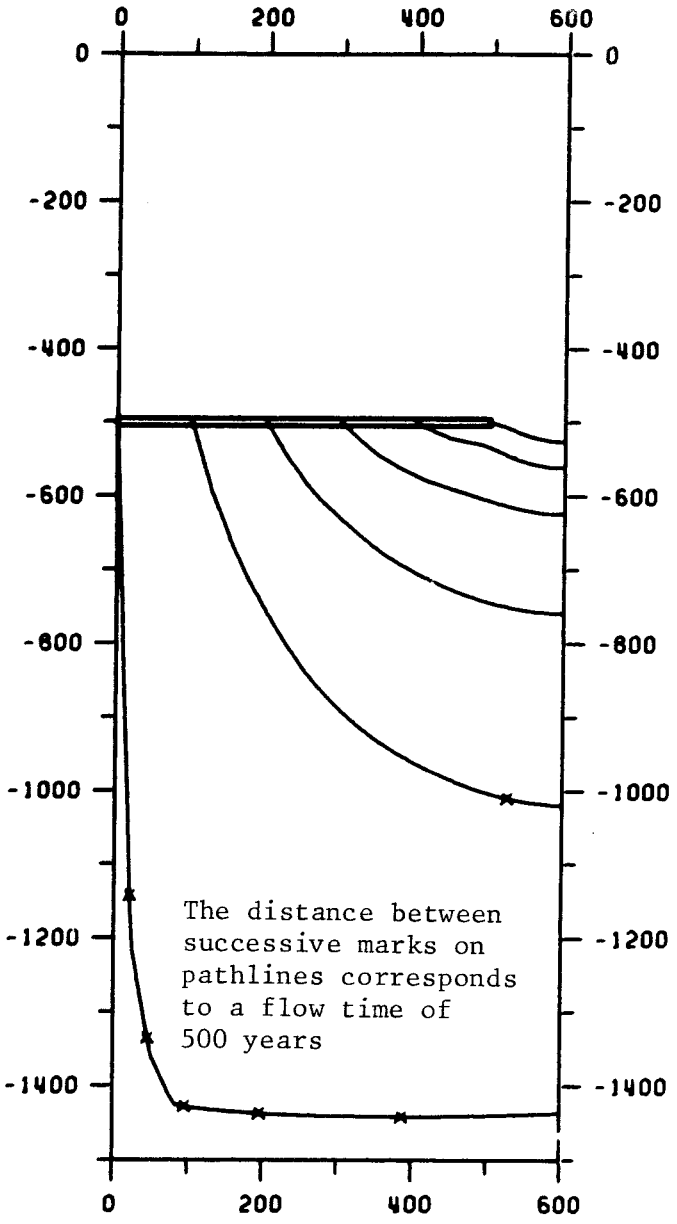

Figure 4.4.1 Pathlines for the flow conditions with the influence of a repository located between two major vertical fracture zones. The distance between the repository and respective fracture zone is 100 metres. The drawdown in the fracture zones is 5 metres. Permeability and porosity are constant.

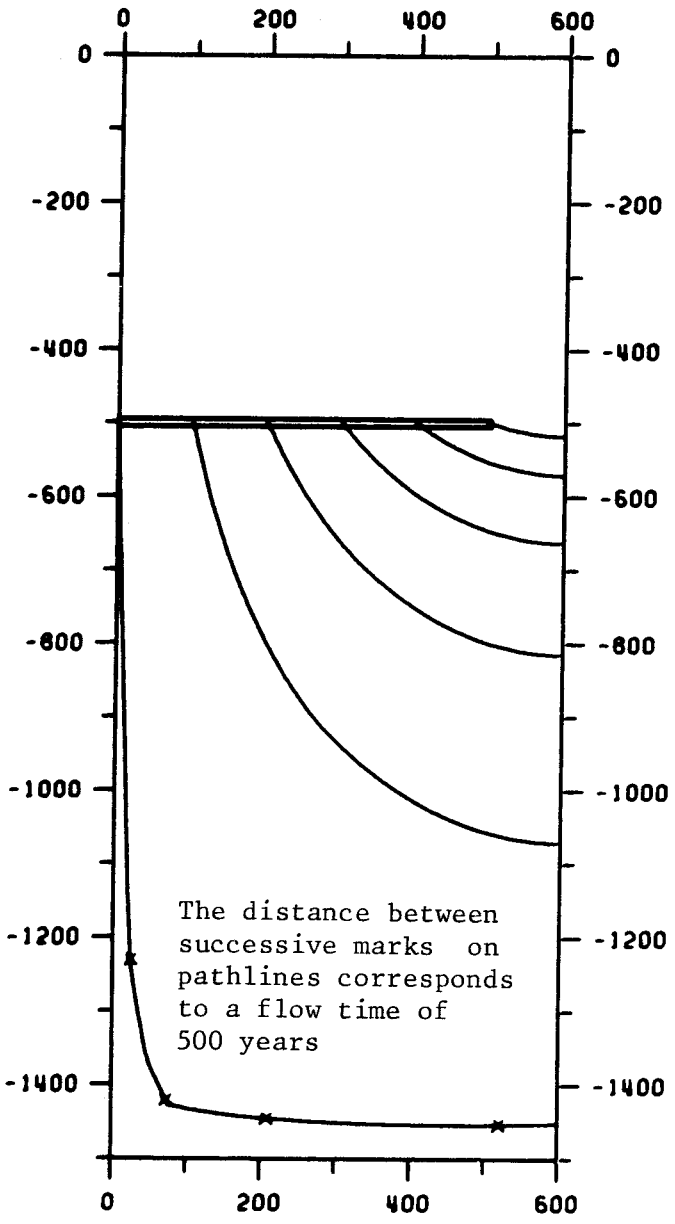

Figure 4.4.2 Pathlines for the natural groundwater flow around a repository located between two major vertical fracture zones. The distance between the repository and respective fracture zone is 100 metres. The drawdown in the fracture zones is 5 metres. Permeability and porosity are constant.

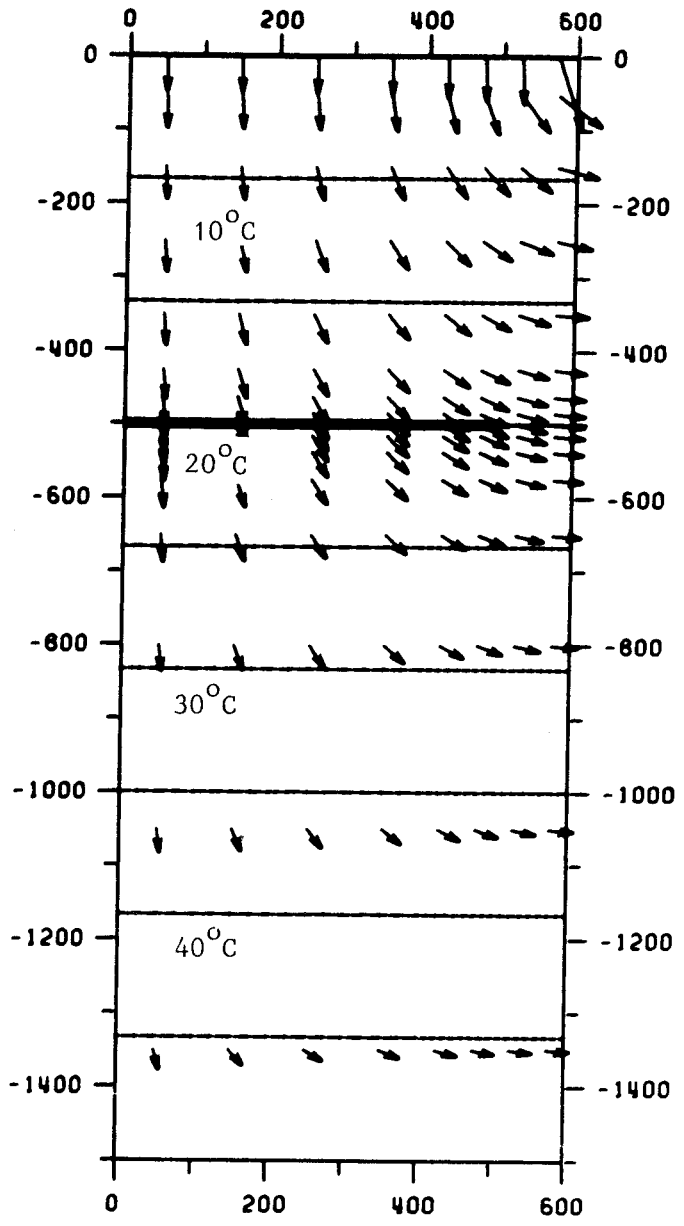

Figure 4.4.3 Groundwater fluxes and isotherms illustrating the hydrothermal flow conditions around a radioactive waste repository situated between two major fracture zones. The distance between the repository and respective fracture zone is 100 metres. The drawdown in the fracture zones is 5 metres. Permeability and porosity are constant. Release time: 0 years.

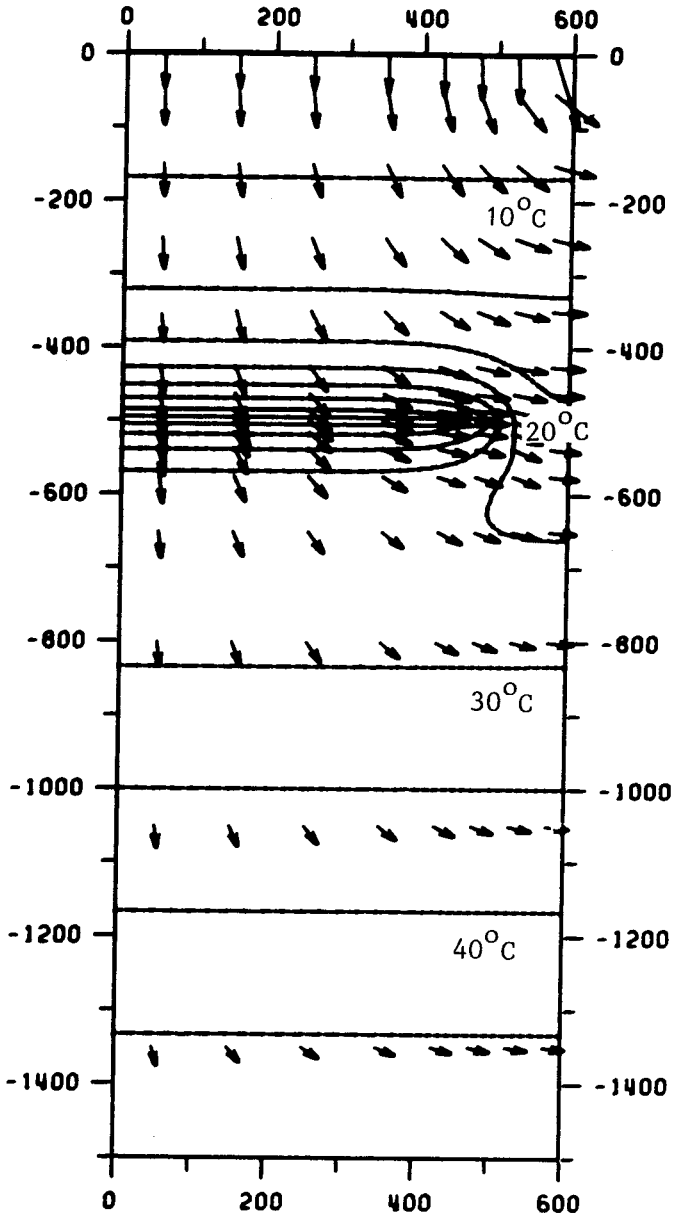

Figure 4.4.4 Groundwater fluxes and isotherms illustrating the hydrothermal flow conditions around a radioactive waste repository situated between two major fracture zones. The distance between the repository and respective fracture zone is 100 metres. The drawdown in the fracture zones is 5 metres. Permeability and porosity are constant. Release time: 59 years.

4.4.2 Repository located between two major vertical fracture zones. The distance between the repository and respective fracture zone is 100 metres. The drawdown in the fracture zones is 5 metres. Permeability and porosity are exponentially decreasing with depth.

Exit time: > 7 years

> 7 without the influence of a repository

The results of the pathline trace are presented in tables 4.4.3 and 4.4.4.

Pathlines for the groundwater flow with the influence of a repository are displayed in figure 4.4.5.

Pathlines for the natural flow conditions are displayed in figure 4.4.6.

Groundwater fluxes and isotherms are displayed in figures 4.4.7 - 4.4.8.

Table 4.4.3 Coordinates of the starting respectively end points and the corresponding travel times in years of pathlines traced from a radioactive waste repository located between two major vertical fracture zones. The distance from the repository to respective fracture zone is 100 metres and the drawdown in the fractures is 5 metres. Permeability and porosity are exponentially decreasing with depth.

No	Starting point		End point		Travel time
1	0	-500	600	-1019	211
2	100	-500	600	-668	77
3	200	-500	600	-597	47
4	300	-500	600	-556	26
5	400	-500	600	-526	15
6	500	-500	600	-508	7

Table 4.4.4 Coordinates of the starting respectively end points and the corresponding travel times in years of pathlines traced from a radioactive waste repository located between two major vertical fracture zones. The distance from the repository to respective fracture zone is 100 metres and the drawdown in the fractures is 5 metres. Permeability and porosity are exponentially decreasing with depth. No heat is released from the repository.

No	Starting point		End point		Travel time
1	0	-500	600	-1041	190
2	100	-500	600	-684	80
3	200	-500	600	-607	44
4	300	-500	600	-560	27
5	400	-500	600	-527	16
6	500	-500	600	-507	7

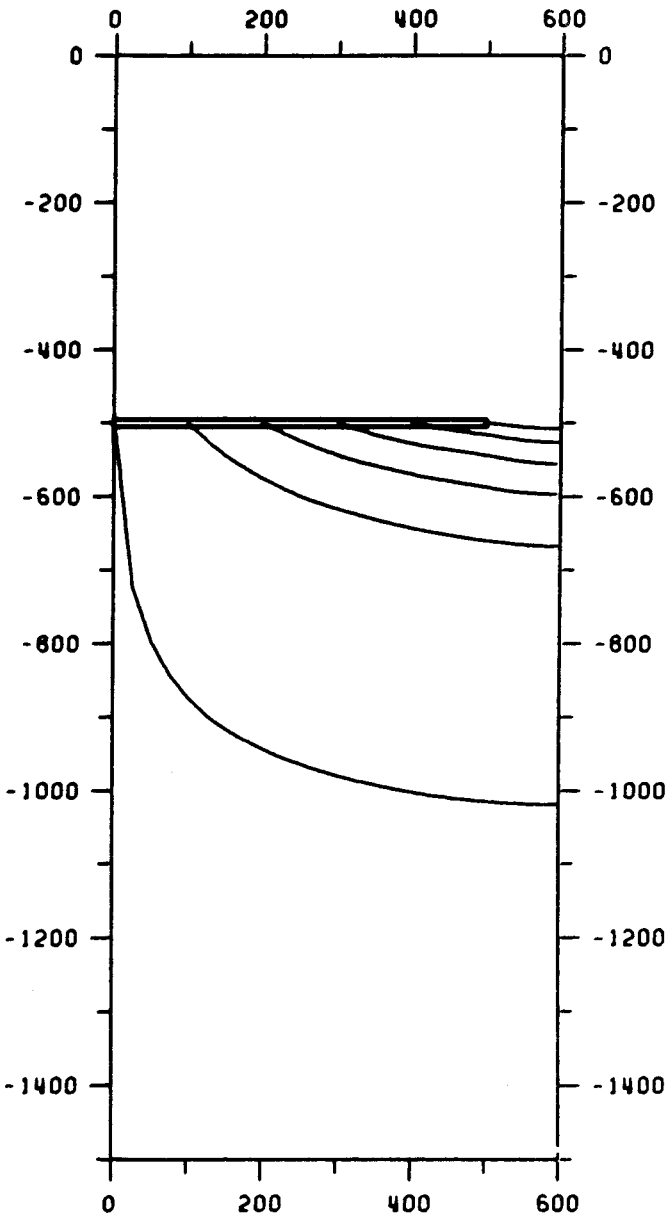

Figure 4.4.5 Pathlines for the groundwater flow with the influence of a repository located between two major vertical fracture zones. The distance between the repository and respective fracture zone is 100 metres. The drawdown in the fractures is 5 metres. Permeability and porosity are exponentially decreasing with depth.

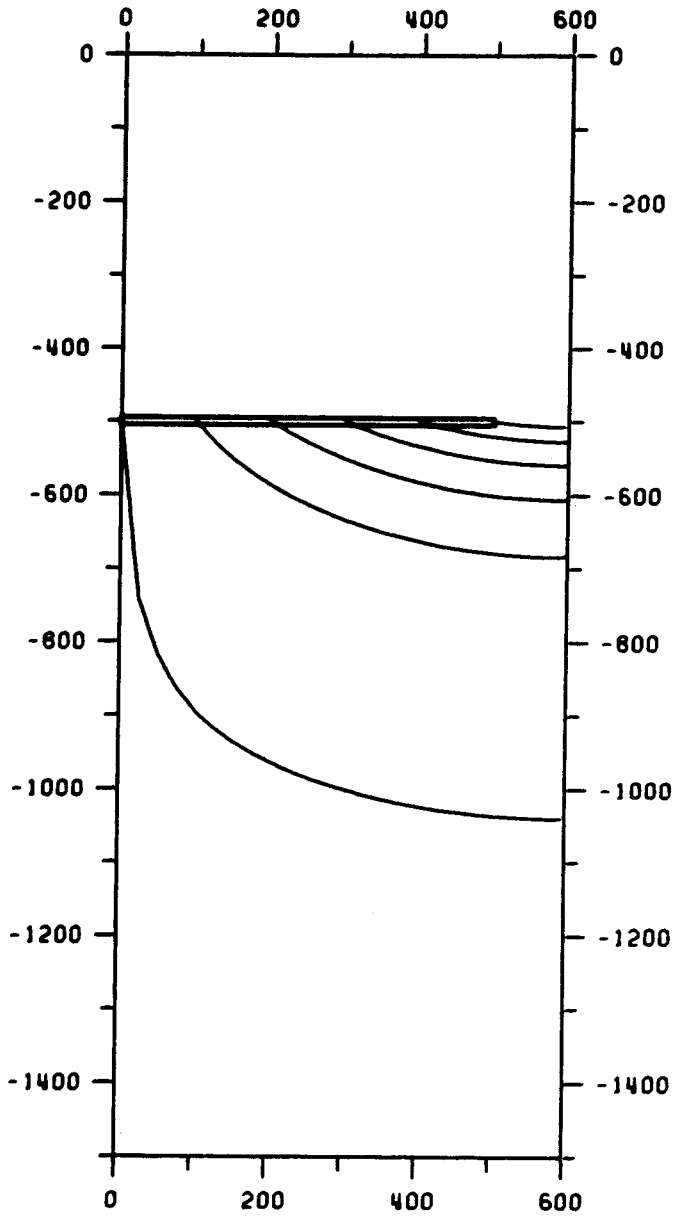

Figure 4.4.6 Pathlines for the natural groundwater flow around a repository located between two major vertical fracture zones. The distance between the repository and respective fracture zone is 100 metres. The drawdown in the fractures is 5 metres. Permeability and porosity are exponentially decreasing with depth.

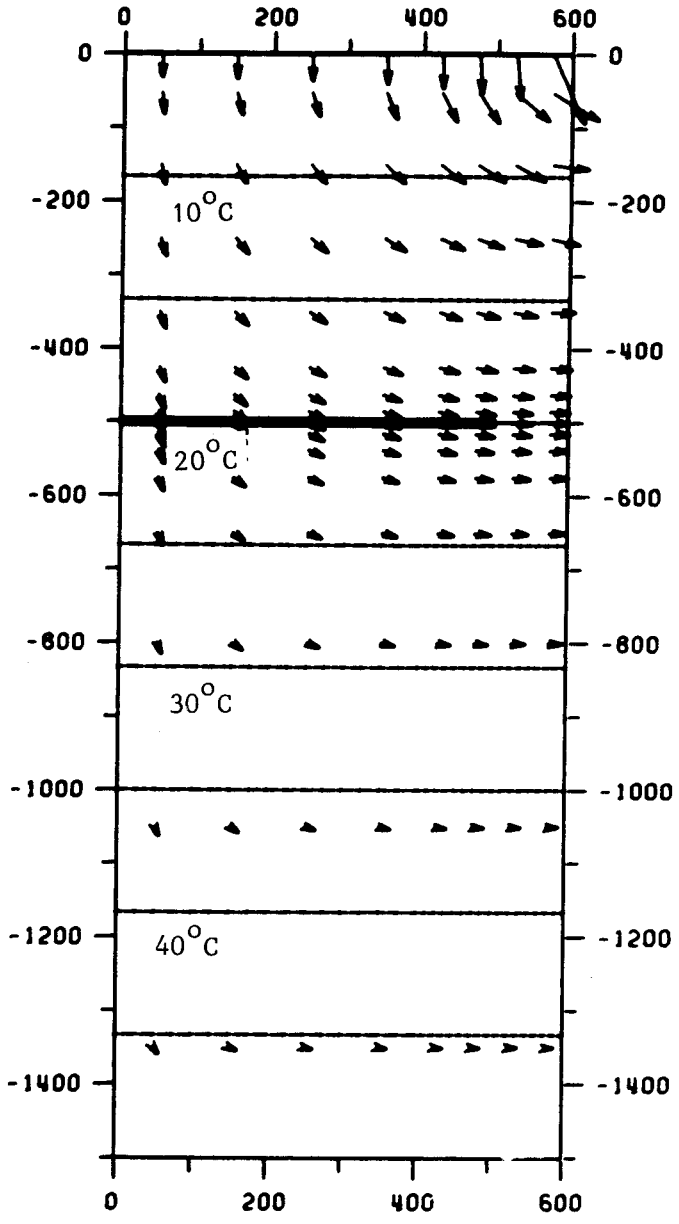

Figure 4.4.7 Groundwater fluxes and isotherms illustrating the hydrothermal flow conditions around a radioactive waste repository situated between two major fracture zones. The distance between the repository and respective fracture zone is 100 metres. The drawdown in the fracture zones is 5 metres. Permeability and porosity are exponentially decreasing with depth. Release time: 0 years.

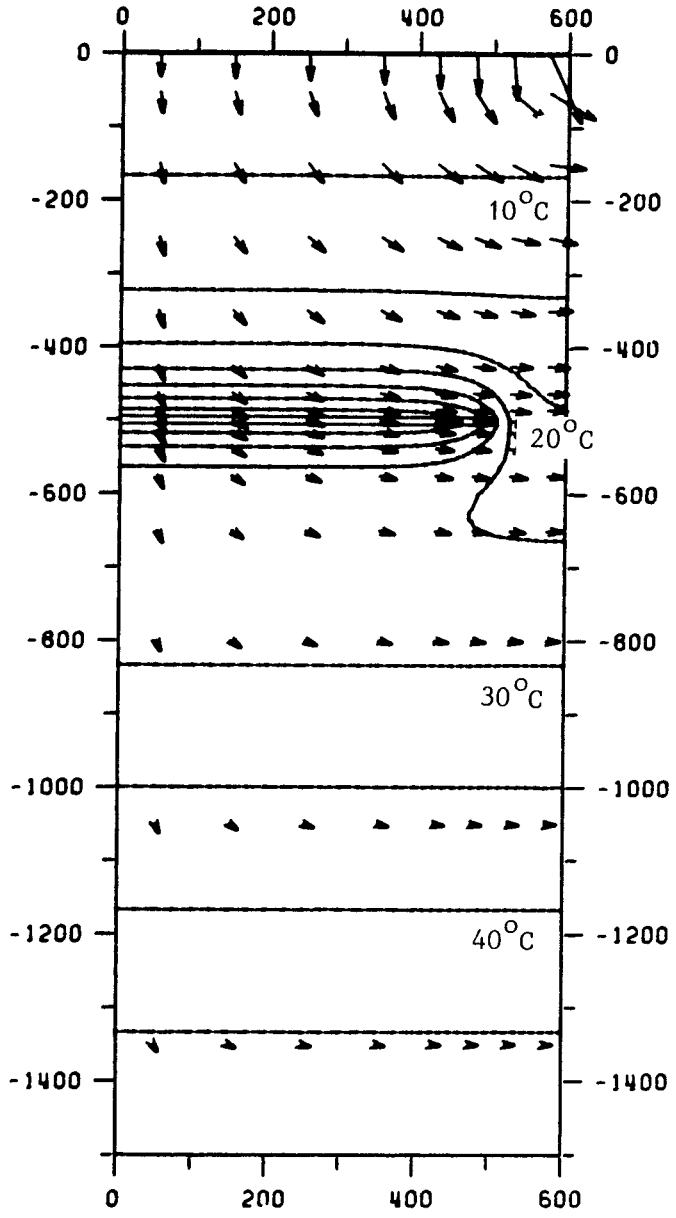

Figure 4.4.8 Groundwater fluxes and isotherms illustrating the hydrothermal flow conditions around a radioactive waste repository situated between two major fracture zones. The distance between the repository and respective fracture zone is 100 metres. The drawdown in the fracture zones is 5 metres. Permeability and porosity are exponentially decreasing with depth. Release time: 53 years.

4.4.3 Repository located between two major vertical fracture zones. The distance between the repository and respective fracture zone is 200 metres. The drawdown in the fracture zones is 3 metres. Permeability and porosity are constant.

Exit time: > 110 years

> 88 without the influence of a repository

The results of the pathline trace are presented in tables 4.4.5 and 4.4.6.

Pathlines for the flow conditions with the influence of a repository are displayed in figure 4.4.9.

Pathlines for the natural flow conditions without the influence of a repository are displayed in figure 4.4.10.

Groundwater fluxes and isotherms are displayed in figures 4.4.11 - 4.4.12.

Table 4.4.5 Coordinates of the starting respectively end points and the corresponding travel times in years of pathlines traced from a radioactive waste repository located between two major vertical fracture zones. The distance from the repository to respective fracture zone is 200 metres and the drawdown in the fractures is 3 metres. Permeability and porosity are constant over the flow domain.

No	Starting point		End point		Travel time
1	0	-500	700	-1425	4500
2	100	-500	700	-1141	1300
3	200	-500	700	-888	651
4	300	-500	700	-740	384
5	400	-500	700	-673	226
6	500	-500	700	-609	110

Table 4.4.6 Coordinates of the starting respectively end points and the corresponding travel times in years of pathlines traced from a radioactive waste repository located between two major vertical fracture zones. The distance from the repository to respective fracture zone is 200 metres and the drawdown in the fractures is 3 metres. Permeability and porosity are constant over the flow domain. No heat is released from the repository.

No	Starting point		End point		Travel time
1	0	-500	700	-1451	2981
2	100	-500	700	-1173	919
3	200	-500	700	-925	481
4	300	-500	700	-759	274
5	400	-500	700	-642	159
6	500	-500	700	-562	88

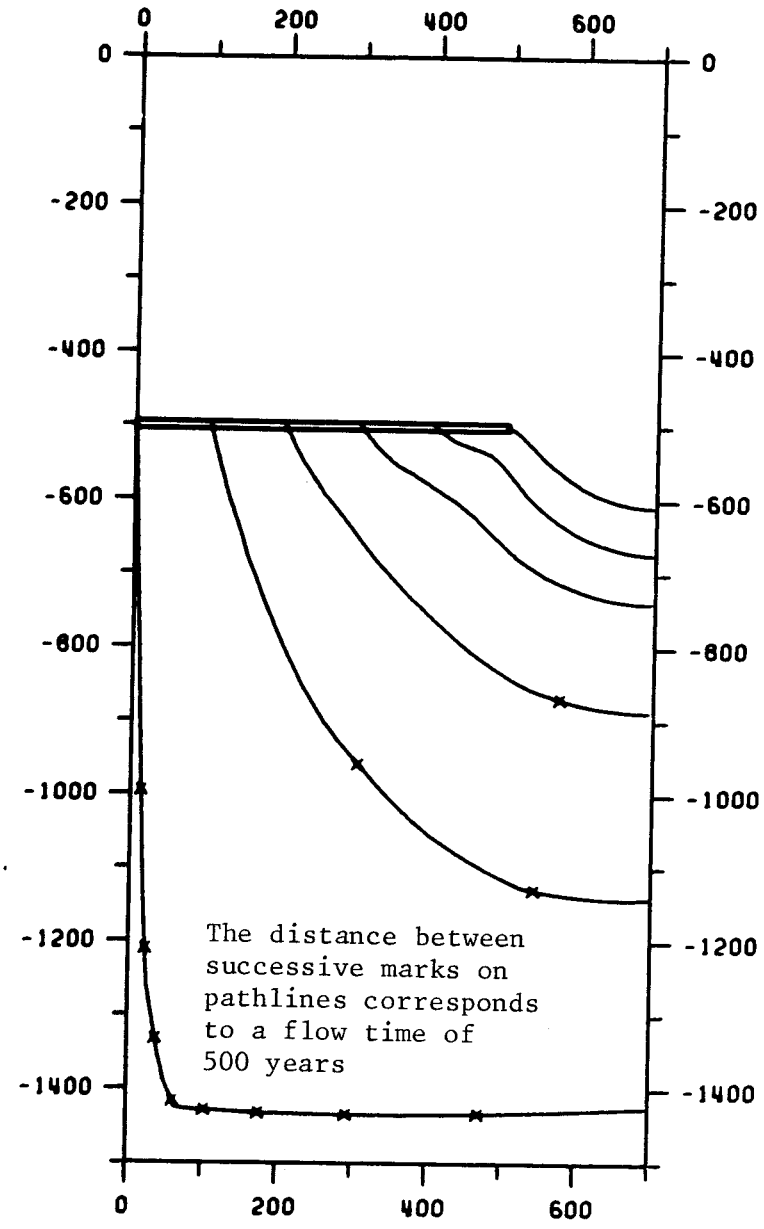

Figure 4.4.9 Pathlines for the flow conditions with the influence of a repository located between two major vertical fracture zones. The distance between the repository and respective fracture zone is 200 metres. The drawdown in the fracture zones is 3 metres. Permeability and porosity are constant.

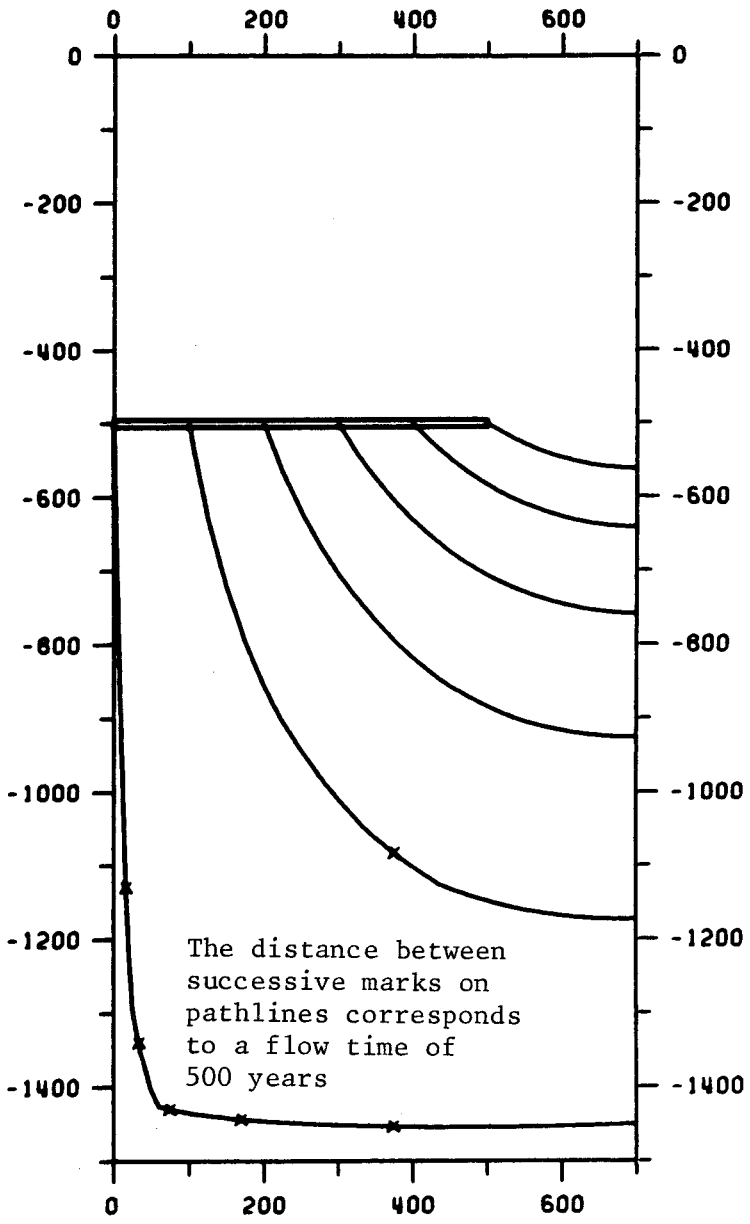

Figure 4.4.10 Pathlines for the natural groundwater flow around a repository located between two major vertical fracture zones. The distance between the repository and respective fracture zone is 200 metres. The drawdown in the fracture zones is 3 metres. Permeability and porosity are constant.

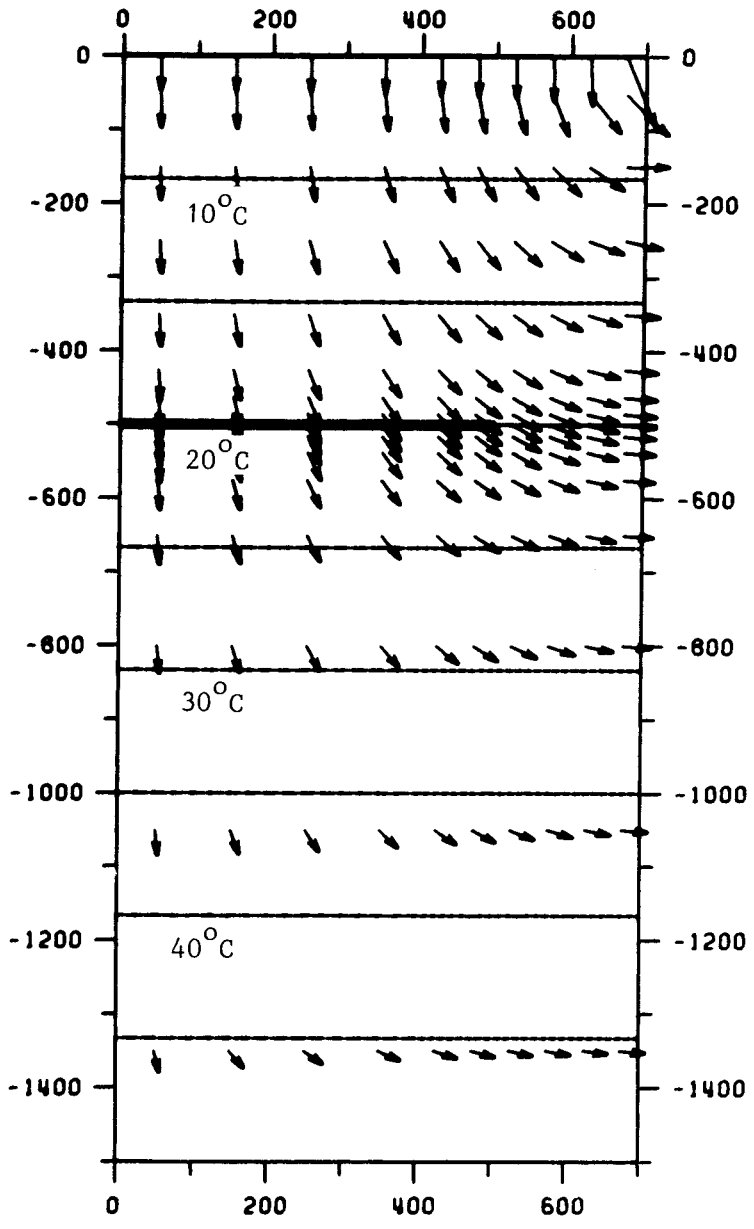

Figure 4.4.11 Groundwater fluxes and isotherms illustrating the hydrothermal flow conditions around a radioactive waste between two major fracture zones. The distance between the repository and respective fracture zones is 200 metres. The drawdown in the fracture zones is 3 metres. Permeability and porosity are constant. Release time: 0 years.

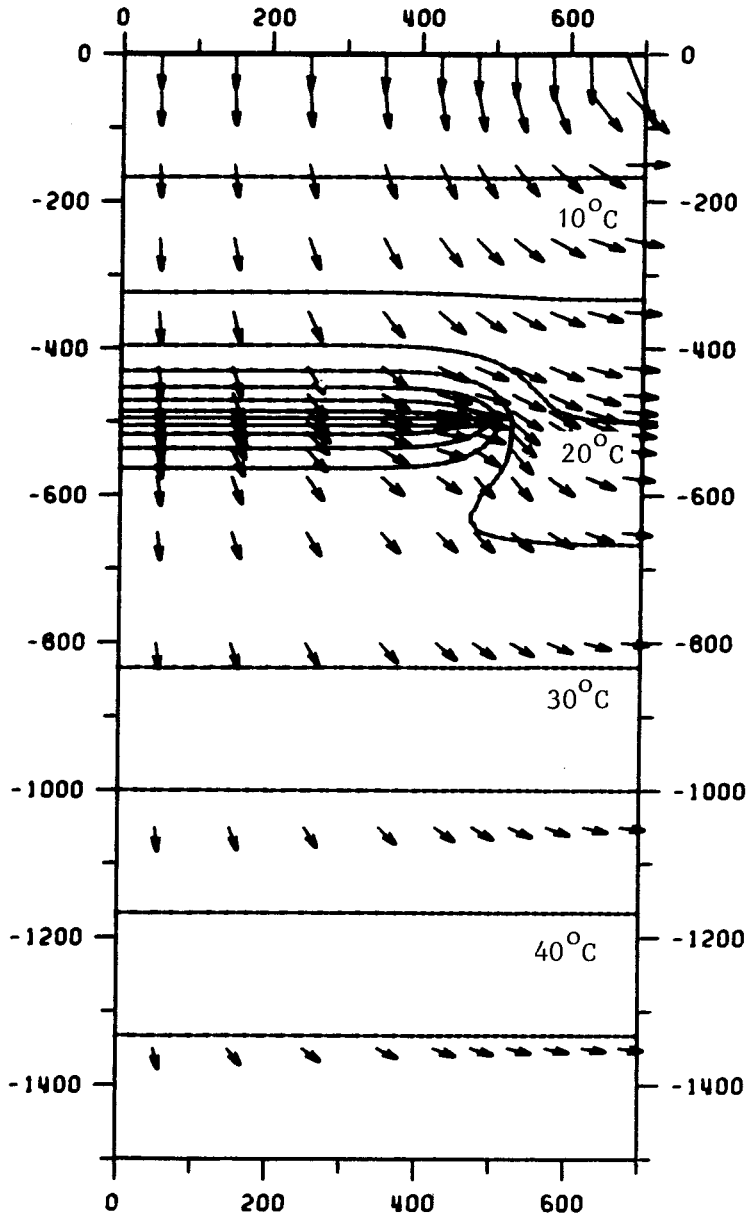

Figure 4.4.12 Groundwater fluxes and isotherms illustrating the hydrothermal flow conditions around a radioactive waste between two major fracture zones. The distance between the repository and respective fracture zones is 200 metres. The drawdown in the fracture zones is 3 metres. Permeability and porosity are constant. Release time: 53 years.

4.4.4 Repository located between two major vertical fracture zones at a distance of 200 metres to the fracture zones. The drawdown in the fracture zones is 3 metres. Permeability and porosity are exponentially decreasing with depth.

Exit time: > 27 years

> 27 without the influence of a repository

The results of the pathline trace are presented in tables 4.4.7 and 4.4.8.

Pathlines for the groundwater flow with the influence of a repository are displayed in figure 4.4.13.

Pathlines for the natural flow conditions are displayed in figure 4.4.14.

Groundwater fluxes and isotherms are displayed in figures 4.4.15 - 4.4.16.

Table 4.4.7 Coordinates of the starting respectively end points and the corresponding travel times in years of pathlines traced from a radioactive waste repository located between two major vertical fracture zones. The distance from the repository to respective fracture zone is 200 metres and the drawdown in the fractures is 3 metres. Peremeability and porosity are exponentially decreasing with depth.

No	Starting point		End point		Travel time
1	0	-500	700	-1062	551
2	100	-500	700	-709	207
3	200	-500	700	-636	121
4	300	-500	700	-599	82
5	400	-500	700	-566	46
6	500	-500	700	-533	27

Table 4.4.8 Coordinates of the starting respectively end points and the corresponding travel times in years of pathlines traced from a radioactive waste repository located between two major vertical fracture zones. The distance from the repository to respective fracture zone is 200 metres and the drawdown in the fractures is 3 metres. Peremeability and porosity are exponentially decreasing with depth. No heat is released from the repository.

No	Starting point		End point		Travel time
1	0	-500	700	-1087	465
2	100	-500	700	-725	173
3	200	-500	700	-645	107
4	300	-500	700	-594	75
5	400	-500	700	-554	45
6	500	-500	700	-525	27

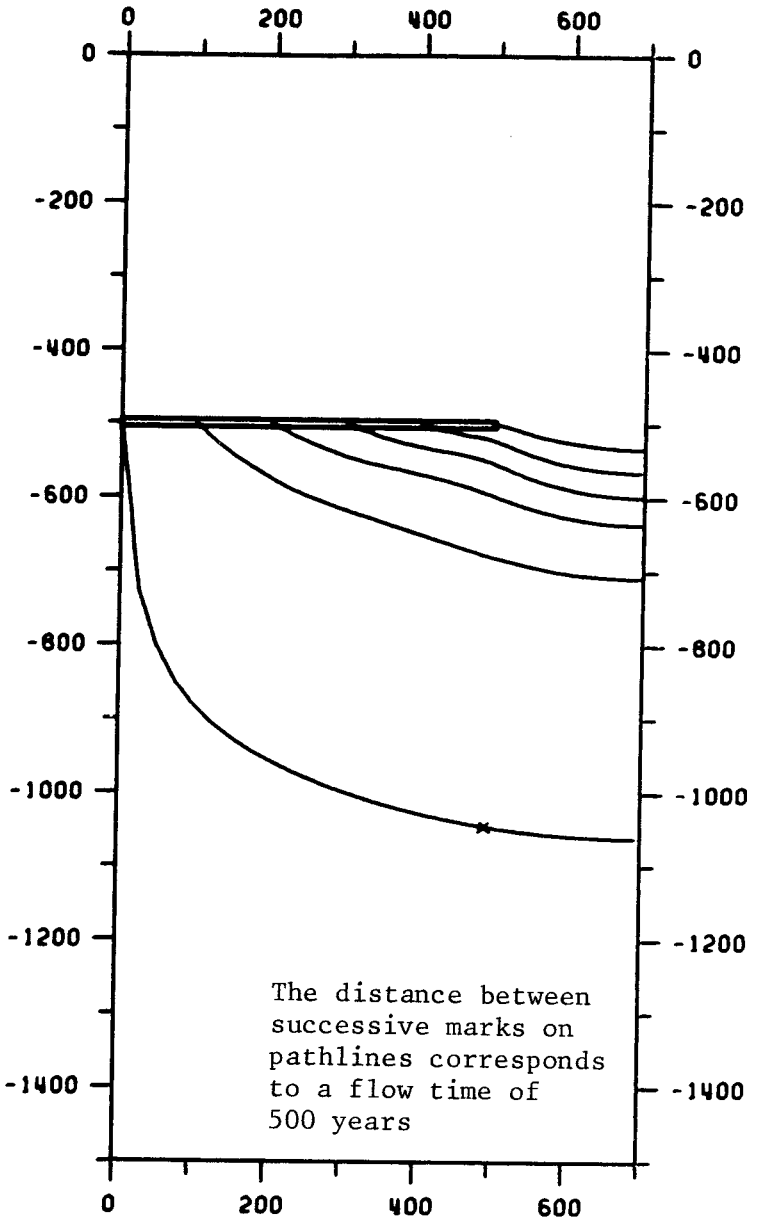

Figure 4.4.13 Pathlines for the groundwater flow with the influence of a repository located between two major vertical fracture zones. The distance between the repository and respective fracture zone is 200 metres. The drawdown in the fractures is 3 metres. Permeability and porosity are exponentially decreasing with depth.

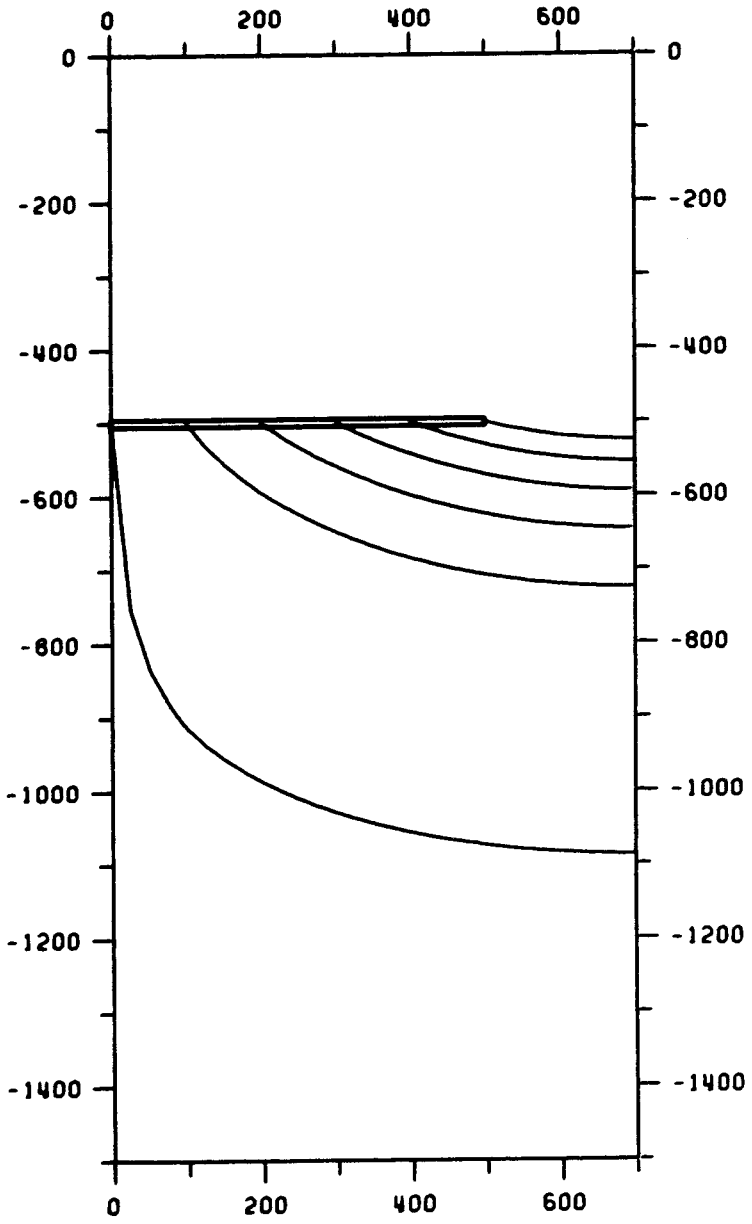

Figure 4.4.14 Pathlines for the natural groundwater flow around a repository located between two major vertical fracture zones. The distance between the repository and respective fracture zone is 200 metres. The drawdown in the fracture zones is 3 metres. Permeability and porosity are exponentially decreasing with depth.

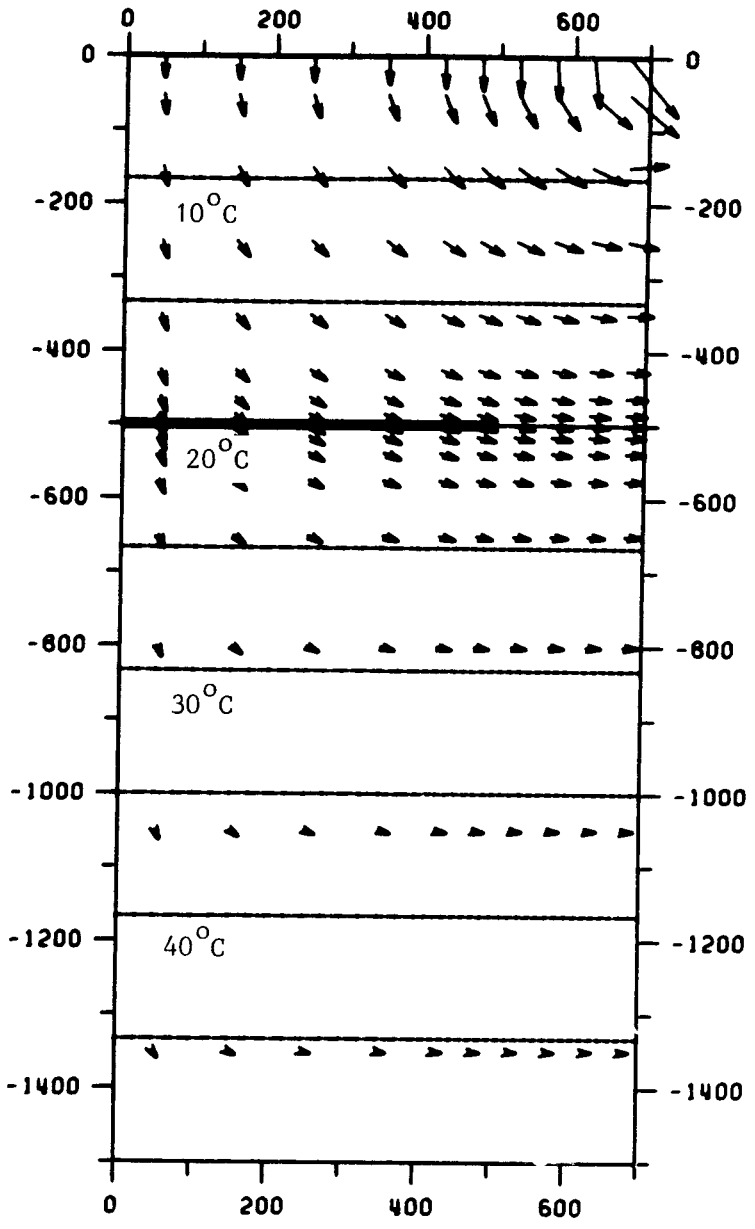

Figure 4.4.15 Groundwater fluxes and isotherms illustrating the hydrothermal flow conditions around a radioactive waste repository situated between two major fracture zones. The distance between the repository and respective fracture zone is 200 metres. The drawdown in the fracture zones is 3 metres. Permeability and porosity are exponentially decreasing with depth. Release time 0 years.

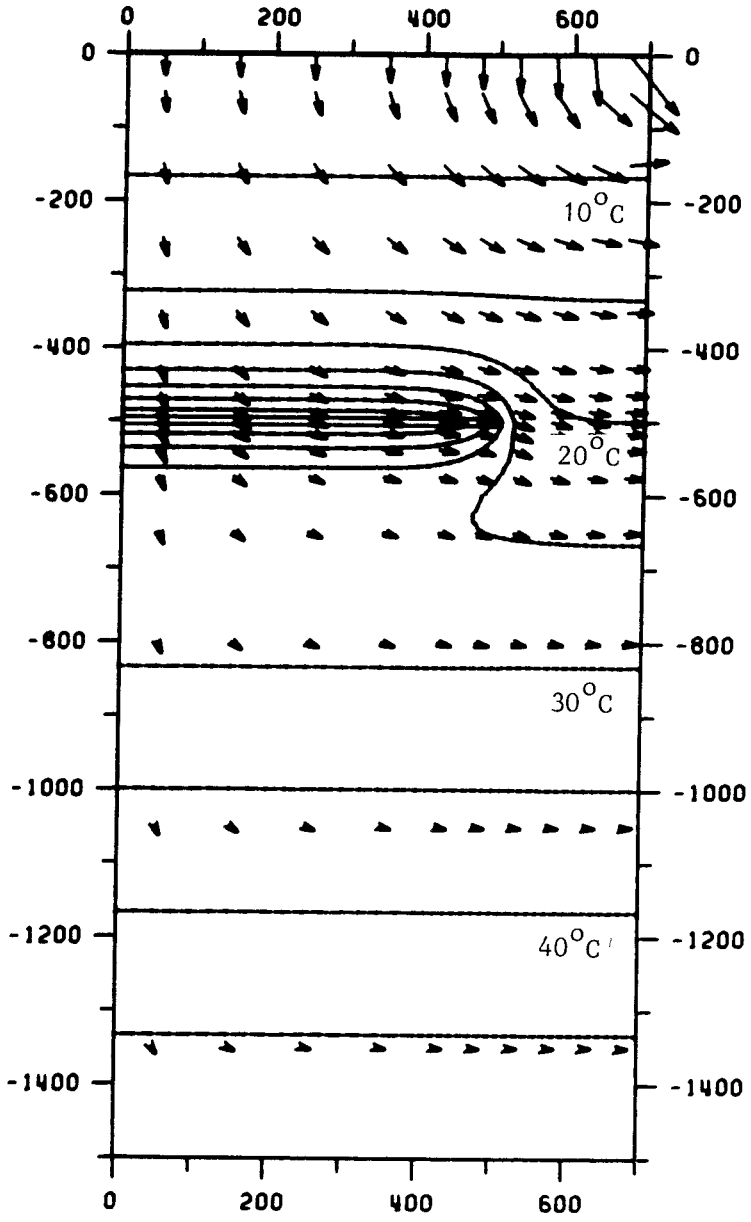

Figure 4.4.16 Groundwater fluxes and isotherms illustrating the hydrothermal flow conditions around a radioactive waste repository situated between two major fracture zones. The distance between the repository and respective fracture zone is 200 metres. The drawdown in the fracture zones is 3 metres. Permeability and porosity are exponentially decreasing with depth. Release time 53 years.

5. CONCLUSIONS AND DISCUSSION

The purpose of this chapter is to relate some general conclusions based on the presented examples and to discuss various further aspects of the heat flow problem that may have to be considered in the forthcoming investigations.

The primary objective of the investigation has been to exemplify the influence of a radioactive waste repository on the groundwater in the surrounding rock qualitatively rather than quantitatively. Thus, no specific site is referred to in the analysis. Therefore, simplified assumptions were made regarding the physical properties as well as the geometry of the flow domain. As a consequence, owing to the great complexity in the present flow problem, care must be taking in drawing conclusions on the behaviour of the groundwater at a specific site, based on the presented solutions.

The flow domain was limited downwards by an impervious bottom and laterally by noflow boundaries or alternatively hydrostatic bounaries, representing some major fracture zones. Upwards, the flow domain was bounded by the water table, assumed to coincide with the ground surface and water is allowed to pass freely through this boundary, depending on the piezometric gradients in the flow domain. Furthermore, the repository was located at equal distances from the lateral boundaries.

For simplicity in the calculations the radioactive waste was assumed to be loaded into the repository at the same time. However, this was considered a conservative assumption, resulting in a more concentrated thermal load in the initial stage.

Four main cases were considered in the analysis:

1) A repository situated below a horizontal ground surface.
2) A repository situated below the crest of a hill.
3) A repository situated below a hillside.
4) A repository situated between two major fracture zones.

Each case was worked out for constant respectively exponentially decreasing permeability with depth over the flow domain.

The overall effect of the heat emitted by the decaying waste was to modify the initial fluxes and subsequently also the flow times from the repository. Although the temperature reached its maximum after about 50 years, the heat released from the repository continued to exert influence on the flow field for many thousands of years, before the initial flow conditions were reestablished.

In case 1, the groundwater flow is only induced by the heat from the repository. In the example with constant permeability the flow time from the centre of the repository was about 650 years. However, in the example with permeability decreasing with depth the initial hydrostatic conditions were reestablished before any water particles could reach the ground surface. Thus, in the latter example the driving force on the groundwater attenuated after about 7500 years and the water particles traced from the repository halted at a depth of about 175 metres below the ground surface.

In case 2, the groundwater flow is initially governed by topography and the repository was symmetrically situated below the crest of the hill. Generally, this case represents a desirable location

of a radioactive waste repository. This is due to the fact that the repository is situated below an inflow area. As a result, the travel times from the repository to the ground surface become relatively long if the groundwater is only governed by topography. Two different values of the slope of the hillsides were applied, 1 in 1000 and 1 in 100. Two examples were worked out for a slope of 1 in 1000. In these examples the heat from the repository had a significant effect on the flow pattern of the groundwater. Convection currents were created, and the flow pattern was influenced by the heat for about 10000 years. In the two examples with a slope of 1 in 100, topography is the dominating factor and only a minor influence on the flow times could be noted.

In case 3, the slope of the hillside was 1 in 1000. This case is characterized by mainly horizontal flow at the repository area. The effect of the repository was most significant for the example with constant permeability. In this example, rotative convection currents were created at both edges of the repository. As a result, the pathlines, which under the initial flow conditions appeared fairly concentrated from the repository to the surface, diverged owing to the heat and from some areas the flow times became shorter, while from other areas they became longer. In the example with constant permeability over the flow domain, the effect of the heat from the repository was to shorten the minimum travel times by about 30 per cent. In the example with exponentially decreasing permeability with depth over the flow domain, the minimum travel time was increased by about 20 per cent.

Case 4 differs from the foregoing cases because the lateral boundaries are treated as hydrostatic or discharge boundaries, instead

of impervious boundaries, as for the previous three cases. In this case the hydrostatic boundaries are assumed to represent major vertical fracture zones, whose orientation is perpendicular to the study area. The assumption here was that the piezometric gradient in the fractures was high compared to that of the rock, but yet low enough to allow the Dupuit assumption to be made. Thus means that the flow in the fracture zones may be treated as horizontal and that the piezometric head is constant in the vertical direction. Furthermore, steady state conditions were assumed to prevail in the fracture zones. Two different settings were worked out. In the first one, the distance between the repository and respective fracture zone was 100 metres and the drawdown in the fractures was 5 metres. In the second one the distance between the repository and the fracture zones was 3 metres. Each setting was solved for constant and for exponentially decreasing permeability and porosity. All of the examples gave as a result very short travel times from the repository to the fracture zones. The shortest travel times were obtained for water particles starting at the edge of the repository. The flow times in the second setting were about four times longer than those in the first one. The exponential decrease in the permeability resulted in about 30 per cent shorter travel times compared with constant permeability.

The presented examples show that heat released from a radioactive waste repository may have a significant impact on the flow regime around the repository. A general impression of the results is that the effect of the heat released from a repository on the groundwater flow pattern is highly sensitive to the physical properties as well as the boundary conditions of the considered flow domain. Although the hypothetical repository in the presented

examples causes a very moderate increase in the temperature of the surrounding rock, it significantly effects the flow patterns and consequently also the flow times for water particles from the repository to the ground surface or to a major fracture zone.

Especially remarkable is the fact, that the heat from the repository may increase as well as decrease the travel times, depending on the conditions in and around the repository. Moreover, the conditions differ from place to place in the repository. Thus, at the centre of the repository the effect of the heat is to push the groundwater upwards. At the lateral boundaries of the repository, the effect of the heat is to develop rotational movements. As a consequence, if the repository is situated below a horizontal ground surface or a hillside, the transit times are in general shorter at the centre of the repository and significantly longer at the edges. On the other hand, in the latter case the repository becomes subject to a higher leaching of hazardous waste material, since the groundwater may pass through the repository several times before reaching the bioshpere.

The presented examples show that under certain conditions, major fracture zones situated in the vicinity of the repository may have a strong impact on the flow conditions. However, the examples were based on very simplified and conservative assumptions. Therefore, further investigations based on more realistic assumptions should be carried out to examine the influence of major discontinuities in the flow domain.

All of the presented examples exhibit a very strong influence of decreasing permeability with depth on the flow patterns. This is

due to the fact that the decrease in permeability with depth particularly reduces the vertical groundwater fluxes, implying that the effect of heat released from a radioactive waste repository becomes less significant under these conditions.

In the calculations with exponentially decreasing permeability the same degree of decrease with depth was used for porosity as for the permeability. This assumes that there is a linear relationship between permeability and porosity. However, this probably yields unreasonably low values of porosity at depth. Although porosity itself does not significantly affect the solutions for the groundwater fluxes, it is crucial in evaluating the travel times for water particles. Thus, the travel times are inversely proportional to porosity. The actual decrease in porosity with depth is probably much less than the assumed one in the presented examples. This means that the travel times given in the examples with exponentially decreasing permeability and porosity should in reality be significantly longer than the presented ones.

In addition to pressure and temperature, the fluid density is also dependent on the salt concentration in the water. Thus, if the considered flow domain comprises any significant salt deposits which are liable to be leached out, then the effect of both temperature and salt concentration on the flow pattern should be taken into account.

Other factors which may have to be taken into account in future investigations are changes in the rock stress distribution, resulting in modifications in the initial fracture pattern, changing permeabilities and flow paths of the groundwater.

Furthermore, the flow patterns may be influenced by the repository during the construction and operation period. During this period, water must be pumped out from the tunnels and shafts and as a result the surrounding rock will be drained, lowering the water table.

The travel times for water particles from the repository to the ground surface in the presented examples are computed applying Darcy's law to the groundwater fluxes obtained from the used flow model and dividing the results by porosity. Thus, various phenomena resulting in retention of the radionuclides due to chemical reactions with the rock, diffusion into the rock and dispersion are not being accounted for.

6. REFERENCES

1 Braester, C., 1977, Theory of Flow through Fractured Rocks, International Seminar of Groundwater in Hard Rocks, Stockholm-Cagliary Sept.-Oct. 1977, Dept. Land Improvement and Drainage, Royal Institute of Technology, Stockholm, Sweden.

2 Jeffry, J.A., Chan, T., Cook, N.G.W., Witherspoon, P.A., 1979, Determination of In-situ Thermal Properties of Stripa Granite from Temperature measurements in the Full-scale Heater experiments - Method and Preliminary Results, LBL-8423, Lawrence Berkeley Laboratory, University of California.

3 Ratigan, J.L., 1977, Groundwater Movements around a Repository - Thermal analyses, Hagconsult AB, KBS-TR-54:02.

4 Stokes, J., Thunvik, R., 1978, Investigations of Groundwater Flow in Rock around Repositories for Nuclear Waste, KBS-TR-47.

5 Stokes, J., 1980, On the Description of the Properties of Fractured Rock using the Concept of a Porous Medium, SKBF-KBS-TR-80-05.

FÖRTECKNING ÖVER KBS TEKNISKA RAPPORTER

1977-78

TR 121 KBS Technical Reports 1 - 120.
Summaries. Stockholm, May 1979.

1979

TR 79-28 The KBS Annual Report 1979.
KBS Technical Reports 79-01--79-27.
Summaries. Stockholm, March 1980.

1980

TR 80-01 Komplettering och sammanfattning av geohydrologiska undersökningar inom sternöområdet, Karlshamn
Lennart Ekman
Bengt Gentzschein
Sveriges geologiska undersökning, mars 1980

TR 80-02 Modelling of rock mass deformation for radioactive waste repositories in hard rock
Ove Stephansson
Per Jonasson
Department of Rock Mechanics
University of Luleå

Tommy Groth
Department of Soil and Rock Mechanics
Royal Institute of Technology, Stockholm
1980-01-29

TR 80-03 GETOUT - a one-dimensional model for groundwater transport of radionuclide decay chains
Bertil Grundfelt
Mark Elert
Kemakta konsult AB, January 1980

TR 80-04 Helium retention
Summary of reports and memoranda
Gunnar Berggren
Studsvik Energiteknik AB, 1980-02-14

TR 80-05 On the description of the properties of fractured rock using the concept of a porous medium
John Stokes
Royal Institute of Technology, Stockholm
1980-05-09

TR 80-06 Alternativa ingjutningstekniker för radioaktiva jonbytarmassor och avfallslösningar
Claes Thegerström
Studsvik Energiteknik AB, 1980-01-29

TR 80-07 A calculation of the radioactivity induced in PWR cluster control rods with the origen and casmo codes
Kim Ekberg
Studsvik Energiteknik AB, 1980-03-12

TR 80-08 Groundwater dating by means of isotopes
A brief review of methods for dating old groundwater by means of isotopes
A computing model for carbon - 14 ages in groundwater
Barbro Johansson
Naturgeografiska Institutionen
Uppsala Universitet, August 1980

TR 80-09 The Bergshamra earthquake sequence of December 23, 1979
Ota Kulhánek, Norris John, Klaus Meyer, Torild van Eck and Rutger Wahlström
Seismological Section, Uppsala University
Uppsala, Sweden, August 1980

TR 80-10 Kompletterande permeabilitetsmätningar i finnsjö-området
Leif Carlsson, Bengt Gentzschein, Gunnar Gidlund, Kenth Hansson, Torbjörn Svenson, Ulf Thoregren
Sveriges geologiska undersökning, Uppsala, maj 1980

TR 80-11 Water uptake, migration and swelling characteristics of unsaturated and saturated, highly compacted bentonite
Roland Pusch
Luleå 1980-09-20
Division Soil Mechanics, University of Luleå

TR 80-12 Drilling holes in rock for final storage of spent nuclear fuel
Gunnar Nord
Stiftelsen Svensk Detonikforskning, september 1980

TR 80-13 Swelling pressure of highly compacted bentonite
Roland Pusch
Division Soil Mechanics, University of Luleå
Luleå 1980-08-20

TR-80-14 Properties and long-term behaviour of bitumen and radioactive waste-bitumen mixtures
Hubert Eschrich
Eurochemic, Mol, October 1980

TR 80-15 Aluminium oxide as an encapsulation material for unreprocessed nuclear fuel waste - evaluation from the viewpoint of corrosion
Final Report 1980-03-19
Swedish Corrosion Institute and its reference group

TR 80-16 Permeability of highly compacted bentonite
Roland Pusch
Division Soil Mechanics, University of Luleå
1980-12-23

TR 80-17 Input description for BIOPATH
Jan-Erik Marklund
Ulla Bergström
Ove Edlund
Studsvik Energiteknik AB, 1980-01-21

TR 80-18 Införande av tidsberoende koefficientmatriser i BIOPATH
Jan-Erik Marklund
Studsvik Energiteknik AB, januari 1980

TR 80-19 Hydrothermal conditions around a radioactive waste repository
Part 1 A mathematical model for the flow of groundwater and heat in fractured rock
Part 2 Numerical solutions
Roger Thunvik
Royal Institute of Technology, Stockholm, Sweden
Carol Braester
Israel Institute of Technology, Haifa, Israel
December 1980

TR 80-20 BEGAFIP. Programvård, utveckling och benchmarkberäkningar
Göran Olsson
Stanley Svensson
Studsvik Energiteknik AB, 1980-10-14

TR 80-21 Report on techniques and methods for surface characterization of glasses and ceramics
Bengt Kasemo
Mellerud, augusti 1980

TR 80-22 Evaluation of five glasses and a glass-ceramic for solidification of Swedish nuclear waste
Larry L Hench
Ladawan Urwongse
Ceramics Division
Department of Materials Science and Engineering
University of Florida, Gainesville, Florida
1980-08-16